AD-A040 477 MISSISSIPPI UNIV UNIVERSITY DEPT OF ELECTRICAL ENGIN--ETC F/G 9/5
THEORETICAL ANALYSIS OF THE WIRE BICONICAL ANTENNA.(U)
JAN 75 C M BUTLER, K R UMASHANKAR, C E SMITH DAEA18-74-C-0173

UNCLASSIFIED

1 OF 2

AD A040477

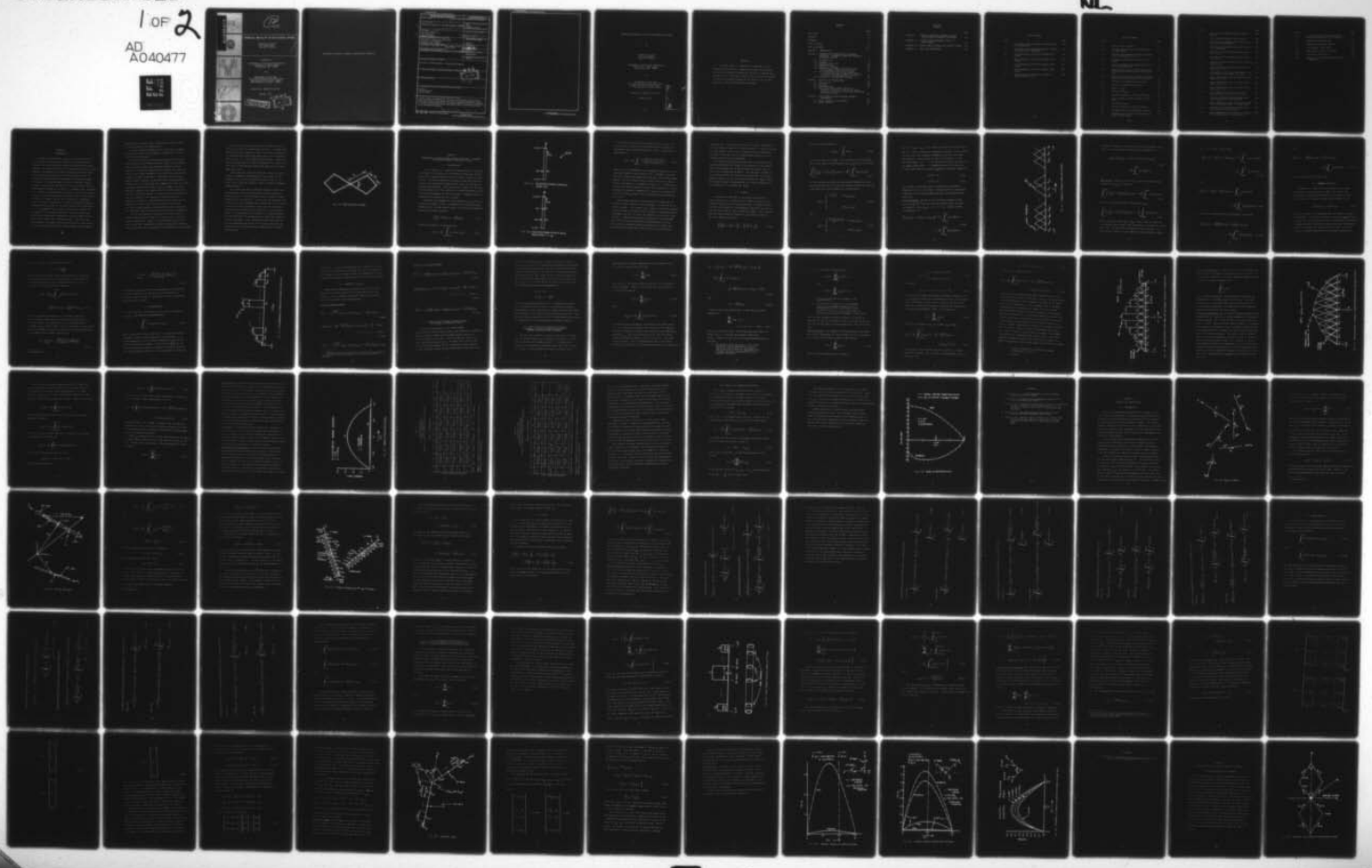

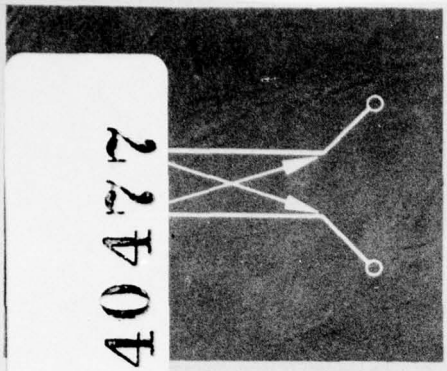

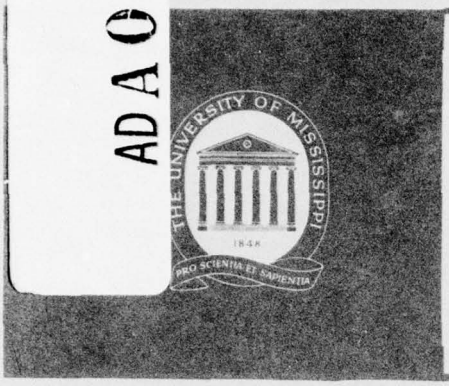

THEORETICAL ANALYSIS OF THE WIRE BICONICAL ANTENNA

Chalmers M. Butler
K.R. Umashankar
Charles E. Smith

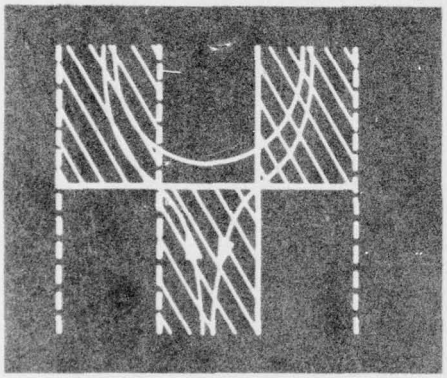

Prepared by

Department of Electrical Engineering
University of Mississippi
University, MS 38677

for

Department Of The Army
U.S. Army Communications-Electronics
Engineering Installation Agency
Fort Huachuca, Arizona 85613

Contract No. DAEA18-74-C-0173

January, 1975

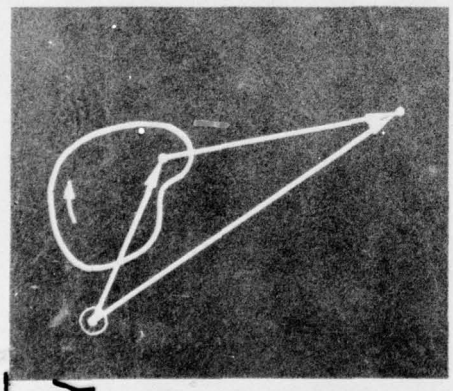

Approved for public release; distribution unlimited

UNCLASSIFIED

SECURITY CLASSIFICATION OF THIS PAGE (When Data Entered)

REPORT DOCUMENTATION PAGE

READ INSTRUCTIONS BEFORE COMPLETING FORM

1. REPORT NUMBER

2. GOVT ACCESSION NO.

3. RECIPIENT'S CATALOG NUMBER

4. TITLE (and Subtitle)

THEORETICAL ANALYSIS OF THE WIRE BICONICAL ANTENNA

5. TYPE OF REPORT & PERIOD COVERED

Final rept.

6. PERFORMING ORG. REPORT NUMBER

7. AUTHOR(s)

Chalmers M. Butler,
K.R. Umashankar
Charles E. Smith

8. CONTRACT OR GRANT NUMBER(s)

DAEA18-74-C-0173

9. PERFORMING ORGANIZATION NAME AND ADDRESS

Department of Electrical Engineering
University of Mississippi
University, MS 38677

10. PROGRAM ELEMENT, PROJECT, TASK AREA & WORK UNIT NUMBERS

PCN-18-74

11. CONTROLLING OFFICE NAME AND ADDRESS

Department of the Army, U.S. Army Communications-Electronics
Engineering Installation Agency
Fort Huachuca, AZ 85613

12. REPORT DATE

January, 1975

13. NUMBER OF PAGES

146 p.

14. MONITORING AGENCY NAME & ADDRESS (if different from Controlling Office)

15. SECURITY CLASS. (of this report)

UNCLASSIFIED

15a. DECLASSIFICATION/DOWNGRADING SCHEDULE

16. DISTRIBUTION STATEMENT (of this Report)

Approved for Public Release: Distribution Unlimited

17. DISTRIBUTION STATEMENT (of the abstract entered in Block 20, if different from Report)

18. SUPPLEMENTARY NOTES

19. KEY WORDS (Continue on reverse side if necessary and identify by block number)

Antennas
Numerical Methods
Wire Biconical

20. ABSTRACT (Continue on reverse side if necessary and identify by block number)

A general theory is presented for analysis of wire antennas and scatterers. Sample applications are provided, and selected theoretical/numerical results are compared with measured data. Particular attention is given to the analysis of the wire biconical antenna and the special case of this structure often called the bow-tie antenna.

DD FORM 1 JAN 73 1473 EDITION OF 1 NOV 65 IS OBSOLETE

UNCLASSIFIED

SECURITY CLASSIFICATION OF THIS PAGE (When Data Entered)

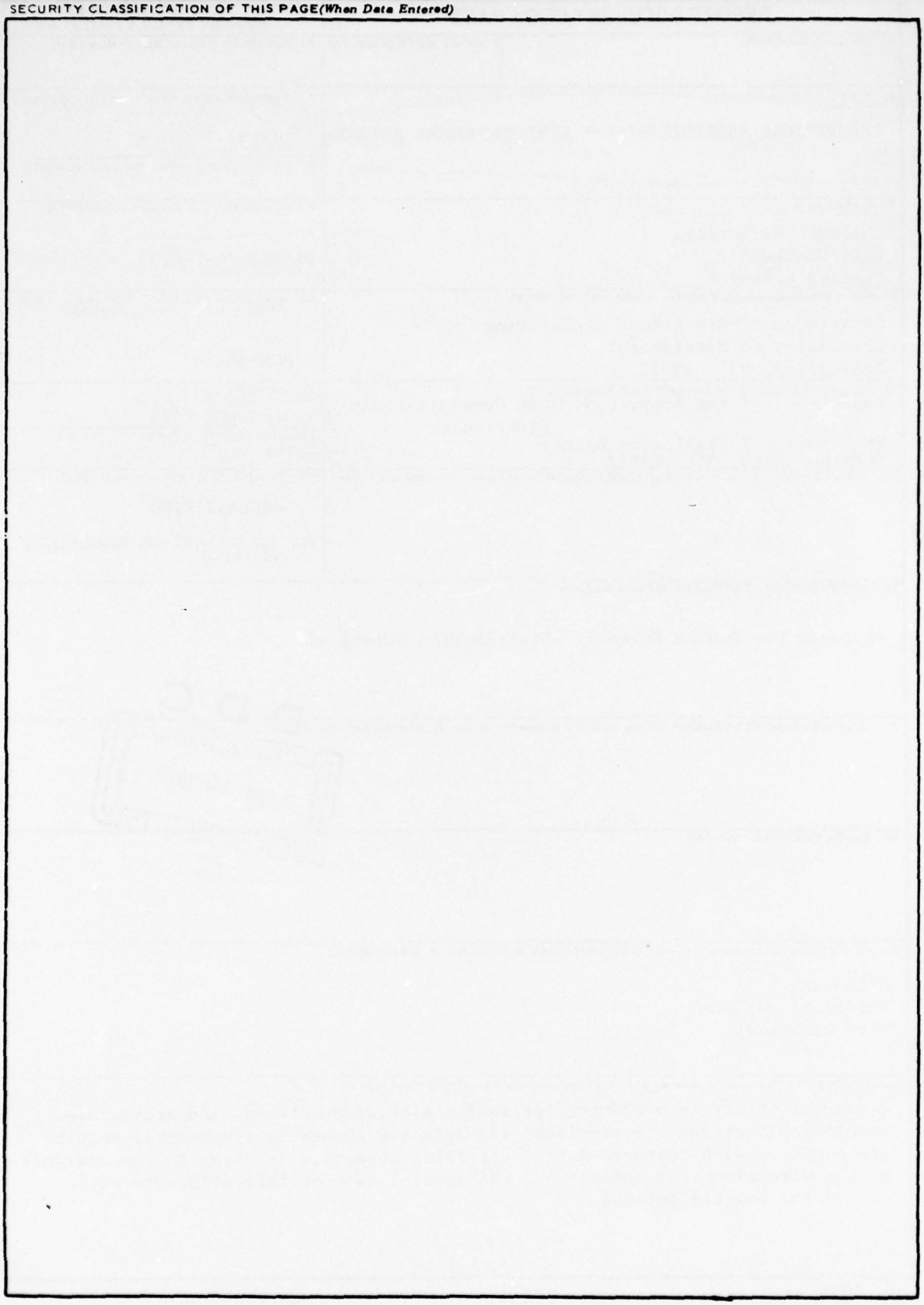

THEORETICAL ANALYSIS OF THE WIRE BICONICAL ANTENNA

BY

Chalmers M. Butler
K.R. Umashankar
Charles E. Smith

Department of Electrical Engineering
University of Mississippi
University, MS 38677

for

Department Of The Army
U.S. Army Communications-Electronics
Engineering Installation Agency
Fort Huachuca, Arizona 85613

Contract No. DAEA18-74-C-0173

January, 1975

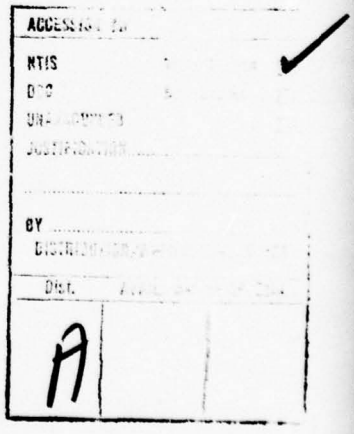

ABSTRACT

A general theory is presented for analysis of wire antennas and scatterers. Sample applications are provided, and selected theoretical/numerical results are compared with measured data. Particular attention is given to the analysis of the wire biconical antenna and the special case of this structure often called the bow-tie antenna.

CONTENTS

CONTENTS
(Cont'd)

LIST OF TABLES

LIST OF FIGURES

CHAPTER 1

INTRODUCTION

In numerous applications, there is a pressing need for a short distance HF antenna which exhibits desired electrical characteristics but which also possesses acceptable mechanical features. For an HF antenna to be of greatest utility, its input impedance and VSWR must not vary outside of prescribed bounds over the frequency band, and its radiation pattern must be essentially omni-directional throughout this frequency range of interest. The antenna must be quickly erectable, highly portable, light weight, and must be able to withstand natural environmental hazards such as wind, ice loading, rain, corrosion, etc. Finally, the antenna must be simple, of low cost, and its properties under varying ambient conditions must be well known. Of course, to achieve such an ideal radiator is impossible, but it certainly is desirable to attempt to realize a physical structure having as many of the above features as is practical.

It is apparent that a careful analysis must precede the development of an optimum HF antenna, since any design task necessitates intelligent compromises involving trade-offs and modifications among ideal characteristics. Only after full understanding of a generic antenna structure and a delineation of its properties and their interrelationships can an engineer

undertake the difficult task of designing a structure which is near optimum for his applications.

A basic radiating element which can be made to operate satisfactorily over a broad range of frequencies is the so-called biconical antenna.

Biconical dipoles have been used extensively as broad-band antennas in the VHF-UHF frequency range. The biconical type structure in free space has been studied by various authors as a spherical boundary-value problem, and, from this point of view, input impedance can be predicted from analytic formulas for small cone angles. Impedance data for large angle biconical antennas is derived mainly from experimental studies, and it is well-known from these results that the input resistance and reactance remain fairly constant over a wide frequency range for cone angles from 20^{o} to 90^{o} as compared to the thin cylindrical dipole. The gain of the biconical structure also exhibits this resonably constant behavior as a function of frequency. Experimentalists have found that, by adjusting the total length and the angle of the conical sections, optimum radiation characteristics can be obtained for frequency range variations of several orders of magnitude.

In the size needed for operation at HF, the solid or shell biconical antenna would be so massive that it would be totally impractical. However, the properties of the bicone are so near ideal compared with those of other simple antennas, one is naturally led to investigate the possibility of developing

a biconical-like antenna which retains desired electrical features but which is mechanically realistic. A simple radiator which may be viewed as a form of a biconical antenna can be fabricated from conducting wires having the configuration shown in Fig. 1-1. More sophisticated antennas, comprising various combinations or arrays of elemental wire bicone radiators, may be desired where prescribed applications warrant added complexity.

Even though the classical biconical antenna is known to exhibit a remarkably wide bandwidth, how similar are the properties of the wire structure depicted in Fig. 1-1 to those of the classical radiator? Does it exhibit broadband characteristics?

This report describes a research program in which are developed the tools for investigating the wire biconical antenna of Fig. 1-1 in free space as well as above an ideal ground (three orientations). A new theory for analyzing wire structures has been developed and is described in this report. A numerical solution procedure, based upon the new theory and applicable to general wire structures, is discussed and sample calculated data are presented. A computer program has been developed for implementing the theory and numerical solution procedure. Also, calculations have been made for various configurations of the wire biconical antennas, and selected results are presented and compared with available measured data.

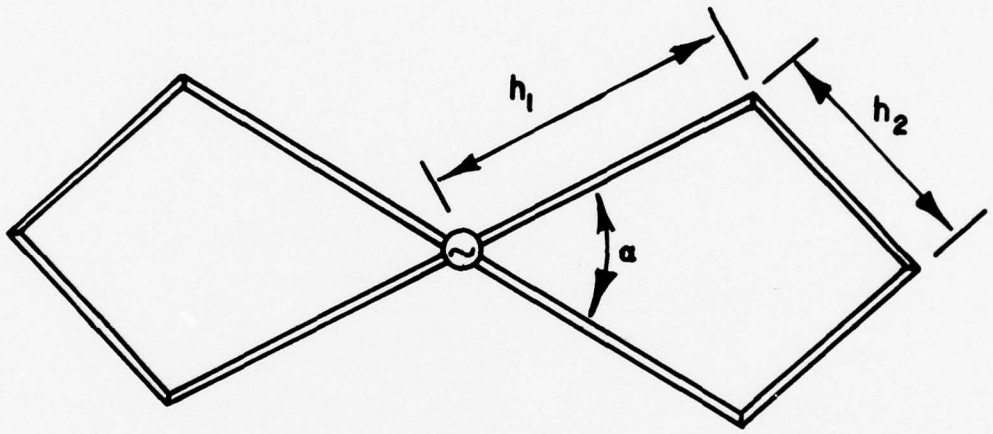

FIG. 1.1 WIRE BICONICAL ANTENNA

CHAPTER 2

FORMULATION OF STRAIGHT-WIRE INTEGRAL EQUATIONS: PIECEWISE LINEAR AND PIECEWISE SINUSOIDAL TESTING

2.1 INTRODUCTION

In this section a particular moment method [1] analysis of straight-wire scatterers and antennas is developed, and the associated integral equation for the straight element is formulated. The method emphasizes piecewise linear and sinusoidal testing, and interrelationships between these two testing procedures are delineated. Both pulses and triangles [1] are used for representation of the current and a brief discussion of the utility and advantages of each is provided. Example results of straight-wire calculations are included.

From basic electromagnetic theory applied to the perfectly conducting cylinder of Fig. 2.1, assumed to be excited by some incident field, one may readily derive the following fundamental integro-differential equation,

$$\left(\frac{d^2}{dz^2} + k^2\right) A_z(z) = -j\frac{k^2}{\omega} E_z^i(z) \ , \qquad (2.1)$$

relating the magnetic vector potential,

$$A_z(z) = \frac{\mu}{4\pi} \int_{z'=-L/2}^{L/2} i(z')K(z-z')dz' \ , \qquad (2.2)$$

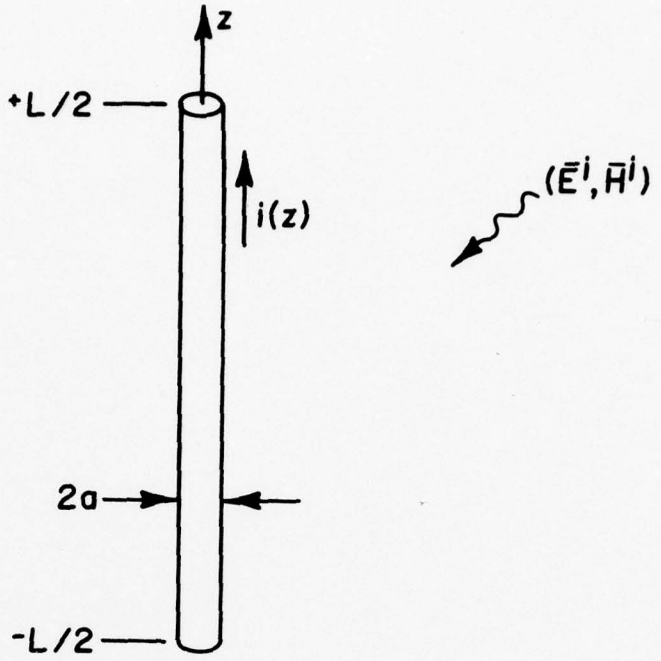

FIG. 2.1. STRAIGHT-WIRE SCATTERER ILLUMINATED BY INCIDENT FIELD

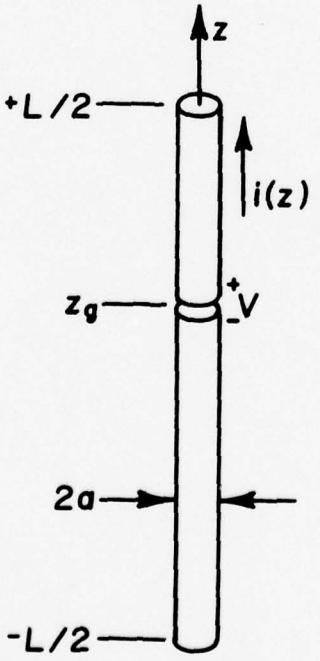

FIG. 2.2. STRAIGHT-WIRE ANTENNA EXCITED BY VOLTAGE SOURCE LOCATED AT $z = z_g$

to the unknown incident electric field having an axial component E_z^i on the surface of the cylinder, which resides in a homogeneous space characterized by $(\mu,\varepsilon,\sigma=0)$. The kernel in (2.2) above is

$$K(\xi) = \frac{1}{2\pi} \int_{\phi'=-\pi}^{\pi} \frac{e^{-jk[\xi^2+4a^2 \sin^2\phi'/2]^{\frac{1}{2}}}}{[\xi^2+4a^2 \sin^2\phi'/2]^{\frac{1}{2}}} d\phi' \qquad (2.3)$$

where k is $2\pi/\lambda$ (wavelength) at the angular frequency ω of the suppressed harmonic time variation $e^{j\omega t}$. Through (2.2), Equation (2.1) relates the known excitation E_z^i to the unknown axial current i on the scatterer which is specified to be a tube of radius a and length L as suggested in Fig. 2.1. If one wishes to treat the antenna problem in which the excitation is a slice generator of voltage V impressed at a point z_g, he replaces E_z^i of (2.1) by $V\delta(z-z_g)$ where $\delta(z)$ is the familiar delta function (Fig. 2.2).

For present purposes, the wire radius is looked upon as being very small relative to the wavelength λ as well as to the cylinder length. Such restrictions, common in thin-wire analyses, assure one that the current on the cylinder is circumferentially independent and that it can be accounted for by the total axial current i. Under these thin-wire assumptions, one could make use of the so-called reduced kernel approximation to (2.3), but, since the solution procedures below are not unduly complicated by the exact kernel, $K(\xi)$ of (2.3) is used without

approximation. Even though thin wires are under investigation here the analysis applies to a thick cylinder, if only an axially directed current exists and is circumferentially independent, as would be the case for an isolated antenna driven by a circularly uniform source or generator.

The solution procedure presented here is essentially the moment method [1], but a change in the sequence of the method's usual steps enables one to gain interesting insight into the nature of the numerical procedure. The alteration alluded to is that one performs the testing of the equation to be solved (2.1) with elements T_m of the selected testing set $\{T_m\}$ before the unknown current is approximated as a linear combination of the elements i_n of the basis set $\{i_n\}$.

2.2 TESTING

To ensure the stability of the anticipated system of linear equations to be formed in the solution procedure, only subdomain testing sets are considered here. Pursuant to such a system, one equates the corresponding projections of the two sides of (2.1) onto the space spanned by $\{T_m\}$, which implies that the scalar products formed by T_m and the two sides of (2.1) are equated for each m:

$$\left\langle \left(\frac{d^2}{dz^2} + k^2 \right) A_z, T_m \right\rangle = \left\langle -j\frac{k^2}{\omega} E_z^i, T_m \right\rangle , \qquad (2.4a)$$

where the scalar product is

$$\langle f,g\rangle = \int_{-L/2}^{L/2} fg^* dz \quad . \tag{2.4b}$$

For real testing sets $\{T_m\}$ of the subdomain type considered here, where $T_m(z)$ is zero outside $z\varepsilon(z_{m-1},z_{m+1})$, (2.4) is simply

$$\int_{z=z_{m-1}}^{z_{m+1}} \left[\left(\frac{d^2}{dz^2} + k^2\right) A_z(z)\right] T_m(z)dz = -j\frac{k^2}{\omega} \int_{z=z_{m-1}}^{z_{m+1}} E_z^i(z)T_m(z)dz. \tag{2.5}$$

The two testing sets which are particularly amenable to numerical solutions of (2.1) are the piecewise linear and piecewise sinusoidal sets whose elements are, respectively,

$$\Lambda_m^{\ell}(z) = \begin{cases} \dfrac{\Delta-|z-z_m|}{\Delta} & , \quad z\varepsilon(z_{m-1},z_{m+1}) \\ 0 & , \quad z\notin(z_{m-1},z_{m+1}) \end{cases} \tag{2.6a}$$

and

$$\Lambda_m^{s}(z) = \begin{cases} \dfrac{\sin k(\Delta-|z-z_m|)}{\sin k\Delta} & , \quad z\varepsilon(z_{m-1},z_{m+1}) \\ 0 & , \quad z\notin(z_{m-1},z_{m+1}) \end{cases} \tag{2.6b}$$

where $2\Delta = (z_{m+1} - z_{m-1})$. The former set above is illustrated in Fig. 2.3 where one observes overlapping triangles on the interior intervals with half-triangles (dashed) on the lower and upper end intervals. Testing with the end half-triangles, or end "half-sinusoids" in the case of piecewise sinusoidal testing, in the moment method admits the representation of the current in a series which does not satisfy a priori the boundary conditions,

$$i(+L/2) = 0 \quad , \tag{2.7a}$$

$$i(-L/2) = 0 \quad , \tag{2.7b}$$

and provides a convenient way to incorporate the boundary conditions (2.7) of the problem. Having a means to incorporate conditions at wire ends becomes important in situations where wires join.

Interior Testing Testing of (2.1) with the elements (2.6a) of the piecewise linear set over the interior full intervals of length 2Δ, (z_{m-1}, z_{m+1}), $m = 0 \pm 1, \pm 2, \ldots, \pm[M-1]$, yields (See Appendix I)

$$\frac{1}{\Delta}\left[A_z(z_{m+1}) - 2A_z(z_m) + A_z(z_{m-1})\right] + k^2 \int_{z=z_{m-1}}^{z_{m+1}} A_z(z)\Lambda_m^{\ell}(z)dz$$

$$= -j\frac{k^2}{\omega} \int_{z=z_{m-1}}^{z_{m+1}} E_z^i(z)\Lambda_m^{\ell}(z)dz \quad . \tag{2.8a}$$

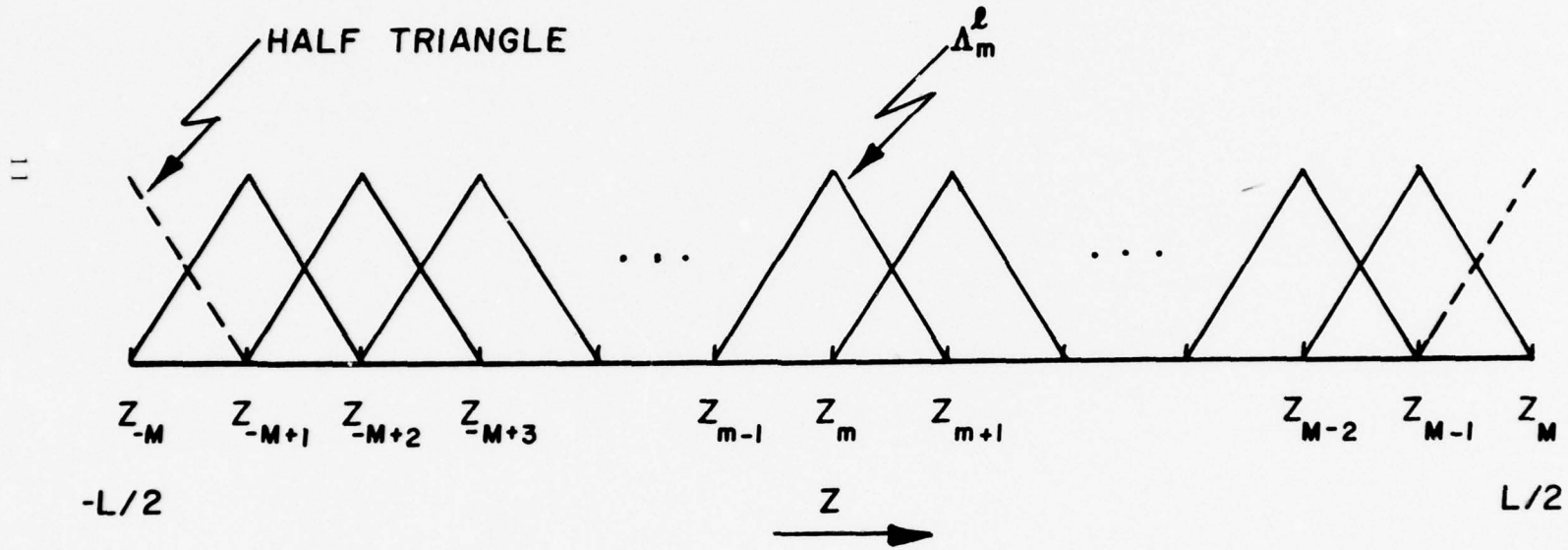

FIG. 2.3. TRIANGLES IN PIECEWISE LINEAR TESTING SCHEME

Similarly, testing of (2.1) with (2.6b) of the piecewise sinusoidal set over the full intervals yields (Appendix I)

$$\frac{k}{\sin k\Delta}\left[A_z(z_{m+1}) - 2\cos k\Delta\, A_z(z_m) + A_z(z_{m-1})\right]$$

$$= -j\frac{k^2}{\omega}\int_{z=z_{m-1}}^{z_{m+1}} E_z^i(z)\Lambda_m^s(z)dz \quad . \tag{2.8b}$$

End Testing Testing of (2.1) with T_m over the lower-end half interval (z_{-M}, z_{-M+1}) is written

$$\int_{z=z_{-M}}^{z_{-M+1}} \left[\left(\frac{d^2}{dz^2} + k^2\right)A_z(z)\right] T_{-M}(z)dz = -j\frac{k^2}{\omega}\int_{z=z_{-M}}^{z_{-M+1}} E_z^i(z)T_{-M}(z)dz \tag{2.9a}$$

and, over the upper-end half interval (z_{M-1}, z_M),

$$\int_{z=z_{M-1}}^{z_M} \left[\left(\frac{d^2}{dz^2} + k^2\right)A_z(z)\right] T_M(z)dz = -j\frac{k^2}{\omega}\int_{z=z_{M-1}}^{z_M} E_z^i(z)T_M(z)dz \tag{2.9b}$$

where $T_{\pm M}$ may be either $\Lambda_{\pm M}^{\ell}$ or $\Lambda_{\pm M}^{s}$. Notice that the limits of the integrals above render (2.9) equivalent to testing (Eq. (2.4)) over (-L/2, L/2) with half-triangles or half-sinusoids. For end testing as above, or with equivalent half-triangles, (2.9a)

and (2.9b) become, respectively,

$$- \frac{d}{dz}A_z(z_{-M}) - \frac{1}{\Delta}A_z(z_{-M}) + \frac{1}{\Delta}A_z(z_{-M+1}) + k^2 \int_{z=z_{-M}}^{z_{-M+1}} \Lambda_{-M}^{\ell}(z)A_z(z)\,dz$$

$$= -j\frac{k^2}{\omega} \int_{z=z_{-M}}^{z_{-M+1}} \Lambda_{-M}^{\ell}(z)E_z^i(z)\,dz \qquad (2.10a)$$

and

$$\frac{d}{dz}A_z(z_M) - \frac{1}{\Delta}A_z(z_M) + \frac{1}{\Delta}A_z(z_{M-1}) + k^2 \int_{z=z_{M-1}}^{z_M} A_z(z)\Lambda_M^{\ell}(z)\,dz$$

$$= -j\frac{k^2}{\omega} \int_{z=z_{M-1}}^{z_M} E_z^i(z)\Lambda_M^{\ell}(z)\,dz \quad . \qquad (2.10b)$$

Also, for end testing with half-sinusoids, one obtains

$$- \frac{d}{dz}A_z(z_{-M}) - k\,\frac{\cos k\Delta}{\sin k\Delta}\,A_z(z_{-M}) + \frac{k}{\sin k\Delta}\,A_z(z_{-M+1})$$

$$= -j\frac{k^2}{\omega} \int_{z=z_{-M}}^{z_{-M+1}} E_z^i(z)\Lambda_{-M}^{s}(z)\,dz \qquad (2.11a)$$

and

$$\frac{d}{dz}A_z(z_M) - k\,\frac{\cos k\Delta}{\sin k\Delta}\,A_z(z_M) + \frac{k}{\sin k\Delta}\,A_z(z_{M-1})$$

$$= -j\frac{k^2}{\omega}\int_{z=z_{M-1}}^{z_M} E_z^i(z)\Lambda_M^s(z)dz \quad , \qquad (2.11b)$$

where $T_{\pm M}$ may be either $\Lambda_{\pm M}^{\ell}$ or $\Lambda_{\pm M}^{s}$.

2.3 BOUNDARY CONDITIONS

Attention is called to the derivatives of the vector potential at $z_{\pm M}$ which appear in Eqs. (2.9) and (2.10). Appealing to the Lorentz condition, one can readily relate these terms to the electric scalar potential Φ by use of

$$\frac{d}{dz}\,A_z(z_{\pm M}) = -j\frac{k^2}{\omega}\,\Phi(z_{\pm M}) \qquad (2.12)$$

where, of course, Φ is calculated from the electric charge on the cylinder. If one does not enforce $i(z_{\pm M})=0$ <u>a priori</u>, then, in order that the charge and current on the cylinder constitute a complete electric system [2], rings of discrete charge must reside on the upper and lower rims of the tube. Since the current is assumed uniform over any cylinder circumference,

each ring charge is uniform and has density*

$$\rho_{\ell}^{r\pm} = \mp j \frac{i(z_{\pm M})}{2\pi\omega a}$$

where the upper and lower signs are associated with quantities at z_M and z_{-M} (L/2 and -L/2), respectively. Now one may write the expression below for the scalar potential at a point $z\varepsilon(-L/2, L/2)$ on the cylinder in the form

$$\Phi(z) = j\frac{1}{4\pi\omega\varepsilon} \int_{z'=-L/2}^{L/2} \frac{d}{dz'} i(z')\ K(z-z')dz'$$

$$-j\frac{i(z_M)}{4\pi\omega\varepsilon}\ K(z-z_M) + j\frac{i(z_{-M})}{4\pi\omega\varepsilon}\ K(z-z_{-M}) \quad (2.13)$$

where the integral contribution to the potential is due to the distributed charge and the remaining two terms come from the ring charges. The potential is to be evaluated on the cylinder at $z_{\pm M}$ at which points (2.13) is unbounded. Specifically, one can show* that the potential exhibits the following properites at the upper and lower ends, respectively:

$$\Phi^{+} = \lim_{z \uparrow z_M} \Phi(z) = \frac{i(z_M)}{j4\pi^2\omega\varepsilon a}\left[\lim_{z \uparrow z_M}\left[\ell n\left(\frac{2a}{z_M - z}\right)\right]\right] \quad (2.14a)$$

*See Appendix II.

and

$$\Phi^{-} = \lim_{z \downarrow z_{-M}} \Phi(z) = -\frac{i(z_{-M})}{j4\pi^2 \omega \varepsilon \mathbf{a}} \left[\lim_{z \downarrow z_{-M}} \left[\ell n \left(\frac{2a}{z - z_{-M}} \right) \right] \right] . \tag{2.14b}$$

Even though (2.14a) and (2.14b) are unbounded, the derivatives of vector potential in (2.10) and (2.11) are replaced by equivalent terms involving $\Phi^{\pm}$ explicitly in order to facilitate discussions which follow.

2.4 APPROXIMATIONS

For a function f sufficiently smooth over the interval (z_{m-1}, z_{m+1}) one employs the approximation,

$$\int_{z=z_{m-1}}^{z_{m+1}} f(z) T_m(z) dz \doteq \Delta f(z_m) \tag{2.15}$$

where T_m here may be either Λ_m^{ℓ} or Λ_m^{s}. In a numerical solution procedure, Δ must be small compared to the wavelength λ, if (1) the excitation is to be sampled adequately along the wire and (2) the number of elements in the basis set $\{i_n\}$ for the current approximation (hence the number of equations obtained from testing Equation (2.1)) is to be large enough to accurately

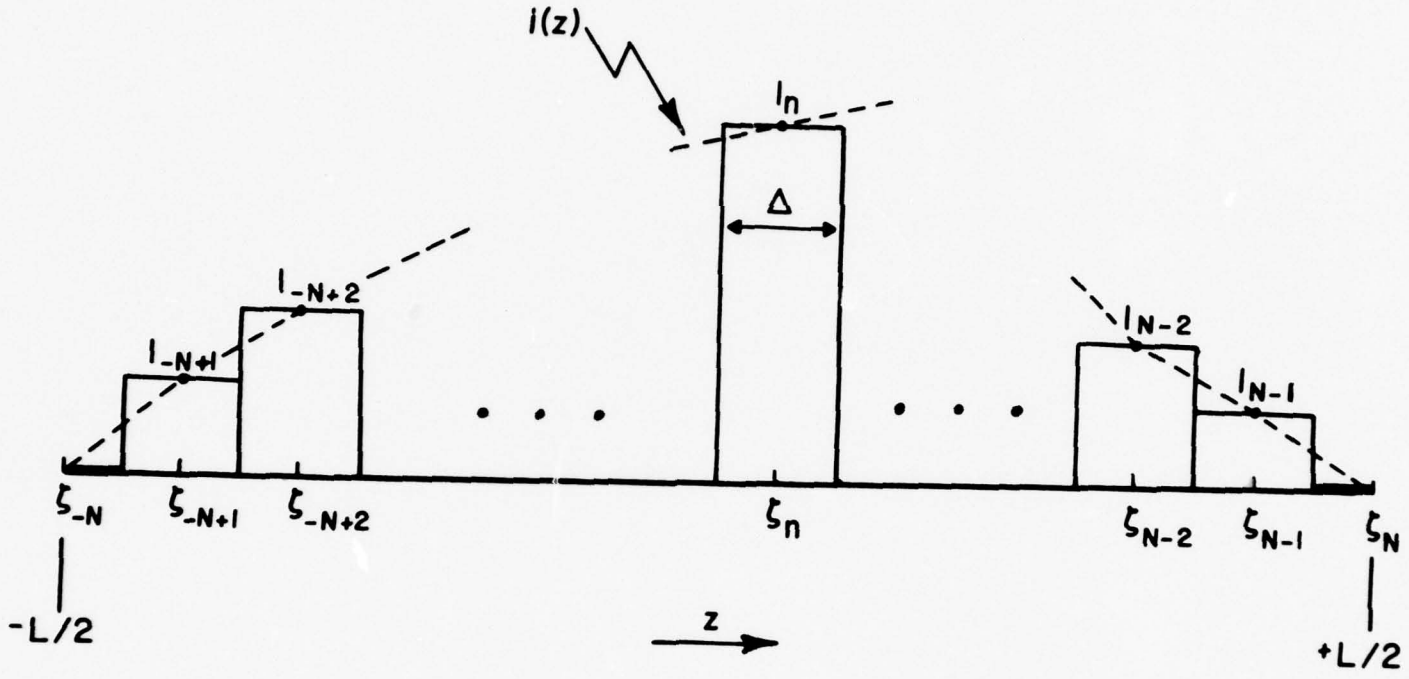

FIG. 2.4. PULSE ARRANGEMENT FOR APPROXIMATING CURRENT ON STRAIGHT WIRE

represent i. A similar approximation may be made for testing over the end intervals with the right side of (2.15) replaced by $\frac{1}{2}\,\Delta f(z_{\pm M})$, since, for end testing, the integration is over an interval of length Δ rather than 2Δ as is the case in (2.15).

2.5 SUMMARY OF TESTING

Employing the approximations above in (2.8)-(2.11) and making use of (2.12) and (2.14) in (2.10) and (2.11), one arrives at the two systems of equations below for piecewise linear and piecewise sinusoidal testing.*

Piecewise Linear Testing

$$j\frac{k^2}{\omega}\,\Phi^- - \frac{1-\frac{(k\Delta)^2}{2}}{\Delta}\,A_z(z_{-M}) + \frac{1}{\Delta}\,A_z(z_{-[M-1]}) \doteq -j\frac{k^2}{\omega}\,\frac{\Delta}{2}\,E_z^i(z_{-M}) \tag{2.16a}$$

$$\frac{1}{\Delta}\left[A_z(z_{m+1}) - 2\left(1 - \frac{(k\Delta)^2}{2}\right)A_z(z_m) + A_z(z_{m-1})\right] \doteq -j\frac{k^2}{\omega}\,\Delta E_z^i(z_m)\,,$$

$$m = 0, \pm 1, \pm 2, \ldots, \pm[M-1], \tag{2.16b}$$

$$-j\frac{k^2}{\omega}\,\Phi^+ - \frac{1-\frac{(k\Delta)^2}{2}}{\Delta}\,A_z(z_M) + \frac{1}{\Delta}\,A_z(z_{[M-1]}) \doteq -j\frac{k^2}{\omega}\,\frac{\Delta}{2}\,E_z^i(z_M) \tag{2.16c}$$

---

*Another form of the equations resulting from end testing is convenient for some purposes; this form is discussed in Chapter 3.

$$j\frac{k^2}{\omega}\,\Phi^- - k\,\frac{\cos k\Delta}{\sin k\Delta}\,A_z(z_{-M}) + \frac{k}{\sin k\Delta}\,A_z(z_{-[M-1]}) \doteq -j\frac{k^2}{\omega}\,\frac{\Delta}{2}\,E_z^i(z_{-M}) \tag{2.17a}$$

$$\frac{k}{\sin k\Delta}\left[A_z(z_{m+1}) - 2\cos k\Delta\, A_z(z_m) + A_z(z_{m-1})\right] \doteq -j\frac{k^2}{\omega}\,\Delta E_z^i(z_m),$$

$$m = 0, \pm 1, \pm 2, \ldots, \pm[M-1], \tag{2.17b}$$

$$-j\frac{k^2}{\omega}\,\Phi^+ - k\,\frac{\cos k\Delta}{\sin k\Delta}\,A_z(z_M) + \frac{k}{\sin k\Delta}\,A_z(z_{[M-1]}) \doteq -j\frac{k^2}{\omega}\,\frac{\Delta}{2}\,E_z^i(z_M) \tag{2.17c}$$

2.6 RELATIONSHIPS BETWEEN PIECEWISE LINEAR AND PIECEWISE SINUSOIDAL TESTING

For sufficiently small Δ, one observes that Λ_m^ℓ and Λ_m^s do not differ significantly, and, therefore, operations with one testing element should produce results similar to those achieved via the other. Such is indeed the case as is seen from the discussion below. To obtain (2.16) from (2.8a) and (2.10), approximation (2.15) is applied to two integrals in each equation, whereas (2.17) follows from (2.8b) and (2.11)

subject to approximation of a single integral per equation. In this sense, Eqs. (2.17) resulting from piecewise sinusoidal testing are more nearly exact than are (2.16) resulting from piecewise linear testing. Of course, in a numerical solution one may make use of Eqs. (2.8), (2.10), and (2.11) which are exact, but, as one would suspect in view of the closeness of Λ_m^{ℓ} to Λ_m^{s} for $\Delta<<\lambda$, (2.16) and (2.17) are seen to be the same set of equations within the approximations,

$$\sin k\Delta \doteq k\Delta \quad ,$$

$$\cos k\Delta \doteq 1 - \frac{(k\Delta)^2}{2} \quad ,$$

which are quite good whenever $k\Delta<<1$. Of additional interest is the observation that (2.16b) is the difference equation approximation to (2.1) arrived at by replacing the second derivative operator by the second central difference operator. Thus, piecewise linear testing of Eq. (2.1) is approximately equivalent to replacing it by the corresponding difference equation.

2.7 USE OF PIECEWISE LINEAR AND PIECEWISE SINUSOIDAL TESTING IN NUMERICAL SOLUTION OF CURRENT ON STRAIGHT-WIRE SCATTERER

At this point attention is given to the task of solving for the unknown current i(z) induced on a straight-wire scatterer by a specified incident field $\bar{E}^i$. To obtain such a solution one establishes a procedure based upon either (2.16) or (2.17). In the procedure the unknown current i(z) is

approximated as a linear combination of known elements $i_n(z)$ of a suitably chosen basis set $\{i_n\}$:

$$i(z) = \sum_{n=-N}^{N} I_n i_n(z) \tag{2.18}$$

where the I_n's are unknown complex constants to be calculated in the procedure. With i(z) of (2.18), the vector potential of (2.2) can be written

$$A_z(z) = \sum_{n=-N}^{N} I_n A_{z_n}(z) \tag{2.19a}$$

where

$$\mathbf{A}_{z_n}(z) = \frac{\mu}{4\pi} \int_{z'=-L/2}^{L/2} i_n(z')K(z-z')dz' \tag{2.19b}$$

is a partial vector potential contributed by the basis element i_n. Once a basis set $\{i_n\}$ has been selected in the numerical solution technique, i_n would be known and one could immediately determine A_{z_n}. Next one substitutes (2.19) into the tested integro-differential equation ((2.16) or (2.17)). For illustrative purposes (2.16) is employed here and, to facilitate explanation, one finds the following definitions to be convenient:

$$S_{mn} = \frac{1}{\Delta}\left[A_{z_n}(z_{m+1}) - 2\left(1-\frac{(k\Delta)^2}{2}\right)A_{z_n}(z_m) + A_{z_n}(z_{m-1})\right]$$

$$= \frac{1}{\Delta}\cdot\frac{\mu}{4\pi}\int_{z'=-L/2}^{L/2} i_n(z')\left[K(z_{m+1}-z') - 2\left(1-\frac{(k\Delta)^2}{2}\right)K(z_m-z') + K(z_{m-1}-z')\right]dz' \qquad (2.20a)$$

and

$$V_m = -j\frac{k^2}{\omega}\Delta E_z^i(z_m) \quad . \qquad (2.20b)$$

In terms of the above definitions, (2.16b) may be written compactly as

$$\sum_{n=-N}^{N} I_n S_{mn} = V_m \quad ,$$

$$m = 0, \pm 1, \pm 2, \ldots, \pm(M-1) \quad , \qquad (2.21)$$

which is a system of (2M-1) linear equations with (2N+1) unknowns (I_n's). To satisfy the boundary conditions, $i(-L/2) = i(L/2) = 0$, one of the following approaches may be employed.

1. Equations (2.16a) and (2.16c), with (2.18) and (2.19), may be appended to (2.21) in which case the presence of the terms Φ^- and Φ^+ of (2.16) in such an augmented system of equations forces satisfaction of the boundary conditions.

2. The boundary conditions imply

$$i(-L/2) = \sum_{n=-N}^{N} I_n i_n(-L/2) = 0$$

and

$$i(L/2) = \sum_{n=-N}^{N} I_n i_n(L/2) = 0$$

which two equations may be added to the system (2.21).

3. If the basis set $\langle i_n \rangle$ is of the subdomain type [1], the boundary conditions may be incorporated directly by setting i_{-N} and i_N equal to zero; i_{-N} and i_N exist over the lower-end and upper-end subdomains, respectfully.

With the wire boundary conditions honored, the system of equations (2.21) can be solved for the I_n's, which in conjunction with (2.18) lead to an approximation for the wire current $i(z)$.

Pulse Basis Set As an example of how the procedure described here may be implemented, we choose pulses [1] for the elements of the basis set, in terms of which (2.18) becomes

$$i(z) = \sum_{n=-N}^{N} I_n p_n(z) \qquad (2.22)$$

where the pulse function $p_n(z)$ is given by

$$p_n(z) = \begin{cases} 1, & z\varepsilon(\zeta_n-\Delta/2,\ \zeta_n+\Delta/2) \\ \\ 0, & z\not\varepsilon(\zeta_n-\Delta/2,\ \zeta_n+\Delta/2)\ . \end{cases} \tag{2.23}$$

and where

$$\zeta_n = n\Delta\ ,\ n = 0,\ \pm1,\ \pm2,\ldots,\ \pm N\ . \tag{2.24}$$

In Fig. 2.4 a current approximated by pulses is depicted and ζ_n of (2.23) is shown as the coordinate location of the center of the n^{th} pulse. Notice in Fig. 2.4 that I_{-N} and I_N are made zero in order that boundary conditions are satisfied by the current approximation; thus, (2.22) reduces to

$$i(z) = \sum_{n=-(N-1)}^{N-1} I_n p_n(z) \tag{2.25}$$

and, with i_n replaced by p_n in (2.20a), S_{mn} becomes

$$S_{mn} = \frac{1}{\Delta}\frac{\mu}{4\pi}\int_{z'=\zeta_n-\Delta/2}^{\zeta_n+\Delta/2}\left[K(z_{m+1}-z') - 2\left(1-\frac{(k\Delta)^2}{2}\right)K(z_m-z') + K(z_{m-1}-z')\right]dz' \tag{2.26}$$

since $p_n(z)$ is zero outside $z\varepsilon(\zeta_n-\Delta/2,\ \zeta_n+\Delta/2)$. A simple change of variables, use of (2.24), and replacement of z_m by (see Fig. 2.4)

$$z_m = m\Delta \quad , \quad m = 0, \pm 1, \pm 2, \ldots \quad , \tag{2.27}$$

allow one to convert (2.26) to

$$S_{mn} = \frac{\mu}{4\pi\Delta} \int_{\zeta'=-\Delta/2}^{\Delta/2} \left[K(\Delta[m+1-n]+\zeta') - 2\left(1 - \frac{(k\Delta)^2}{2}\right) K(\Delta[m-n]+\zeta') \right.$$

$$\left. + K(\Delta[m-1-n]+\zeta') \right] d\zeta' \quad , \tag{2.28}$$

a form which is computationally more convenient than (2.26). With N=M and with (2.25) and (2.28) in (2.21), one has a system of (N-1) equations in (N-1) unknowns from which he can determine the I_n's (unknowns). Fig. 2.5 shows a wire of length L partitioned into 10 segments of length Δ with the current approximated by 9 pulses. Notice the geometric relationships between the location of the piecewise linear testing functions Λ_m^{ℓ} and of the pulses and observe that the current on each end is represented by half-pulses, each of which is made zero so that the current approximation satisfies the boundary condition from the outset. From this figure we generalize as follows. For a wire of length L one may select any number P (odd number for convenience) of unknown pulses and partition L into (P+1) segments of length Δ=L/(P+1), which lead one to specify the number of equations in the linear system (2.21) to be, of course, P.

P - number of unknown I_n's (pulses) and number of equations in (2.21)

Δ - L/(P+1)

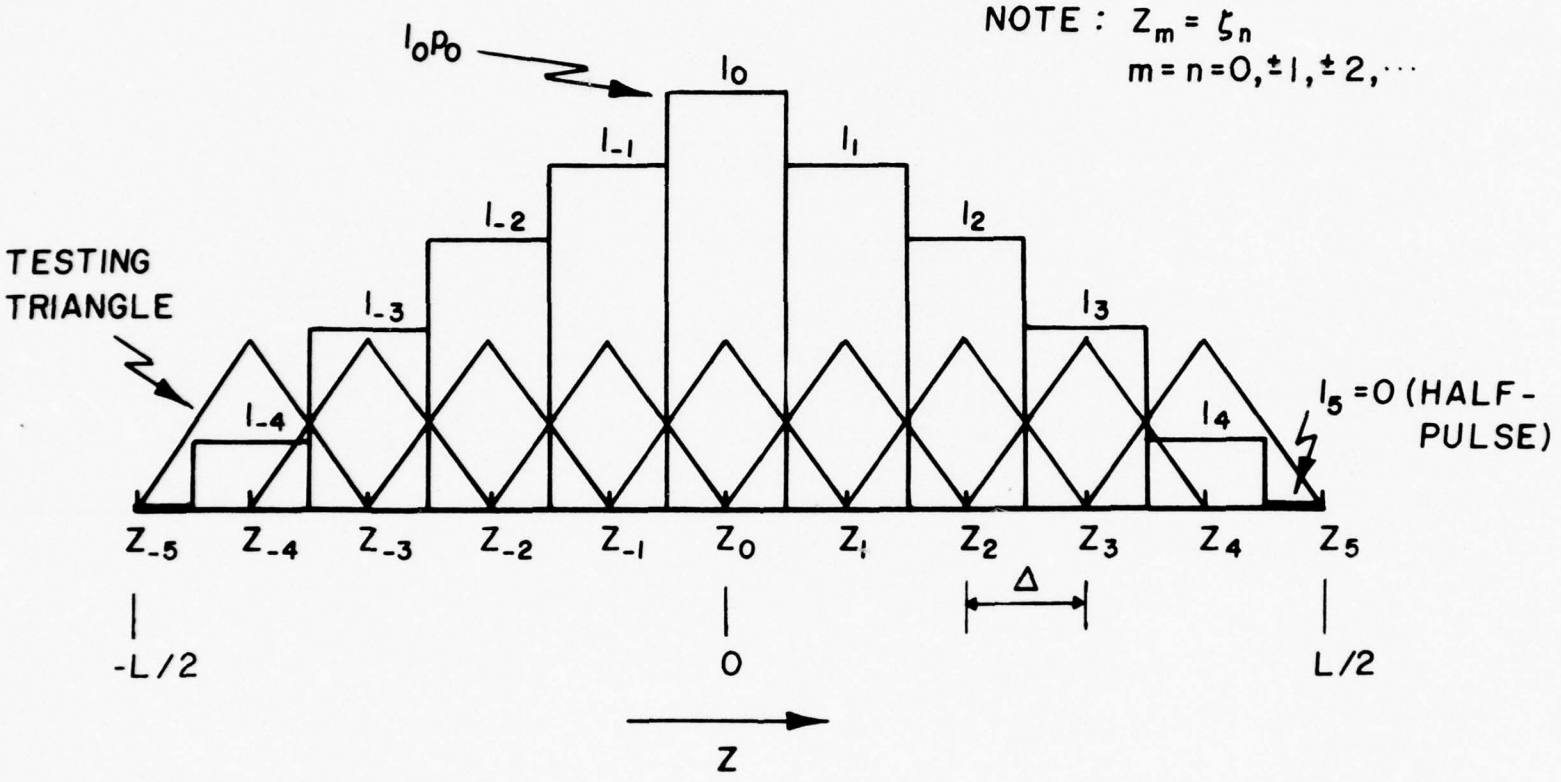

FIG. 2.5. RELATIVE LOCATIONS OF PULSES (BASES SET) AND TRIANGLES (TESTING SET) ON STRAIGHT WIRE

Numerical Calculations We observe from (2.3) and (2.28) that, when m and n are related by either m=n-1, m=n, or m=n+1, one of the three integrands of (2.28) is singular leaving one with the need to evaluate integrals like

$$\int_{\zeta'=-\Delta/2}^{\Delta/2} K(\zeta')d\zeta' \quad .$$

with a singular integrand. This integral is discussed and evaluated in a forthcoming paper [3] by Butler. All combinations of n and m other than those cited above give rise to nonsingular integrands of (2.28) which may be integrated numerically with great ease and accuracy.

Piecewise Linear Basis Set As another example, one may consider representing the current as a linear combination of piecewise linear functions Λ_n^ℓ , where the Λ_n^ℓ's of (2.6a) replace the p_n's of (2.18). These are often called triangles or triangular pulses and are illustrated in Fig. 2.6 where one sees the current approximated by 9 triangles and their relative positions to the 9 testing triangles. The peak of a given triangle used in the set to approximate current is equal to current at the point where the peak occurs, i.e., the peak of Λ_n^ℓ is I_n, and triangles are seen to be arranged in such a way that the boundary conditions are satisfied. Also, an approximation of current by a sum of weighted triangles is equivalent to piecewise linear interpolation as suggested by the dashed lines of Fig. 2.6.

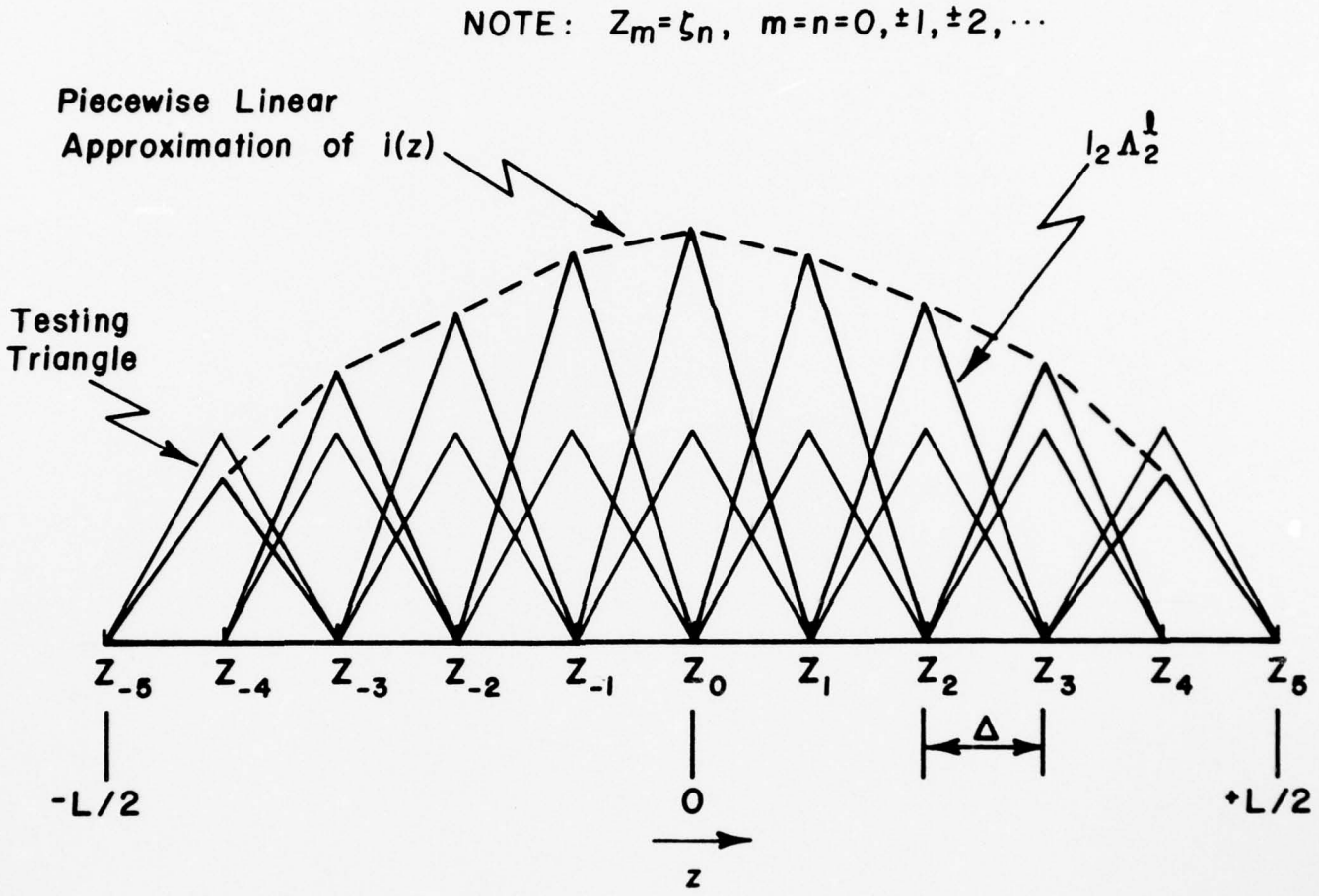

FIG. 2.6. RELATIVE LOCATIONS OF TRIANGLES IN CURRENT APPROXIMATION AND THOSE USED FOR TESTING

The coefficients S_{mn} are needed with $i_n=\Lambda_n^{\ell}$ in order that one may establish the linear system (2.21) when the current is represented by a piecewise linear approximation. To obtain S_{mn} with $i_n=\Lambda_n^{\ell}$, A_{z_n} of (2.19b) is determined, reduced to a useful form, and then substituted into (2.20a). First, from (2.19b),

$$A_{z_n}(z_m) = \frac{\mu}{4\pi}\int_{z'=-L/2}^{L/2}\Lambda_n^{\ell}(z')K(z_m-z')dz'$$

and, since Λ_n^{ℓ} is nonzero only over $z'\varepsilon(\zeta_n-\Delta,\zeta_n+\Delta)$, the above expression becomes

$$A_{z_n}(m\Delta) = \frac{\mu}{4\pi}\int_{z'=(n-1)\Delta}^{(n+1)\Delta}\Lambda_n^{\ell}(z')K(\Delta m-z')dz'$$

where use is made of (2.24) and (2.27). Subject to the change of variables $z'=-\zeta'+n\Delta$, one has

$$A_{z_n}(m\Delta) = \frac{\mu}{4\pi}\int_{\zeta'=-\Delta}^{\Delta}\Lambda_n^{\ell}(n\Delta-\zeta')K(\Delta[m-n]+\zeta')d\zeta'$$

and, as can be seen from (2.6a) or (I-1),

$$\Lambda_n^{\ell}(n\Delta-\zeta') = \frac{1}{\Delta}[\Delta-|\zeta'|] = \Lambda_0^{\ell}(\zeta')$$

so one finally arrives at

$$A_{z_n}(m\Delta) = \frac{\mu}{4\pi} \int_{\zeta'=-\Delta}^{\Delta} \Lambda_0^{\ell}(\zeta') K(\Delta[m-n]+\zeta') d\zeta' \quad . \tag{2.29}$$

Substitution of (2.29) into (2.20a) enables one to obtain S_{mn} for a piecewise linear approximation of i(z):

$$S_{mn} = \frac{\mu}{4\pi\Delta} \int_{\zeta'=-\Delta}^{\Delta} \Lambda_0^{\ell}(\zeta') \left[K(\Delta[m+1-n]+\zeta') - 2\left(1 - \frac{(k\Delta)^2}{2}\right) K(\Delta[m-n]+\zeta') \right.$$

$$\left. + K(\Delta[m-1-n]+\zeta') \right] d\zeta' \quad . \tag{2.30}$$

Equation (2.30) is in a highly convenient form for numerical computation. As is the case in (2.28), the kernels of (2.30) can be singular; such integrals are discussed in [3] and suggestions for evaluation are given.

With S_{mn} available for the current approximated by triangles, one substitutes (2.30) into (2.21) and, with N=M, solves for the I_n's. Knowing these coefficients, one approximates the current by means of

$$i(z) \doteq \sum_{n=-(N-1)}^{(N-1)} I_n \Lambda_n^{\ell}(z) \quad . \tag{2.31}$$

Sample Results The above theory is directly applicable to the problem of calculation of current on a straight-wire scatterer. By solving the set of algebraic equations (2.21) with S_{mn} given by (2.28), one obtains the I_n's of the pulse current expansion (2.25) and, hence, has an approximation for the current i(z); similarly, solution of (2.21) with S_{mn} of (2.30) yields the I_n's associated with a triangle expansion which may be used in (2.31) for determination of current. As an example of results obtained from the present analysis, Fig. 2.7 depicts the current induced by a normally incident field of 1 volt/meter on a straight-wire scatterer of length $L=\lambda/4$ and radius $a=\lambda/1000$. Notice that data obtained by pulse and triangle current expansion are essentially identical.

Convergence In order that one may observe the convergence of the series (2.25) and (2.31) for straight-wire scatterers of various lengths, all of radius $a=\lambda/1000$ and illuminated by a normally incident electric field of 1 volt/meter, Tables I and II are provided. From a careful study of these tabulated data, one sees little difference in convergence rates.

Other Basis and Testing Sets One may choose piecewise sinusoidal testing functions and employ Equation (2.17b) rather than (2.16b) to solve for the current on the scatterer. A procedure based upon (2.17b) would parallel those described above. However, in view of the closeness of Λ_m^s to Λ_m^ℓ for sufficiently small Δ/λ, one would obtain essentially the same numerical results. Furthermore, one may wish to specify the elements of the basis set to be Λ_n^s's but, here again, the close-

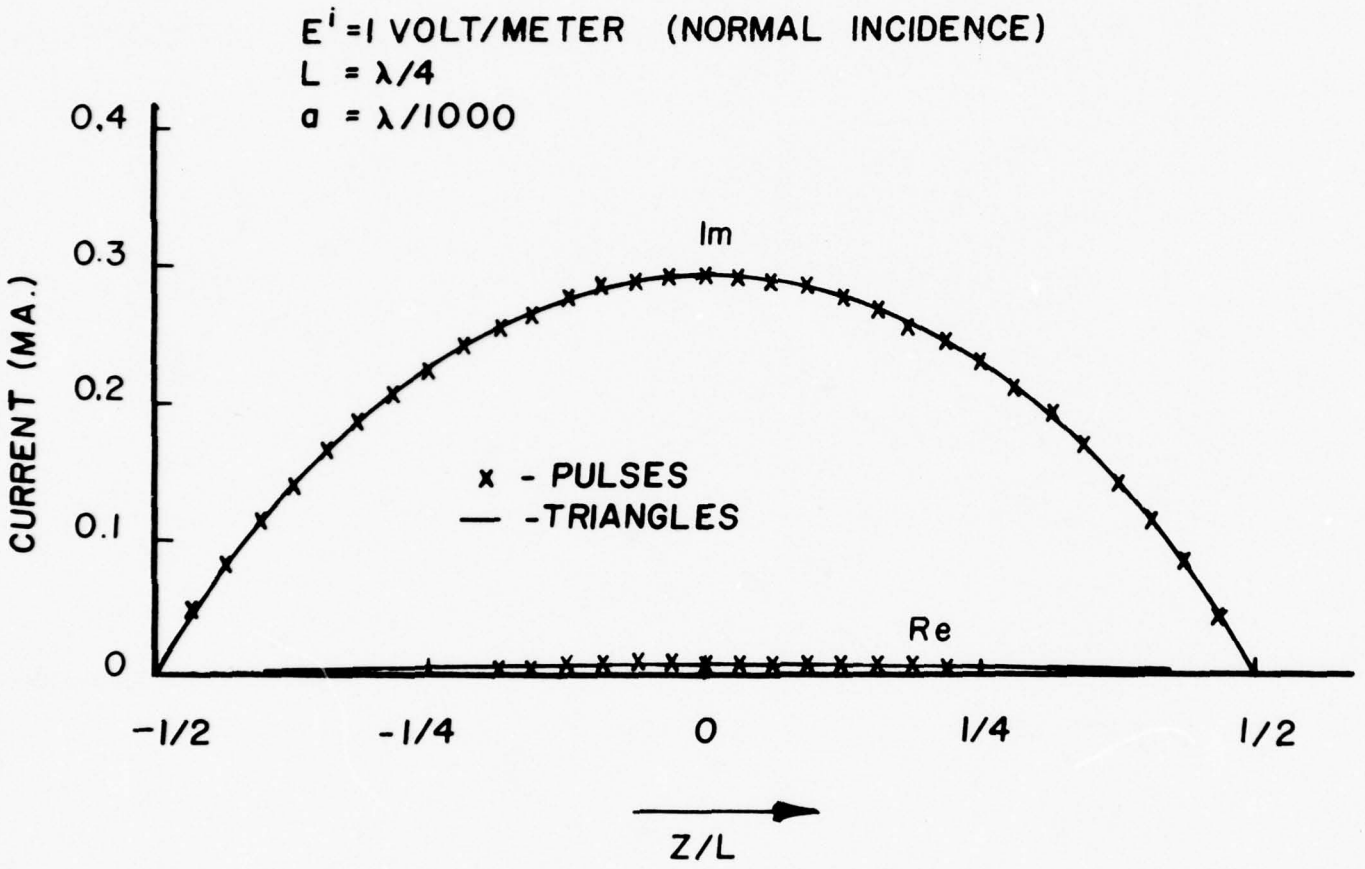

FIG. 2.7. CURRENT ON STRAIGHT-WIRE SCATTERER

TABLE 1

Convergence Data
(Piecewise Linear Testing
Pulse Expansion)
Current at Center of Scatterer (Milliamperes)

Number of Subdomains*

Normalized Length (L/λ)	4	6	8	10	16	20	30
0.4	.476+j1.52 (1.59)**	.470+j1.49 (1.56)	.476+j1.49 (1.56)	.484+j1.49 (1.57)	.502+j1.51 (1.59)	.510+j1.52 (1.60)	
0.5	2.91-j2.11 (3.59)	3.20-j1.91 (3.73)	3.25-j1.86 (3.74)	3.24-j1.85 (3.73)	3.19-j1.85 (3.69)	3.16-j1.87 (3.67)	
0.667	.413-j1.17 (1.24)	.452-j1.20 (1.29)	.473-j1.21 (1.30)	.468-j1.22 (1.30)	.471-j1.22 (1.31)	.471-j1.22 (1.31)	
1.0	.233-j1.02 (1.04)	.242-j.950 (.980)	.245-j.941 (.972)	.247-j.938 (.970)	.248-j.936 (.968)	.248-j.935 (9.67)	.249-j.935 (.967)
1.5	.160-j.382 (.414)	-.057+j.164 (.174)	-4.33+j.525 (.680)	-.860+j.721 (1.12)	-1.69+j.712 (1.83)	-1.91+j.621 (2.01)	-2.11+j.498 (2.17)

Radius (a) = .001λ, Angle of Incidence = 90^{o}, $|E^{i}|$ = 1 Volt/Meter

*Number of Subdomains is One More than Number of Current Elements i_n

**Absolute Value in Parenthesis

TABLE II

Convergence Data
(Piecewise Linear Testing
Piecewise Linear Expansion)
Current at Center of Scatterer (Milliamperes)

Number of Subdomains*

Normalized Length (L/λ)	4	6	8	10	16	20	30
0.4	.59+j1.67 (1.77)**	.55-j1.59 (1.68)	.54+j1.57 (1.66)	.54+j1.56 (1.65)	.54+j1.56 (1.65)	.54+j1.55 (1.65)	
0.5	2.44-j2.21 (3.29)	2.82-j2.07 (3.50)	2.94-j2.00 (3.55)	2.99-j1.97 (3.57)	3.02-j1.93 (3.58)	3.02-j1.93 (3.58)	
0.667	.41-j1.16 (1.23)	.43-j1.18 (1.26)	.45-j1.19 (1.27)	.45-j1.20 (1.28)	.46-j1.21 (1.30)	.46-j1.21 (1.30)	
1.0	.25-j1.1 (1.13)	.24-j.97 (1.00)	.24-j.94 (.97)	.24-j.94 (.97)	.25-j.93 (.97)	.25-j.93 (.97)	.25-j.94 (.97)
1.5	.19-j.40 (.44)	-.06+j.18 (.19)	-.39-j.50 (.64)	-.75+j.69 (1.03)	-1.51+j.76 (1.69)	-1.76+j.69 (1.89)	-2.00+j.57 (2.08)

Straight Wire a/λ = .001, Normal Incidence, E^i = 1 Volt/Meter, Triangles

*Number of Subdomains is One More than Number of Current Elements i_n

**Absolute Value in Parenthesis

ness of Λ_n^s to Λ_n^ℓ suggests that a piecewise sinusoidal approximation of current would lead to solutions which differ only insignificantly from those obtained via a piecewise linear approximation. In summary, then, the two examples given above of solution procedures can be viewed as covering the following combinations of testing/current approximation: (1) piecewise linear/pulses, (2) piecewise linear/piecewise linear, (3) piecewise linear/piecewise sinusoidal, (4) piecewise sinusoidal/pulses, (5) piecewise sinusoidal/piecewise linear, and (6) piecewise sinusoidal/piecewise sinusoidal.

Whenever the wire structure is of sufficiently large magnitude, in terms of numbers of wavelengths of wire, one may not be able to require the increment Δ to be so small relative to wavelength to be assured that piecewise sinusoidal functions (for basis or testing set) yield results which are extremely close to those obtained by means of piecewise linear functions. For $\Delta/\lambda \leq 1/10$ the difference should be less than 6 or 7 percent.

The solution procedure outlined above in which piecewise linear functions, or triangles, are utilized as elements of both the basis and testing sets is an example of a Galerkin method, i.e., a method in which testing functions are the same as basis functions. Since (2) and (6) above are approximately equivalent, the procedure employing triangles for expansion and testing is quite close to Galerkin's method with piecewise sinusoidal functions.

2.8 ANALYSIS OF STRAIGHT-WIRE ANTENNA

The solution methods discussed for the scatterer in Section 2.7 are directly extendable to the case of a straight-wire antenna, driven by a voltage source of V volts and located at some point z_g along the length of the wire (Fig. 2.2). If one adopts the standard slice generator source model [4], then E_z^i of (2.1) becomes

$$E_z^i(z) = V\delta(z-z_g) \tag{2.32}$$

where $\delta(z)$ is the familiar delta function. Without the approximations of Section 2.4, V_m of (2.21) becomes exactly

$$V_m = -j\frac{k^2}{\omega}V\int_{z=z_{m-1}}^{z_{m+1}} \delta(z-z_g)\Lambda_m^{\ell,s}(z)dz = -j\frac{k^2}{\omega}V\Lambda_m^{\ell,s}(z_g) \tag{2.33}$$

for either piecewise linear or piecewise sinusoidal testing and, for either testing set, reduces to

$$V_m = -j\frac{k^2}{\omega}V \quad , (z_g=z_m) \tag{2.34}$$

when z_g and z_m coincide. For multiple excitation (2.33) becomes

$$V_m = -j\frac{k^2}{\omega}\sum_{\nu=1}^{N_g} V_\nu^g\Lambda_m^{\ell,s}(z_{g_\nu}) \tag{2.35}$$

for N_g sources located at $z_{g_1}, z_{g_2},\ldots, z_{N_g}$ and having emf's of $V_1^g, V_2^g,\ldots, V_{N_g}^g$ volts, respectively.

The remaining terms in (2.21), S_{mn} and I_n, are handled in exactly the same way that they are for a scatterer. Hence, with the appropriate definition of V_m in (2.33)--(2.35) and with S_{mn} for pulse or triangle representation of current discussed in Section 2.7, one may calculate current on an arbitrarily excited, straight-wire antenna.

Sample results for a center-driven, half-wavelength antenna are depicted in Fig. 2.8. Current, calculated by means of piecewise linear expansion and testing, is seen in Fig. 2.8, where for comparison is also displayed current calculated from a pulse expansion with collocation numerical solution to Hallen's equation [5].

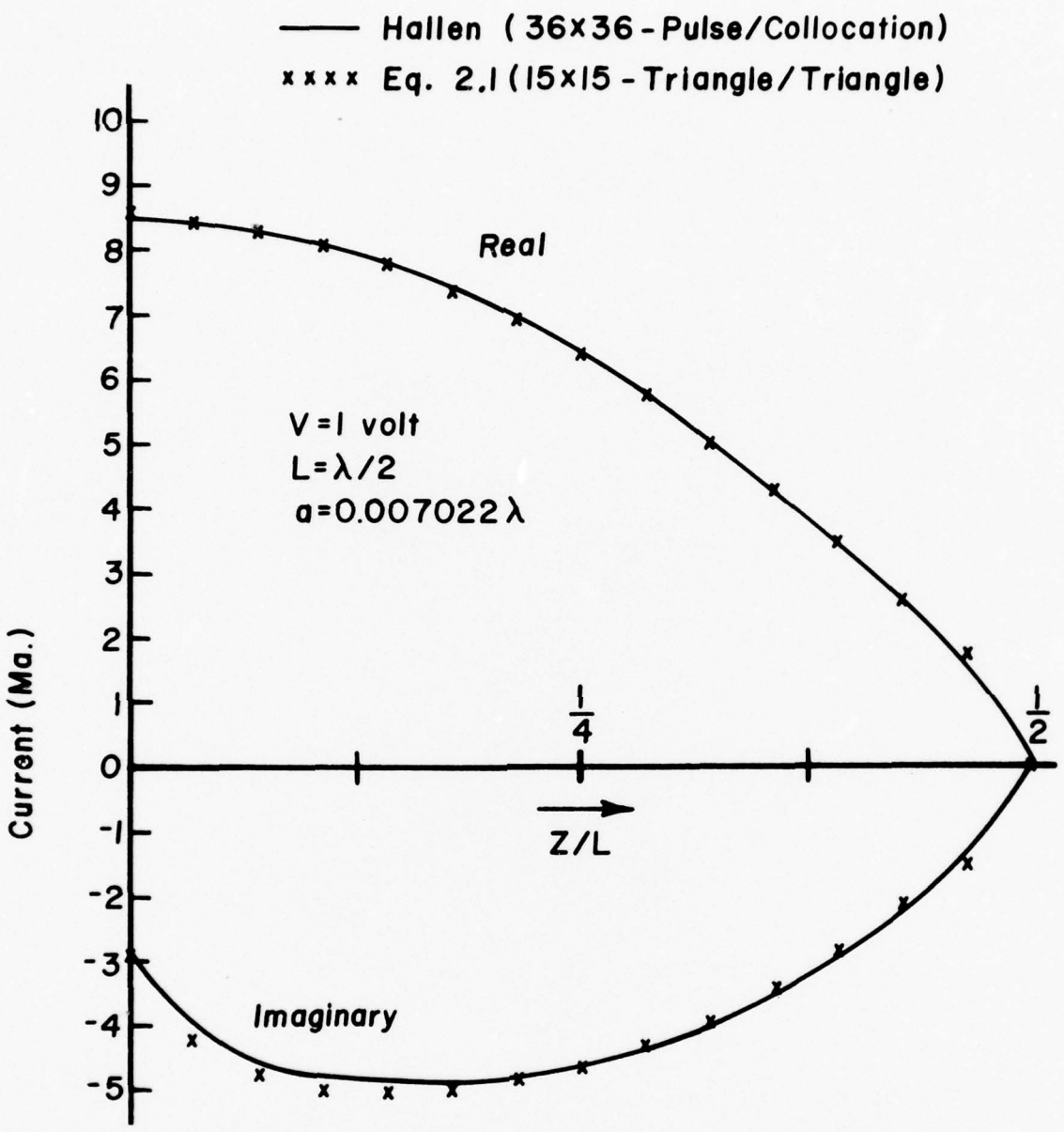

FIG. 2.8. CURRENT ON CENTER-DRIVEN DIPOLE

REFERENCES

1. Harrington, R.F., Field Computation by Moment Methods, MacMillan, New York; 1968.

2. King, R.W.P., Fundamental Electromagnetic Theory, Dover Publication, New York; 1963.

3. Butler, C.M., "Evaluation of Potential Integral at Singularity of Exact Kernel in Thin-Wire Calculations," to be published in March, 1975, issue of IEEE Trans. Ant. and Prop.

4. King, R.W.P., The Theory of Linear Antennas, Harvard University Press, Cambridge, Mass.; 1956.

5. Butler, C.M., and D.R. Wilton, "Analysis of Various Numerical Techniques Applied to Thin-Wire Scatterers," accepted for publication in IEEE Trans. Ant. and Prop.

CHAPTER 3

ANALYSIS OF COUPLED WIRES

3.1 INTRODUCTION

With the foundation being established in Chapter 2, the next step in the procedure for developing a general analytical technique for characterizing wire structures is the treatment of a particular wire in the presence of others. The electromagnetic influence on one wire in an ensemble due to all others plus itself must be fully accounted for in any analysis. Such coupling, mutual and self, must be taken into consideration for each wire in an ensemble.

In this Chapter are presented the analysis of wire structures and the formulation of pertinent integral equations. Numerical solution procedures are discussed as are symmetry conditions. To support the theory, results of sample calculations are included and compared with data obtained elsewhere.

In Fig. 3.1 are shown several wires, one designated the p^{th} wire and another designated the q^{th}. We focus major attention upon the p^{th} wire and investigate how one may calculate the electric field on this wire due to the current i_p on itself plus that due to i_q, the current on the q^{th} wire. The contribution on the p^{th} wire due to the presence of wires other than the q^{th} may be calculated in an identical way, and then the total contribution from wires other than the p^{th} is simply a summation over

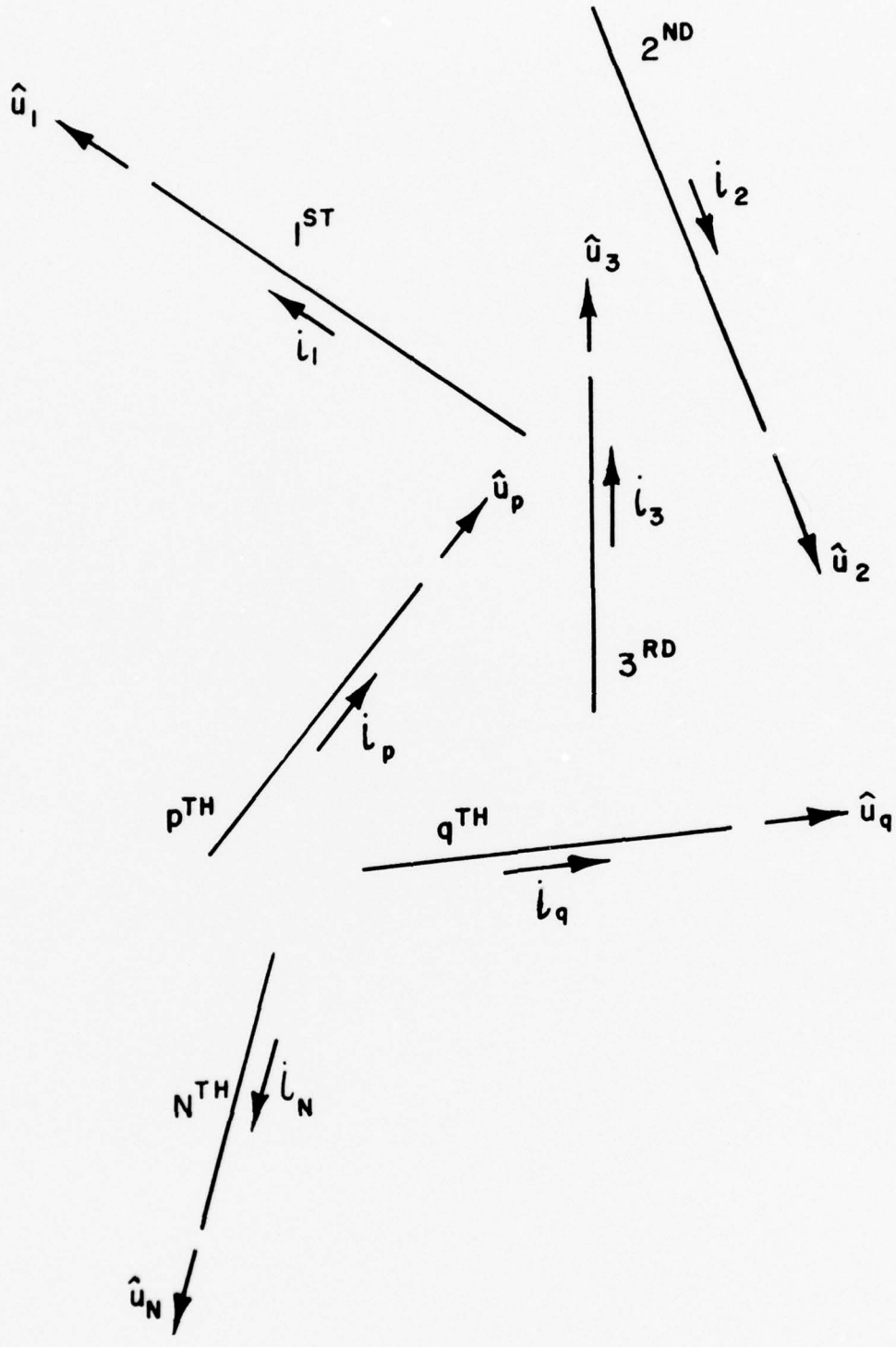

FIG. 3.1 WIRES IN SPACE

all wires, $q=1, 2, \ldots, N (q \neq p)$. Written symbolically, the electric field directed along the axis of the p^{th} wire and evaluated on its surface is

$$E_\zeta(\zeta) = E_{p_\zeta}(\zeta) + \hat{u}_p \cdot \sum_{\substack{q=1 \\ (q \neq p)}}^{N} \bar{E}_q(\zeta) \tag{3.1}$$

where E_ζ is the total axially directed field on the surface of the p^{th} wire produced by all charges and currents on the structure, E_{p_ζ} is that due to the current i_p, and $\bar{E}_q$ is that due to the q^{th} wire. In Eq. (3.1) $\hat{u}_p$ is the unit vector along the p^{th} wire (and has the sense of the current i_p), and ζ is an independent variable denoting axial displacement along $\hat{u}_p$ of the p^{th} wire in a local coordinate system with origin at the center of the p^{th} wire. Fig. 3.2 depicts the two wires and serves to define geometric quantities of interest.*

At a general point in space (x,y,z) one may write E_{p_ζ} in the following form:

$$E_{p_\zeta}(\bar{r}) = -j\omega A_p(\bar{r}) - \frac{\partial}{\partial \zeta} \Phi_p(\bar{r}) \tag{3.2}$$

where A_p and Φ_p are the vector and scalar potentials, respectively, calculated from the sources on the p^{th} wire. Subject to the thin-wire approximations, these potentials may be written

---

*See Appendix III.

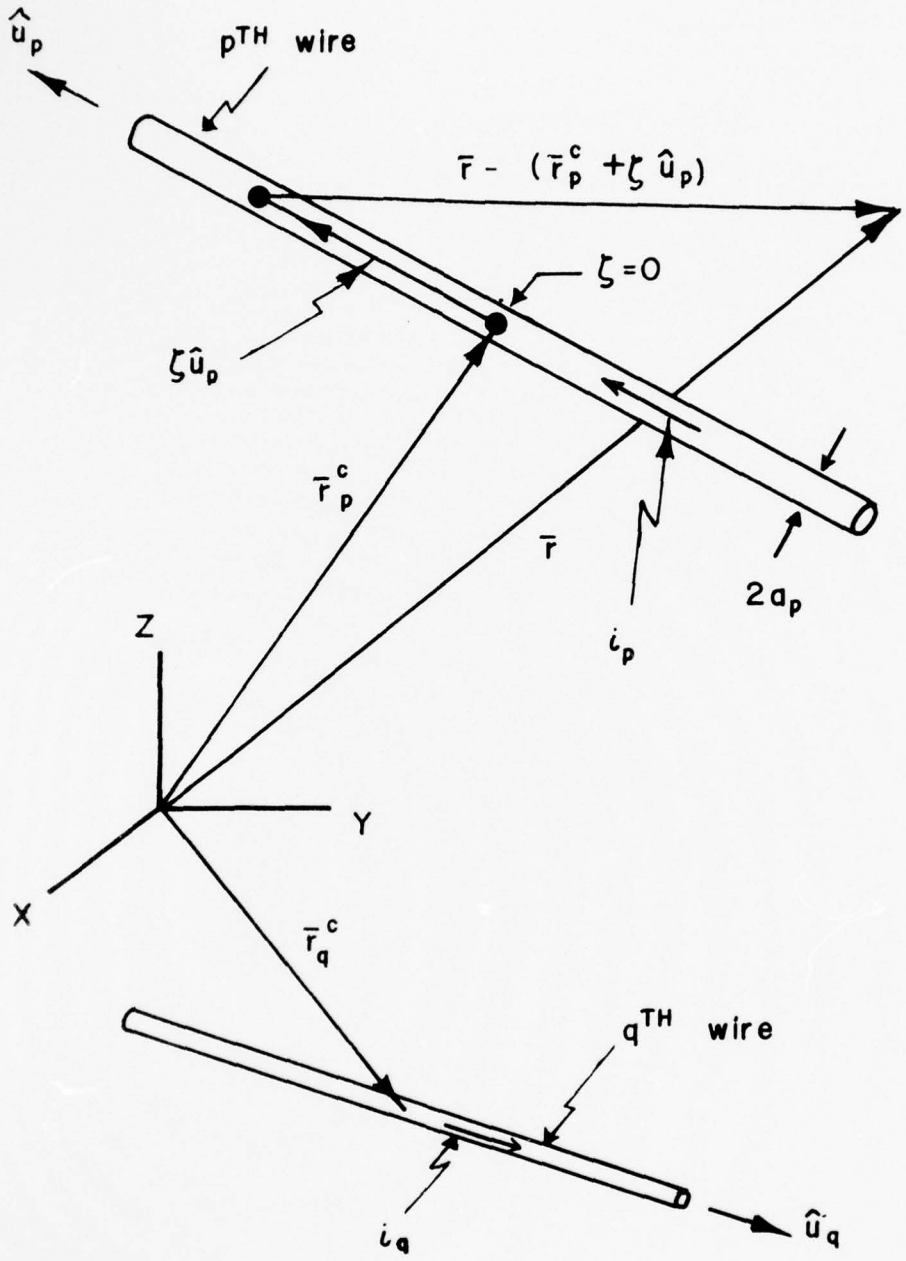

FIG. 3.2 P^{TH} AND Q^{TH} WIRES

$$A_p(\bar{r}) = \frac{\mu}{4\pi} \int_{\zeta'=-L_p/2}^{L_p/2} i_p(\zeta') \frac{e^{-jk|\bar{r}-\bar{r}'_p|}}{|\bar{r}-\bar{r}'_p|} d\zeta' \qquad (3.3a)$$

and

$$\Phi_p(\bar{r}) = \frac{1}{4\pi\varepsilon} \int_{\zeta'=-L_p/2}^{L_p/2} \rho_{\ell_p}(\zeta') \frac{e^{-jk|\bar{r}-\bar{r}'_p|}}{|\bar{r}-\bar{r}'_p|} d\zeta'$$

$$+ \Phi_p^{r+}(\bar{r}) + \Phi_p^{r-}(\bar{r}) \qquad (3.3b)$$

where the general point (x,y,z) is located by

$$\bar{r} = x\hat{u}_x + y\hat{u}_y + z\hat{u}_z \qquad (3.4)$$

and a source point on the p^{th} wire by

$$\bar{r}'_p = \bar{r}^c_p + \zeta'\hat{u}_p \quad . \qquad (3.5)$$

In (3.5), $\bar{r}^c_p$ is a vector which locates* the center of the p^{th} wire so (3.5) itself is simply the equation of a straight line in space along the axis of the p^{th} wire. The linear charge density on the p^{th} wire is denoted ρ_{ℓ_p} and is, of course, related to the p^{th} wire current by the continuity equation,

---

*See Appendix III.

$$\frac{d}{d\zeta} i_p(\zeta) + j\omega\rho_{\ell_p}(\zeta) = 0 \quad . \tag{3.6}$$

In (3.3) the two terms, Φ_q^{r+} and Φ_q^{r-}, represent contributions to the scalar potential from the rings of discrete charge located, respectively, at the upper and lower ends of the p^{th} wire. These charges are present whenever the current is not zero at the ends as is necessary, if the analysis is to be extended to structures involving wires which join at their end-points.

Similarly, the electric field $\bar{E}_q(\bar{r})$ due to sources on the q^{th} wire may be written

$$\bar{E}_q(\bar{r}) = -j\omega A_q(\bar{r})\hat{u}_q - \text{grad } \Phi_q \tag{3.7}$$

where $A_q\hat{u}_q$ and Φ_q are the vector and scalar potentials, respectively, calculated from the sources on the q^{th} wire. A_q and Φ_q can be expressed in terms of potential integrals like those of (3.3) with p replaced by q. The unit vector $\hat{u}_q$ is directed along the q_{th} wire and has the sense of the defined current on this wire.

Since the contributions on the p^{th} wire due to currents on the other wires are all of the form of (3.7), only two wires are treated in general below (Fig.3.3) so that the discussion is not rendered overly complex. The extension to more than two wires is quite direct and can be done readily after the present two-wire case foundation has been established.

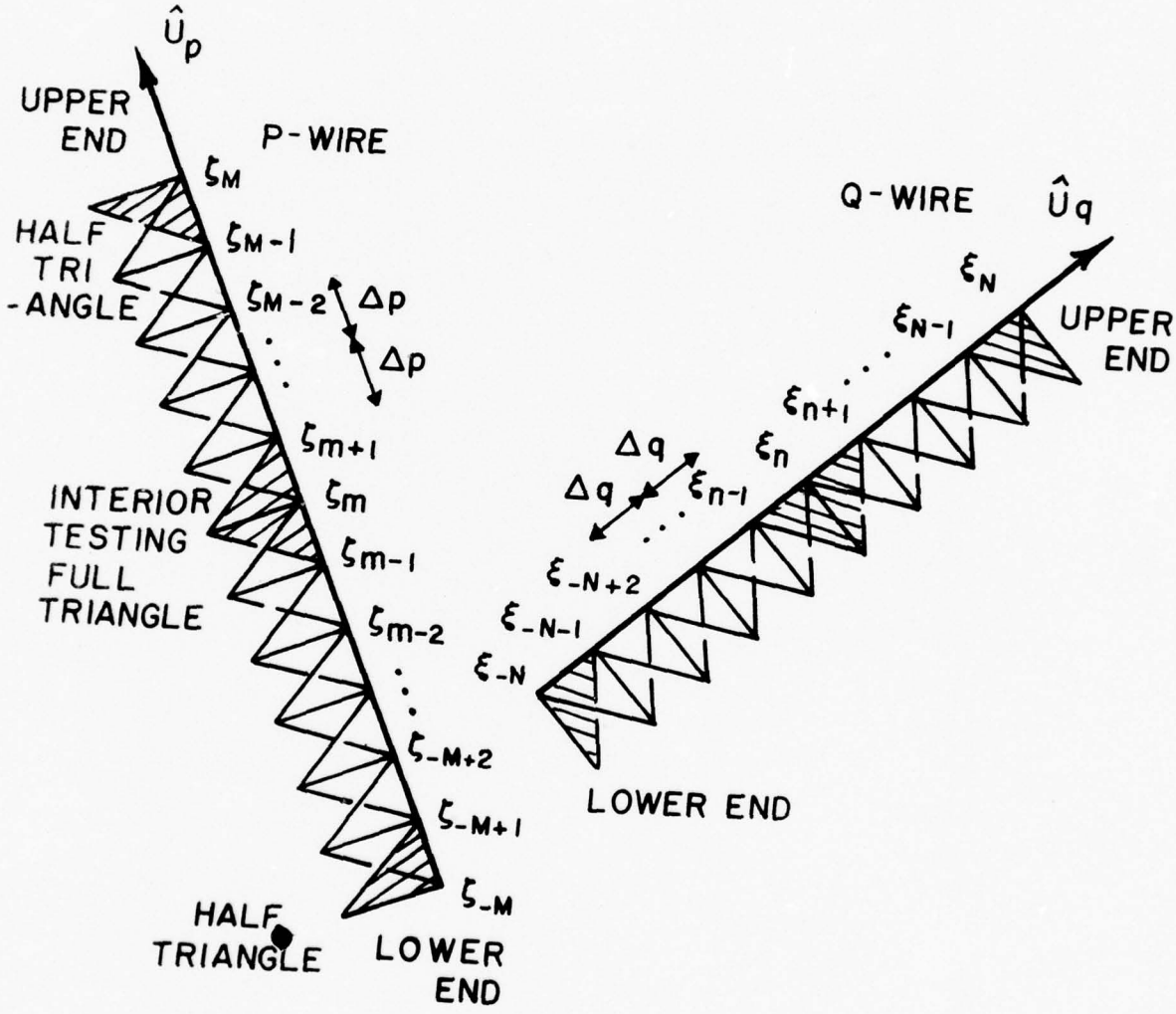

FIG. 3.3. TESTING TRIANGLES ON P^{TH} AND Q^{TH} WIRES

The axially-directed electric field on the surface of the p^{th} wire shown in Fig. 3.2, due to sources on both the p^{th} and q^{th} wires, is

$$E_\zeta = -j\omega A_p - \frac{\partial}{\partial \zeta} \Phi_p$$

$$- j\omega A_q (\hat{u}_q \cdot \hat{u}_p) - \frac{\partial}{\partial \zeta} \Phi_q \quad . \tag{3.8}$$

Retaining Φ_q but employing the Lorentz gauge explicity to eliminate Φ_p one may convert (3.8) to an alternate form:

$$j\frac{k^2}{\omega} E_\zeta(\zeta) = \left(\frac{\partial^2}{\partial \zeta^2} + k^2 \right) A_p(\zeta)$$

$$+ k^2 A_q(\zeta)(\hat{u}_q \cdot \hat{u}_p) - j\frac{k^2}{\omega} \frac{\partial}{\partial \zeta} \Phi_q(\zeta) \quad . \tag{3.9}$$

Actually, the Lorentz gauge is invoked implicity relative to Φ_q, for otherwise the potential integral representation of the scalar potential would be inappropriate; however, in (3.9) the relationship between Φ_q and A_q is not invoked directly. In view of the heterogeneous application above of the relationship between vector and scalar potential under the Lorentz gauge, one must exercise care to avoid violation of the continuity equation, when he calculates Φ_q from the charge on the q^{th} wire. When this wire joins others, as is anticipated by the expression (3.3b), special heed must be given this caution,

and one must recall that explicit application of the Lorentz gauge ensures a complete electric system [1].

3.2 TESTING

As is done above for the isolated wire equations, we seek a set of linear equations by testing with Λ_m^{ℓ} and Λ_m^{s} of (2.6) pursuant to the development of a numerical procedure for performing various calculations on wire structures. As before we distinguish between interior testing and end testing in order that the boundary conditions on wire ends may receive desired attention and may be efficiently incorporated in the numerical solution technique.

Testing of (3.9) with a testing function T_m yields

$$\left\langle \left(\frac{d^2}{d\zeta^2} + k^2 \right) A_p,\ T_m \right\rangle + k^2 (\hat{u}_p \cdot \hat{u}_q) \left\langle A_q,\ T_m \right\rangle$$

$$- j\frac{k^2}{\omega} \left\langle \frac{\partial}{\partial \zeta} \Phi_q,\ T_m \right\rangle = j\frac{k^2}{\omega} \left\langle E_\zeta,\ T_m \right\rangle \qquad (3.10)$$

which, in view of the definition of the scalar product (2.4b) and the subdomain nature of the testing functions to be considered here, can be written

$$\int_{\zeta=\zeta_{m-1}}^{\zeta_{m+1}} \left[\left(\frac{d^2}{d\zeta^2} + k^2\right) A_p(\zeta)\right] T_m(\zeta)\,d\zeta + k^2(\hat{u}_p \cdot \hat{u}_q) \int_{\zeta=\zeta_{m-1}}^{\zeta_{m+1}} A_q(\zeta) T_m(\zeta)\,d\zeta$$

$$-j\frac{k^2}{\omega} \int_{\zeta=\zeta_{m-1}}^{\zeta_{m+1}} \frac{\partial}{\partial\zeta}\Phi_q(\zeta)\, T_m(\zeta)\,d\zeta = j\frac{k^2}{\omega} \int_{\zeta=\zeta_{m-1}}^{\zeta_{m+1}} E_\zeta(\zeta) T_m(\zeta)\,d\zeta \quad . \tag{3.11}$$

As before, in the case of end testing, the limits of the above integrals must be modified; in particular, for testing over the lower interval, $\zeta\varepsilon\ (\zeta_{-M},\zeta_{-M+1})$, the lower and upper limits of each integral are ζ_{-M} and ζ_{-M+1}, respectively, whereas, for testing over the upper interval, $\zeta\varepsilon\ (\zeta_{M-1},\zeta_M)$, the respective lower and upper limits are ζ_{M-1} and ζ_M. Of course, one recognizes that $\zeta_{\pm M} = \pm L_p/2$ and that $\zeta_{\pm(M-1)} = \pm(L_p/2 - \Delta_p)$, where Δ_p is the subdomain interval length defined in Fig. 3.3 .

Interior Testing Making use of the equations in Appendix I, one can perform the operations indicated in (3.11) to achieve the equations resulting from testing with either piecewise linear or piecewise sinusoids over the interior intervals. For piecewise linear testing ($T_m = \Lambda_m^{\ell}$) one obtains Eq. (3.12) and for piecewise sinusoidal testing ($T_m = \Lambda_m^{s}$) he obtains Eq. (3.13), both of which are found on the following page. Eqs. (3.12) and (3.13) are exact in the sense that the testing procedure has introduced no approximations.

Piecewise Linear Testing (Interior)

$$\frac{1}{\Delta_p}\left[A_p(\zeta_{m+1}) - 2A_p(\zeta_m) + A_p(\zeta_{m-1})\right] + k^2\int_{\zeta=\zeta_{m-1}}^{\zeta_{m+1}}\left[A_p(\zeta) + (\hat{u}_p\cdot\hat{u}_q)A_q(\zeta)\right]\Lambda_m^{\ell}(\zeta)d\zeta$$

$$+j\frac{k^2}{\omega\Delta_p}\left[\int_{\zeta=\zeta_{m-1}}^{\zeta_m}\Phi_q(\zeta)d\zeta - \int_{\zeta=\zeta_m}^{\zeta_{m+1}}\Phi_q(\zeta)d\zeta\right] = j\frac{k^2}{\omega}\int_{\zeta=\zeta_{m-1}}^{\zeta_{m+1}}E_\zeta(\zeta)\Lambda_m^{\ell}(\zeta)d\zeta \quad ,$$

$$m = 0, \pm1, \pm2, \ldots, \pm(M-1) \quad . \qquad (3.12)$$

Piecewise Sinusoidal Testing (Interior)

$$\frac{k}{\sin k\Delta_p}\left[A_p(\zeta_{m+1}) - 2\cos k\Delta_p A_p(\zeta_m) + A_p(\zeta_{m-1})\right] + k^2(\hat{u}_p\cdot\hat{u}_q)\int_{\zeta=\zeta_{m-1}}^{\zeta_{m+1}}A_q(\zeta)\Lambda_m^{s}(\zeta)d\zeta$$

$$+j\frac{k^3}{\omega}\left[\int_{\zeta=\zeta_{m-1}}^{\zeta_m}\frac{\cos k(\zeta-\zeta_{m-1})}{\sin k\Delta_p}\Phi_q(\zeta)d\zeta - \int_{\zeta=\zeta_m}^{\zeta_{m+1}}\frac{\cos k(\zeta_{m+1}-\zeta)}{\sin k\Delta_p}\Phi_q(\zeta)d\zeta\right] = j\frac{k^2}{\omega}\int_{\zeta=\zeta_{m-1}}^{\zeta_{m+1}}E_\zeta(\zeta)\Lambda_m^{s}(\zeta)d\zeta \quad ,$$

$$m = 0, \pm1, \pm2, \ldots, \pm(M-1) \quad , \qquad (3.13)$$

End Testing In end testing we consider both Eq. (3.8) and Eq. (3.9) and test with each of the functions $\Lambda^{s}_{\pm M}$ and $\Lambda^{\ell}_{\pm M}$. Of course, these equations are equivalent and either may be used in any wire analysis, or they both may be employed in a mixed fashion. Testing Eq. (3.8) by means of $\Lambda^{\ell}_{\pm M}$ over the upper and lower end intervals yields (3.14a) and (3.14b), respectively, and end testing (3.8) with $\Lambda^{s}_{\pm M}$ yields (3.15a) and (3.15b). Similarly, testing Eq. (3.9) with $\Lambda^{\ell}_{\pm M}$ over the upper and lower end intervals yields (3.16a) and (3.16b), respectively, while end testing of (3.9) with $\Lambda^{s}_{\pm M}$ gives rise to (3.17a) and (3.17b). One should note that, in all end testing cases mentioned here, the scalar product defined in (2.4b) is employed. The limits on the right-hand-side integral in (2.4b) applied to the present case would be $-L_p/2$ and $+L_p/2$, which reduce end testing to integration over only one-half of the domains of the testing functions, $\Lambda^{\ell}_{\pm M}$ or $\Lambda^{s}_{\pm M}$; this is the reason that end testing is treated apart from interior testing.

Piecewise Linear End Testing (Case I - Testing of (3.8))

Upper End:

$$-j\omega \int_{\zeta=\zeta_{M-1}}^{\zeta_M} \left[A_p(\zeta) + \hat{u}_p \cdot \hat{u}_q A_q(\zeta) \right] \Lambda_M^{\ell}(\zeta) d\zeta - \left[\Phi_p(\zeta_M) + \Phi_q(\zeta_M) \right] + \frac{1}{\Delta_p} \int_{\zeta=\zeta_{M-1}}^{\zeta_M} \left[\Phi_p(\zeta) + \Phi_q(\zeta) \right] d\zeta$$

$$= \int_{\zeta=\zeta_{M-1}}^{\zeta_M} E_\zeta(\zeta) \Lambda_M^{\ell}(\zeta) d\zeta \qquad (3.14a)$$

Lower End:

$$-j\omega \int_{\zeta=\zeta_{-M}}^{\zeta_{-M+1}} \left[A_p(\zeta) + \hat{u}_p \cdot \hat{u}_q A_q(\zeta) \right] \Lambda_{-M}^{\ell}(\zeta) d\zeta + \left[\Phi_p(\zeta_{-M}) + \Phi_q(\zeta_{-M}) \right] - \frac{1}{\Delta_p} \int_{\zeta=\zeta_{-M}}^{\zeta_{-M+1}} \left[\Phi_p(\zeta) + \Phi_q(\zeta) \right] d\zeta$$

$$= \int_{\zeta=\zeta_{-M}}^{\zeta_{-M+1}} E_\zeta(\zeta) \Lambda_{-M}^{\ell}(\zeta) d\zeta \qquad (3.14b)$$

Piecewise Sinusoidal End Testing (Case I - Testing of (3.8))

Upper End:

$$-j\omega \int_{\zeta=\zeta_{M-1}}^{\zeta_M} \left[A_p(\zeta) + \hat{u}_p \cdot \hat{u}_q A_q(\zeta) \right] \Lambda_M^s(\zeta) d\zeta - \left[\Phi_p(\zeta_M) + \Phi_q(\zeta_M) \right] + k \int_{\zeta=\zeta_{M-1}}^{\zeta_M} \frac{\cos k(\zeta-\zeta_{M-1})}{\sin k\Delta_p} \left[\Phi_p(\zeta) + \Phi_q(\zeta) \right] d\zeta$$

$$= \int_{\zeta=\zeta_{M-1}}^{\zeta_M} E_\zeta(\zeta) \Lambda_M^s(\zeta) d\zeta \qquad (3.15a)$$

Lower End:

$$-j\omega \int_{\zeta=\zeta_{-M}}^{\zeta_{-M+1}} \left[A_p(\zeta) + \hat{u}_p \cdot \hat{u}_q A_q(\zeta) \right] \Lambda_{-M}^s(\zeta) d\zeta + \left[\Phi_p(\zeta_{-M}) + \Phi_q(\zeta_{-M}) \right] - k \int_{\zeta=\zeta_{-M}}^{\zeta_{-M+1}} \frac{\cos k(\zeta_{-M+1}-\zeta)}{\sin k\Delta_p} \left[\Phi_p(\zeta) + \Phi_q(\zeta) \right] d\zeta$$

$$= \int_{\zeta=\zeta_{-M}}^{\zeta_{-M+1}} E_\zeta(\zeta) \Lambda_{-M}^s(\zeta) d\zeta \qquad (3.15b)$$

Piecewise Linear End Testing (Case II - Testing of (3.9))

Upper End:

$$-j\frac{k^2}{\omega}\,\Phi_p(\zeta_M) - \frac{1}{\Delta_p}\,A_p(\zeta_M) + \frac{1}{\Delta_p}\,A_p(\zeta_{M-1}) + k^2\int_{\zeta=\zeta_{M-1}}^{\zeta_M}\left[A_p(\zeta) + \hat{u}_p\cdot\hat{u}_q A_q(\zeta)\right]\Lambda_M^{\ell}(\zeta)\,d\zeta$$

$$-j\frac{k^2}{\omega}\,\Phi_q(\zeta_M) + j\frac{k^2}{\omega\Delta_p}\int_{\zeta=\zeta_{M-1}}^{\zeta_M}\Phi_q(\zeta)\,d\zeta = j\frac{k^2}{\omega}\int_{\zeta=\zeta_{M-1}}^{\zeta_M} E_\zeta(\zeta)\Lambda_M^{\ell}(\zeta)\,d\zeta \qquad (3.16a)$$

Lower End:

$$+j\frac{k^2}{\omega}\,\Phi_p(\zeta_{-M}) - \frac{1}{\Delta_p}\,A_p(\zeta_{-M}) + \frac{1}{\Delta_p}\,A_p(\zeta_{-M+1}) + k^2\int_{\zeta=\zeta_{-M}}^{\zeta_{-M+1}}\left[A_p(\zeta) + \hat{u}_p\cdot\hat{u}_q A_q(\zeta)\right]\Lambda_{-M}^{\ell}(\zeta)\,d\zeta$$

$$+j\frac{k^2}{\omega}\,\Phi_q(\zeta_{-M}) - j\frac{k^2}{\omega\Delta_p}\int_{\zeta=\zeta_{-M}}^{\zeta_{-M+1}}\Phi_q(\zeta)\,d\zeta = j\frac{k^2}{\omega}\int_{\zeta=\zeta_{-M}}^{\zeta_{-M+1}} E_\zeta(\zeta)\Lambda_{-M}^{\ell}(\zeta)\,d\zeta \qquad (3.16b)$$

Piecewise Sinusoidal End Testing (Case II - Testing of (3.9))

Upper End:

$$-j\frac{k^2}{\omega}\,\Phi_p(\zeta_M) - k\,\frac{\cos k\Delta_p}{\sin k\Delta_p}\,A_p(\zeta_M) + \frac{k}{\sin k\Delta_p}\,A_p(\zeta_{M-1}) + k^2(\hat{u}_p\cdot\hat{u}_q)\int_{\zeta=\zeta_{M-1}}^{\zeta_M} A_q(\zeta)\Lambda_M^s(\zeta)\,d\zeta$$

$$-j\frac{k^2}{\omega}\,\Phi_q(\zeta_M) + j\frac{k^3}{\omega}\int_{\zeta=\zeta_{M-1}}^{\zeta_M}\frac{\cos k(\zeta-\zeta_{M-1})}{\sin k\Delta_p}\,\Phi_q(\zeta)\,d\zeta = j\frac{k^2}{\omega}\int_{\zeta=\zeta_{M-1}}^{\zeta_M} E_\zeta(\zeta)\Lambda_M^s(\zeta)\,d\zeta \qquad (3.17a)$$

Lower End:

$$+j\frac{k^2}{\omega}\,\Phi_p(\zeta_{-M}) - k\,\frac{\cos k\Delta_p}{\sin k\Delta_p}\,A_p(\zeta_{-M}) + \frac{k}{\sin k\Delta_p}\,A_p(\zeta_{-M+1}) + k^2(\hat{u}_p\cdot\hat{u}_q)\int_{\zeta=\zeta_{-M}}^{\zeta_{-M+1}} A_q(\zeta)\Lambda_{-M}^s(\zeta)\,d\zeta$$

$$+j\frac{k^2}{\omega}\,\Phi_q(\zeta_{-M}) - j\frac{k^3}{\omega}\int_{\zeta=\zeta_{-M}}^{\zeta_{-M+1}}\frac{\cos k(\zeta_{-M+1}-\zeta)}{\sin k\Delta_p}\,\Phi_q(\zeta)\,d\zeta = j\frac{k^2}{\omega}\int_{\zeta=\zeta_{-M}}^{\zeta_{-M+1}} E_\zeta(\zeta)\Lambda_{-M}^s(\zeta)\,d\zeta \qquad (3.17b)$$

3.3 APPROXIMATIONS

As was the case in the analysis of the isolated wire of Chapter 2, there are good approximations which can be used to advantage to significantly simplify the present expressions. The integral approximations,

$$\int_{\zeta=\zeta_{-M}}^{\zeta_{-M+1}} f(\zeta)\Lambda_{-M}^{\ell,s}(\zeta)d\zeta \doteq \frac{1}{2}\,\Delta_p f(\zeta_{-M}) \tag{3.18a}$$

and

$$\int_{\zeta=\zeta_{M-1}}^{\zeta_{M}} f(\zeta)\Lambda_{M}^{\ell,s}(\zeta)d\zeta \doteq \frac{1}{2}\,\Delta_p f(\zeta_{M}) \tag{3.18b}$$

are good whenever $f(\zeta)$ is smooth over the lower end interval in the case of (3.18a) and over the upper end interval in the case of (3.18b). These approximations, (2.15) and (3.18), are applied in (3.12) - (3.17) to integrals containing the electric field E_ζ and vector potential terms, A_p and A_q, and one thereby arrives at the following corresponding approximate equations (see following pages).

Piecewise Linear Testing with Approximations (Interior)

$$\frac{1}{\Delta_p}\left[A_p(\zeta_{m+1}) - 2\left(1 - \frac{k^2\Delta_p^2}{2}\right)A_p(\zeta_m) + A_p(\zeta_{m-1})\right] + k^2(\hat{u}_p\cdot\hat{u}_q)\Delta_p A_q(\zeta_m)$$

$$+j\frac{k^2}{\omega\Delta_p}\left[\int_{\zeta=\zeta_{m-1}}^{\zeta_m}\Phi_q(\zeta)d\zeta - \int_{\zeta=\zeta_m}^{\zeta_{m+1}}\Phi_q(\zeta)d\zeta\right] = j\frac{k^2}{\omega}\Delta_p E_\zeta(\zeta_m) \quad ,$$

$$m=0, \pm1, \pm2, \ldots, (M-1) \qquad (3.19)$$

Piecewise Sinusoidal Testing with Approximations (Interior)

$$\frac{k}{\sin k\Delta_p}\left[A_p(\zeta_{m+1}) - 2\cos k\Delta_p A_p(\zeta_m) + A_p(\zeta_{m-1})\right] + k^2(\hat{u}_p\cdot\hat{u}_q)\Delta_p A_q(\zeta_m)$$

$$+j\frac{k^3}{\omega}\left[\int_{\zeta=\zeta_{m-1}}^{\zeta_m}\frac{\cos k(\zeta-\zeta_{m-1})}{\sin k\Delta_p}\Phi_q(\zeta)d\zeta - \int_{\zeta=\zeta_m}^{\zeta_{m+1}}\frac{\cos k(\zeta_{m+1}-\zeta)}{\sin k\Delta_p}\Phi_q(\zeta)d\zeta\right] = j\frac{k^2}{\omega}\Delta_p E_\zeta(\zeta_m) \quad ,$$

$$m=0, \pm1, \pm2, \ldots, (M-1) \qquad (3.20)$$

Piecewise Linear End Testing with Approximation (Case I - Testing of (3.8))

Upper End:

$$-j\omega \frac{\Delta_p}{2}\left[A_p(\zeta_M) + (\hat{u}_p\cdot\hat{u}_q)A_q(\zeta_M)\right] - \left[\Phi_p(\zeta_M) + \Phi_q(\zeta_M)\right] + \frac{1}{\Delta_p}\int_{\zeta=\zeta_{M-1}}^{\zeta_M}\left[\Phi_p(\zeta) + \Phi_q(\zeta)\right]d\zeta$$

$$= \frac{\Delta_p}{2} E_\zeta(\zeta_M) \qquad (3.21a)$$

Lower End:

$$-j\omega \frac{\Delta_p}{2}\left[A_p(\zeta_{-M}) + (\hat{u}_p\cdot\hat{u}_q)A_q(\zeta_{-M})\right] + \left[\Phi_p(\zeta_{-M}) + \Phi_q(\zeta_{-M})\right] - \frac{1}{\Delta_p}\int_{\zeta=\zeta_{-M}}^{\zeta_{-M+1}}\left[\Phi_p(\zeta) + \Phi_q(\zeta)\right]d\zeta$$

$$= \frac{\Delta_p}{2} E_\zeta(\zeta_{-M}) \qquad (3.21b)$$

Piecewise Sinusoidal End Testing with Approximation (Case I - Testing of (3.8))

Upper End:

$$-j\omega \frac{\Delta_p}{2}\left[A_p(\zeta_M) + (\hat{u}_p\cdot\hat{u}_q)A_q(\zeta_M)\right] - \left[\Phi_p(\zeta_M) + \Phi_q(\zeta_M)\right] + k\int_{\zeta=\zeta_{M-1}}^{\zeta_M} \frac{\cos k(\zeta-\zeta_{M-1})}{\sin k\Delta_p}\left[\Phi_p(\zeta) + \Phi_q(\zeta)\right]d\zeta$$

$$= \frac{\Delta_p}{2} E_\zeta(\zeta_M) \qquad (3.22a)$$

Lower End:

$$-j\omega \frac{\Delta_p}{2}\left[A_p(\zeta_{-M}) + (\hat{u}_p\cdot\hat{u}_q)A_q(\zeta_{-M})\right] + \left[\Phi_p(\zeta_{-M}) + \Phi_q(\zeta_{-M})\right] - k\int_{\zeta=\zeta_{-M}}^{\zeta_{-M+1}} \frac{\cos k(\zeta_{-M+1}-\zeta)}{\sin k\Delta_p}\left[\Phi_p(\zeta) + \Phi_q(\zeta)\right]d\zeta$$

$$= \frac{\Delta_p}{2} E_\zeta(\zeta_{-M}) \qquad (3.22b)$$

Other approximations may be made in the present analysis but they are of a type whose error depends on parameters in the calculations being performed. For example, if the derivative of a function $\frac{\partial}{\partial \zeta} f(\zeta)$ is sufficiently smooth over the range of integration indicated below, one may employ the approximations,

$$\int_{\zeta=\zeta_{m-1}}^{\zeta_{m+1}} \frac{\partial}{\partial \zeta} f(\zeta)\ \Lambda_m^{\ell,s}(\zeta)\,d\zeta \doteq \Delta_p \frac{\partial}{\partial \zeta} f(\zeta_m) \quad , \tag{3.23a}$$

$$\int_{\zeta=\zeta_{M-1}}^{\zeta_M} \frac{\partial}{\partial \zeta} f(\zeta)\ \Lambda_M^{\ell,s}(\zeta)\,d\zeta \doteq \frac{\Delta_p}{2} \frac{\partial}{\partial \zeta} f(\zeta_M) \quad , \tag{3.23b}$$

and

$$\int_{\zeta=\zeta_{-M}}^{\zeta_{-M+1}} \frac{\partial}{\partial \zeta} f(\zeta)\ \Lambda_{-M}^{\ell,s}(\zeta)\,d\zeta \doteq \frac{\Delta_p}{2} \frac{\partial}{\partial \zeta} f(\zeta_{-M}) \ . \tag{3.23c}$$

Approximations (3.23) may be applied to terms like the third in(3.11) involving Φ_q to arrive at simpler expressions than those appearing in (3.12) - (3.22). Such approximations are of acceptable accuracy only when $\frac{\partial}{\partial \zeta} \Phi_q$ is sufficiently smooth over the range of integration of the pertinent expression (3.23); $\frac{\partial}{\partial \zeta} \Phi_q$ is smooth enough for (3.23) to apply in

situations where Φ_p is the scalar potential due to an element of current remote (in terms of wavelength) from the interval over which one of the approximations (3.23) is to be employed.

3.4 USE OF PIECEWISE LINEAR TESTING IN NUMERICAL SOLUTION PROCEDURE FOR DETERMINATION OF CURRENT ON SCATTERER COMPRISING TWO COUPLED WIRES

In this section is outlined the theory for calculating currents on a two-wire scatterer illuminated by a specified incident field. So that explanations are not overly complicated, attention here is limited to two wires but the technique is general and can be applied, with little or no modification, to structures of many wires. Pulses are used for representing the current even though other basis sets can be employed, if desirous.

As is done in Chapter 2 for the straight wire, we first approximate the current on each of the two wires by

$$i_p(z) = \sum_{n=-N_p}^{N_p} I_n^p i_n(z) \tag{3.24a}$$

and

$$i_q(z) = \sum_{n=-N_q}^{N_p} I_n^q i_n(z) \tag{3.24b}$$

where $(2N_p+1)$ and $(2N_q+1)$ are the numbers of terms in the approximation for i_p and i_q, respectively. Next the approxima-

tion (3.24a) is substituted into Equations (3.3) and (3.24b), into a similar pair for A_q and Φ_q. With the currents in the potential integrals replaced by (3.24), A_p, Φ_p, A_q, and Φ_q are employed in the selected tested equations--either (3.19) and (3.21) or (3.20) and (3.22)-- which sequence of steps establishes a system of linear equations having many of the features of (2.21). In this study of two wires, and subsequent treatments of multiple wires, the wire currents are approximated by pulses, and piecewise linear functions are used for testing (Equations (3.19) and (3.21)).

In preparation for writing (3.19) and (3.21) as functions of the I_n^p's and I_n^q's, it is desirable to develop expressions for the vector and scalar potential terms appearing in these two equations. The vector potential A_p on the p^{th} wire, due to current i_p on that wire, differs from the corresponding quantity in Chapter 2 only in that contributions from the end half-pulses must be included. One can readily show that at a point ζ_m on the p^{th} wire (in the local coordinates of the p^{th} wire with origin at its center)

$$A_p(\zeta_m) = \frac{\mu}{4\pi}\left\{ I^p_{-N_p}\int_{\zeta'=0}^{\Delta_p/2} K(\Delta_p[m+N_p]-\zeta')\,d\zeta' + \sum_{n=-(N_p-1)}^{N_p-1} I^p_n \int_{\zeta'=-\Delta_p/2}^{\Delta_p/2} K(\Delta_p[m-n]+\zeta')\,d\zeta' + I^p_{N_p}\int_{\zeta'=0}^{\Delta_p/2} K(\Delta_p[m-N_p]+\zeta')\,d\zeta' \right\} \qquad (3.25)$$

where the first and last integrals are contributions from the lower-and upper-end half-pulses, respectively, and where

$$\zeta_m = m\Delta_p,\ m=0,\ \pm1,\ \pm2,\ldots\ . \qquad (3.26)$$

The scalar potential on the p^{th} wire due to the charge on this wire can be calculated with the aid of Fig. 3.4 and Appendix II. As suggested in Fig. 3.4, associated with the n^{th} current pulse of strength I^p_n is a ring charge at $\zeta_n-\Delta_p/2$ having total charge $-I^p_n/j\omega$ and another at $\zeta_n+\Delta_p/2$ having total charge $+I^p_n/j\omega$. The total quantities of charge of the ring charges deposited by the lower-end pulse are $+I^p_{-N_p}/j\omega$ at $-L_p/2$ and $-I^p_{-N_p}/j\omega$ at $-L_p/2+\Delta_p/2$ and those deposited by the upper-end pulse are $-I^p_{N_p}/j\omega$ at $L_p/2-\Delta_p/2$ and $I^p_{N_p}/j\omega$ at $L_p/2$. Therefore, the scalar potential

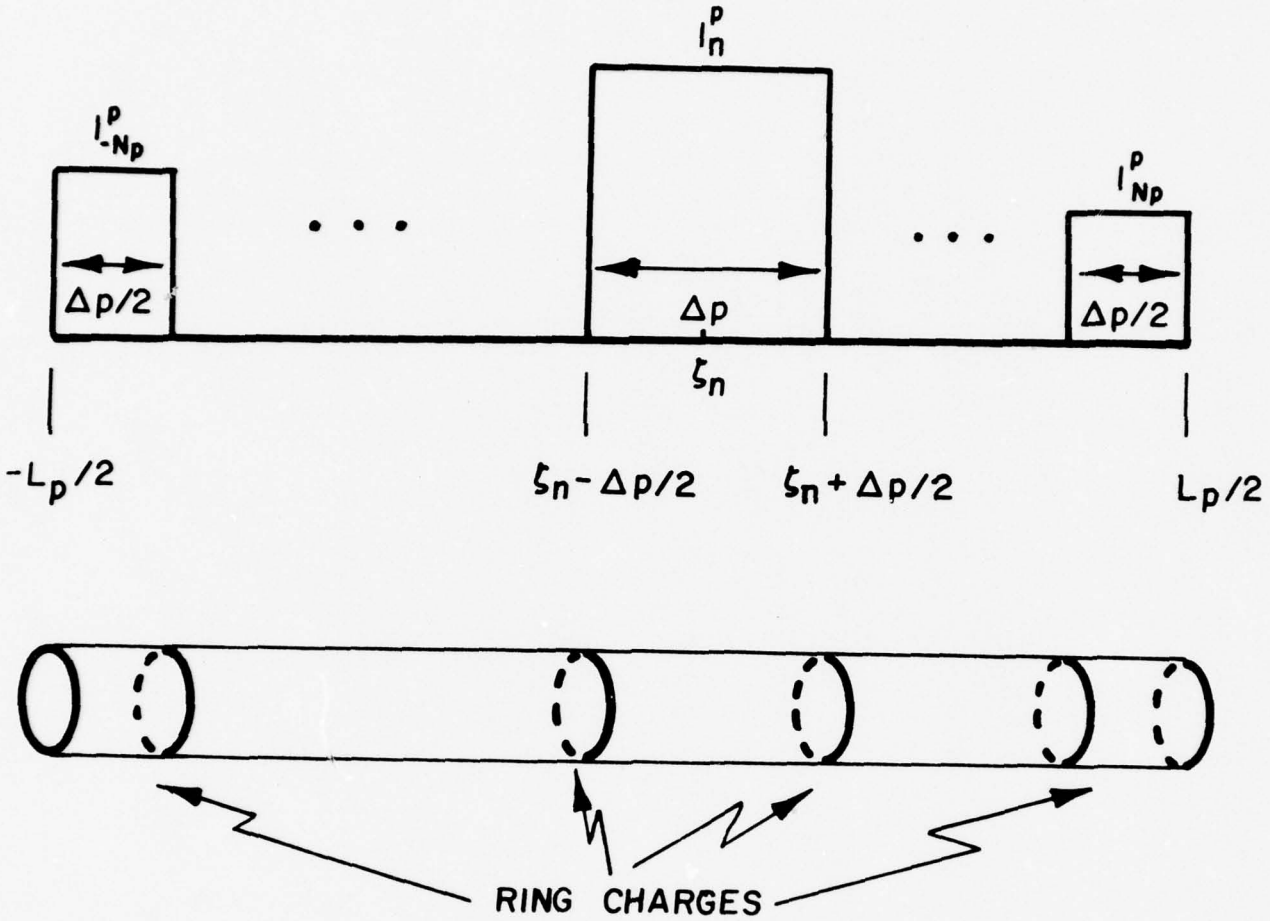

FIG. 3.4. PULSE CURRENTS AND RING CHARGES ON P^{TH} WIRE

at a location ζ on the p^{th} wire due to its own charges is

$$\Phi_p(\zeta) = \frac{1}{j4\pi\omega\varepsilon}\left\{ I^p_{-N_p}\left[K(\zeta+\Delta_p[N_p-\tfrac{1}{2}]) - K(\zeta+\Delta_p N_p)\right] \right.$$

$$+\sum_{n=-(N_p-1)}^{N_p-1} I^p_n\left[K(\zeta-\Delta_p[n+\tfrac{1}{2}]) - K(\zeta-\Delta_p[n-\tfrac{1}{2}])\right]$$

$$\left. + I^p_{N_p}\left[K(\zeta-\Delta_p N_p) - K(\zeta-\Delta_p[N_p-\tfrac{1}{2}])\right]\right\} . \qquad (3.27)$$

Equations (3.25) and (3.27) provide a means of displaying the dependence of quantities bearing subscript p upon I^p_n in (3.19) and (3.2). Quantities bearing subscript q in these two equations are next written with explicit dependence upon I^q_n. Involved in each such quantity is the distance from an appropriate source point on the q^{th} wire to a field point on the surface of the p^{th} wire. This distance D_{pq} is derived in Appendix III where geometric quantities are defined and discussed in detail:

$$D_{pq}(\zeta,\zeta') = \left[a_p^2 + \left|(\bar{r}^c_p+\zeta\hat{u}_p) - (\bar{r}^c_q+\zeta'\hat{u}_q)\right|^2\right]^{\frac{1}{2}} \qquad (3.28)$$

The vector potential A_q at a point ζ_m on the p^{th} wire due to the current (3.24b) on the q^{th} wire is

$$A_q(\zeta_m) = \frac{\mu}{4\pi}\left\{ I^q_{-N_q} \int_{\zeta'=-N_q\Delta_q}^{-(N_q-\frac{1}{2})\Delta_q} G_{pq}(\zeta_m,\zeta')\,d\zeta' \right.$$

$$+ \sum_{n=-(N_q-1)}^{N_q-1} I^q_n \int_{\zeta'=(n-\frac{1}{2})\Delta_q}^{(n+\frac{1}{2})\Delta_q} G_{pq}(\zeta_m,\zeta')\,d\zeta'$$

$$\left. + I^q_{N_q} \int_{\zeta'=(N_q-\frac{1}{2})\Delta_q}^{N_q\Delta_q} G_{pq}(\zeta_m,\zeta')\,d\zeta' \right\} \qquad (3.29)$$

where

$$G_{pq}(\zeta,\zeta') = \frac{e^{-jkD_{pq}(\zeta,\zeta')}}{D_{pq}(\zeta,\zeta')} \quad . \qquad (3.30)$$

The scalar potential Φ_q is formulated in a manner similar to that leading to (3.27) but with the kernel (3.30) playing the role of the usual straight-wire kernel. Using (II-7) of Appendix II, one can show that

$$\Phi_q(\zeta) = \frac{1}{j4\pi\omega\varepsilon}\left\{ I^q_{-N_q}\left[G_{pq}(\zeta, [-N_q+\tfrac{1}{2}]\Delta_q) - G_{pq}(\zeta, -N_q\Delta_q)\right]\right.$$

$$+\sum_{n=-(N_q-1)}^{N_q-1} I^q_n\left[G_{pq}(\zeta, [n+\tfrac{1}{2}]\Delta_q) - G_{pq}(\zeta, [n-\tfrac{1}{2}]\Delta_q)\right]$$

$$\left. + I^q_{N_q}\left[G_{pq}(\zeta, N_q\Delta_q) - G(\zeta, [N_q-\tfrac{1}{2}]\Delta_q)\right]\right\}. \qquad (3.31)$$

Linear System of Equations With A_p of (3.25) and Φ_p of (3.27) written in terms of the unknown coefficients I^p_n's and, also, with A_q of (3.29) and Φ_q of (3.31) written in terms of the I^q_n's, one substitutes these vector and scalar potential quantities into the tested equations (3.19) and (3.21). As a result, with $M=N_p$, one has a system of linear algebraic equations like (2.21),

$$\sum_{n=-N_p}^{N_p} I^p_n S_{mn} + \sum_{n=-N_q}^{N_q} I^q_n C_{mn} = V_m \quad ,$$

$$m=0, \pm1, \pm2, \pm, \ldots, \pm N_p, \qquad (3.32)$$

which is a system of $2N_p+1$ equations in $2(N_p+N_q+1)$ unknowns.

The coefficients S_{mn} are called "self terms" and represent the entries in (3.19) and (3.21), subject to replacement of quantities by their equivalents in (3.25) and (3.27), which

are coefficients of the currents I_n^p. $S_{-N_p,n}$ and $S_{N_p,n}$ are coefficients* of I_n^p, $n=-N_p,\ldots,0,\ldots,N_p$, in (3.21a) and (3.21b), respectively. S_{mn} is the coefficient of I_n^p in (3.19), $m=-(N_p-1),\ldots,0,\ldots,N_p-1$. The coefficients C_{mn} in (3.32) are called "coupling terms" since they are associated with contributions from the current on the q^{th} wire to vector and scalar potential quantities evaluated on the p^{th} wire. These coefficients may be readily identified, if one substitutes (3.29) and (3.31) into (3.19) and (3.21). $C_{-N_p,n}$ and $C_{N_p,n}$, $n=-N_q,\ldots,0,\ldots,N_q$, are coefficients of I_n^q in (3.21a) and (3.21b), respectively, while $C_{m,n}$, $m=-(N_p-1),\ldots,0,\ldots,N_p-1$, is the coefficient of I_n^q in (3.19). In other words, the S_{mn}'s account for contributions to vector and scalar potential at locations along the p^{th} wire from the individual elements of the basis set representing i_p, whereas the C_{mn}'s account for contributions on the p^{th} wire due to elements of the basis set by means of which i_q is approximated.

The inhomogeneous or driving terms V_m's, $m=-N_p,\ldots,0,\ldots,N_p$, are

$$V_{-N_p} = -\frac{\Delta_p}{2}\,\tilde{E}^i(\zeta_{-N_p})\cdot\hat{u}_p \quad , \tag{3.33a}$$

---

*Commas are used to separate subscripts when their being in juxtaposition may lead to misinterpretation; S_{mn} and $S_{m,n}$ are to be looked upon as the same.

$$V_m = -\Delta_p \, \bar{E}^i(\zeta_m)\cdot\hat{u}_p \quad ,$$

$$m=-(N_p-1),\ldots,N_p-1 \qquad (3.33b)$$

and

$$V_{N_p} = -\frac{\Delta_p}{2} \, \bar{E}^i(\zeta_{N_p})\cdot\hat{u}_p \quad , \qquad (3.33c)$$

which are the right-hand side terms in (3.19) and (3.21) with $E_\zeta(\zeta_m)$ replaced by $-\bar{E}^i(\zeta_m)\cdot\hat{u}_p$ so that boundary conditions on the surface of the wire are enforced. In the case of an antenna problem, the modification explained in Section 2.8 is utilized.

The system of equations (3.32) is general in the senses that the p^{th} wire and the q^{th} wire may be any pair in a complex wire structure and that their relative orientation is completely arbitrary (Appendix III). To facilitate subsequent discussions we write (3.32) as a matrix equation,

$$[S_p]\,[I^p] + [C_p^q]\,[I^q] = [V_p] \quad , \qquad (3.34)$$

and define the individual matrices below.

$$[S_p] = \begin{bmatrix} S_{-N_p,-N_p} & \cdots & S_{-N_p,n} & \cdots & S_{-N_p,N_p} \\ \vdots & & \vdots & & \vdots \\ S_{m,-N_p} & & S_{m,n} & & S_{m,N_p} \\ \vdots & & \vdots & & \vdots \\ S_{N_p,-N_p} & \cdots & S_{N_p,n} & \cdots & S_{N_p,N_p} \end{bmatrix} \tag{3.35a}$$

$$[C_p^q] = \begin{bmatrix} C_{-N_p,-N_q} & \cdots & C_{-N_p,n} & \cdots & C_{-N_p,N_q} \\ \vdots & & \vdots & & \vdots \\ C_{m,-N_q} & & C_{m,n} & & C_{m,N_q} \\ \vdots & & \vdots & & \vdots \\ C_{N_p,-N_q} & \cdots & C_{N_p,n} & \cdots & C_{N_p,N_q} \end{bmatrix} \tag{3.35b}$$

$$[I^p] = \begin{bmatrix} I^p_{-N_p} \\ \cdot \\ \cdot \\ \cdot \\ I^p_n \\ \cdot \\ \cdot \\ \cdot \\ I^p_{N_p} \end{bmatrix} \qquad (3.35c)$$

$$[I^q] = \begin{bmatrix} I^q_{-N_q} \\ \cdot \\ \cdot \\ \cdot \\ I^q_n \\ \cdot \\ \cdot \\ \cdot \\ I^q_{N_q} \end{bmatrix} \qquad (3.35d)$$

$$[V_p] = \begin{bmatrix} V_{-N_p} \\ \cdot \\ \cdot \\ \cdot \\ V_m \\ \cdot \\ \cdot \\ \cdot \\ V_{N_p} \end{bmatrix} \qquad (3.35e)$$

The subscript p on the matrices, $[S_p]$, $[C_p^q]$, and $[V_p]$, implies that each of these is associated with evaluation of quantities on the p^{th} wire. The superscript p on $[I^p]$ identifies this matrix as the column vector of current coefficients, I_n^p's, in the expansion of i_p on the p^{th} wire; similarly, $[I^q]$ is the vector of coefficients in the approximation of i_q. The superscript q on $[C_p^q]$ denotes that this is a matrix of coupling terms indicating a contribution from the q^{th} wire current.

Equation (3.32), or its matrix equivalent (3.34), serves to enforce the boundary condition that the axial electric field on the p^{th} wire be zero. Of course, this boundary condition must be satisfied on all wires in a given structure, and (3.32) and (3.34) are totally general so that, by a mere change of subscripts and superscripts, one has available the needed equations to enforce this boundary condition on other wires. For example, if two wires which are located and oriented in

some specified way (Appendix III), are illuminated by an incident field, the entire problem can be characterized by the pair of matrix equations:

$$[S_p]\,[I^p] + [C_p^q]\,[I^q] = [V_p]\ , \tag{3.36a}$$

$$[C_q^p]\,[I^p] + [S_q]\,[I^q] = [V_q]\ . \tag{3.36b}$$

These suggest that the wires are designated p^{th} and q^{th} and (3.36a) is recognized to be (3.34); (3.36b) is the companion equation whose matrix elements are determined from the same procedure used to calculate those in(3.36a) (with indices interchanged). If there were a third wire designated the w^{th} wire in the problem under consideration, the appropriate equations would be

$$[S_p]\,[I^p] + [C_p^q]\,[I^q] + [C_p^w]\,[I^w] = [V_p]$$

$$[C_q^p]\,[I^p] + [S^q]\,[I^q] + [C_q^w]\,[I^w] = [V_q]$$

$$[C_w^p]\,[I^p] + [C_w^q]\,[I^q] + [S^w]\,[I^w] = [V_w]$$

or, as a single matrix equation,

$$\begin{bmatrix} [S_p] & [C_p^q] & [C_p^w] \\ [C_q^p] & [S_q] & [C_q^w] \\ [C_w^p] & [C_w^q] & [S_w] \end{bmatrix} \begin{bmatrix} [I^p] \\ [I^q] \\ [I^w] \end{bmatrix} = \begin{bmatrix} [V_p] \\ [V_q] \\ [V_w] \end{bmatrix}\ . \tag{3.37}$$

Wires Not Joined If the wires in a structure under study are not in electrical contact, the current at the free wire ends must be zero. Therefore, the coefficients of the end current pulses, i.e., I^p_{-N} and I^p_N for the p^{th} wire, are made equal to zero (actually discarded from the set of unknown coefficients). Discarding these upper- and lower-end coefficients reduces the number of unknowns so one in turn discards the equations in the system of linear equations (3.37) which correspond to end testing.

If, for example, the wires in the two-wire problem characterized by (3.36) are not joined electrically, one would set $I^p_{-N_p}$, $I^p_{N_p}$, $I^q_{-N_p}$, and $I^q_{N_q}$ equal to zero. Also, he would delete those equations resulting from end testing. That is, the following matrix elements would be deleted: $S_{-N_p,n}$, $S_{N_p,n}$, $C_{-N_q,n}$, and $C_{N_q,n}$, $n=-N_p,\ldots,0,\ldots,N_p$; $S_{-N_q,n}$, $S_{N_q,n}$, $C_{-N_p,n}$, and $C_{N_p,n}$, $n=-N_q,\ldots,0,\ldots,N_q$; and V_{-N_p}, V_{N_p}, V_{-N_q}, and V_{N_q}. After these deletions, the resulting linear system would contain $2(N_p+N_q-1)$ equations and, of course, the same number of unknowns.

Two Wires Joined As an example of a simple wire structure having a junction, we consider the two wires illustrated in Fig. 3.5 where one sees that the upper end of the p^{th} wire joins the lower end of the q^{th} wire. Of course at the free ends, lower end of the p^{th} wire and upper end of the q^{th},

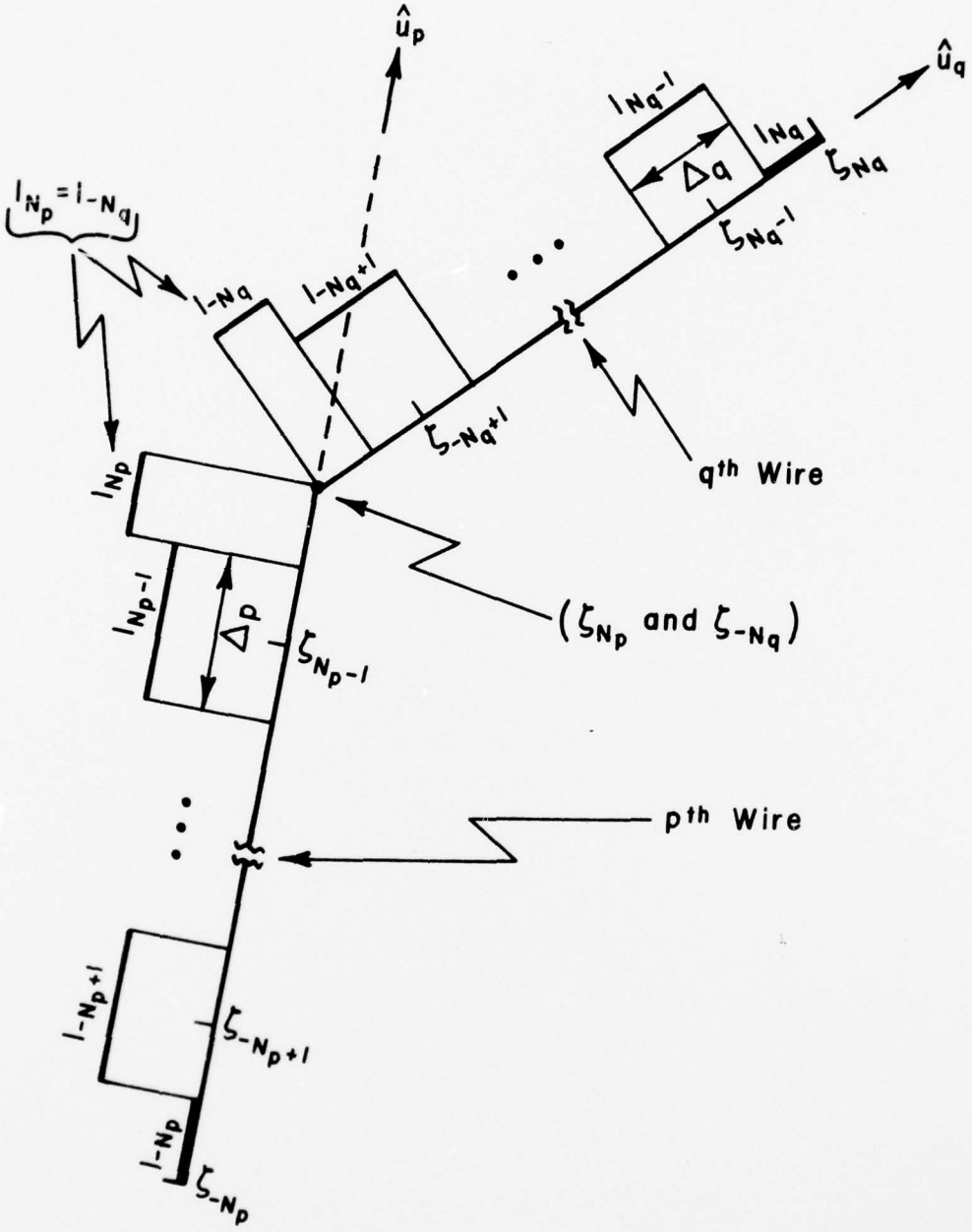

FIG. 3.5. TWO WIRES JOINED

the half-pulse currents are set equal to zero, and the matrix equation is modified, as described above, to be consistent with $I^p_{-N_p} = I^p_{N_q} = 0$. Next, since the current must be continuous at the junction, one requires that $I^p_{N_p}$ be equal to $I^q_{-N_q}$, which, of course, reduces the number of unknowns in the system of equations by one, thereby requiring further modification of the matrix equations (3.36).

With $I^p_{N_p} = I^q_{-N_q} = I^{pq}_J$ (junction current), the columns below both operate on I_J (recall $S_{-N_p,n}$, $C_{-N_p,n}$, $S_{N_q,n}$, $C_{N_q,n}$ are zero--deleted from matrix--to account for $I^p_{-N_p} = I^q_{N_q} = 0$ at the free ends):

$$\begin{bmatrix} S_{-N_p+1,N_p} \\ \vdots \\ S_{N_p,N_p} \\ C_{-N_q,N_p} \\ \vdots \\ C_{N_q-1,N_p} \end{bmatrix} \qquad (3.38a)\ , \qquad \begin{bmatrix} C_{-N_p+1,-N_q} \\ \vdots \\ C_{N_p,-N_q} \\ S_{-N_q,-N_q} \\ \vdots \\ S_{N_q-1,-N_q} \end{bmatrix} \qquad (3.38b)$$

Hence the above two columns are added to reduce the number of columns by one. Next the number of rows must be reduced by one too. Reduction of the number of rows by one is achieved by adding the N_p^{th} and $-N_q^{th}$ rows on both sides of the equation. The summed row on the left-hand side is

$$\left[S_{N_p,-N_p+1} + C_{-N_q,-N_p+1} \quad . \quad . \quad . \right.$$

$$S_{N_p,N_p} + C_{N_p,-N_q} + C_{-N_q,N_p} + S_{-N_q,-N_q}$$

$$\left. . \quad . \quad . \quad C_{N_p,N_q-1} + S_{-N_q,N_q-1} \right] \tag{3.39}$$

while that on the right-hand side is simply

$$\left[V_{N_p} + V_{-N_q} \right] . \tag{3.40}$$

The center entry in (3.39) comprises four terms because these terms are members of the summed column vectors (3.38) as well as of the summed row vectors.

As an alternative to the first step in the modification described above, one may elect to append to the system (3.36) an additional equation enforcing continuity of current at the junction, $I_{N_p}=I_{-N_q}$, rather than to add the column vectors (3.38). Of course, the second step of adding rows must be done regardless of how the current continuity is handled.

With the matrix modifications discussed above, the resulting linear system of equations possesses the same number of equations and unknowns, and, therefore, one may employ standard methods to determine the unknown current coefficients, I_n^p's and I_n^q's.

Sample Results As examples of the utility of the coupled thin-wire theory and numerical techniques outlined in this Chapter, calculated currents on bent-wire (joined) scatterers are presented in Figs. 3.6, 3.7, and 3.8. Wire configuration and dimensions, as well as excitation, are indicated in the figures, and, where available, results from other calculations are provided for comparison.

Extensive data calculated by means of the theory given in Chapters 2 and 3 can be found in Chapter 4.

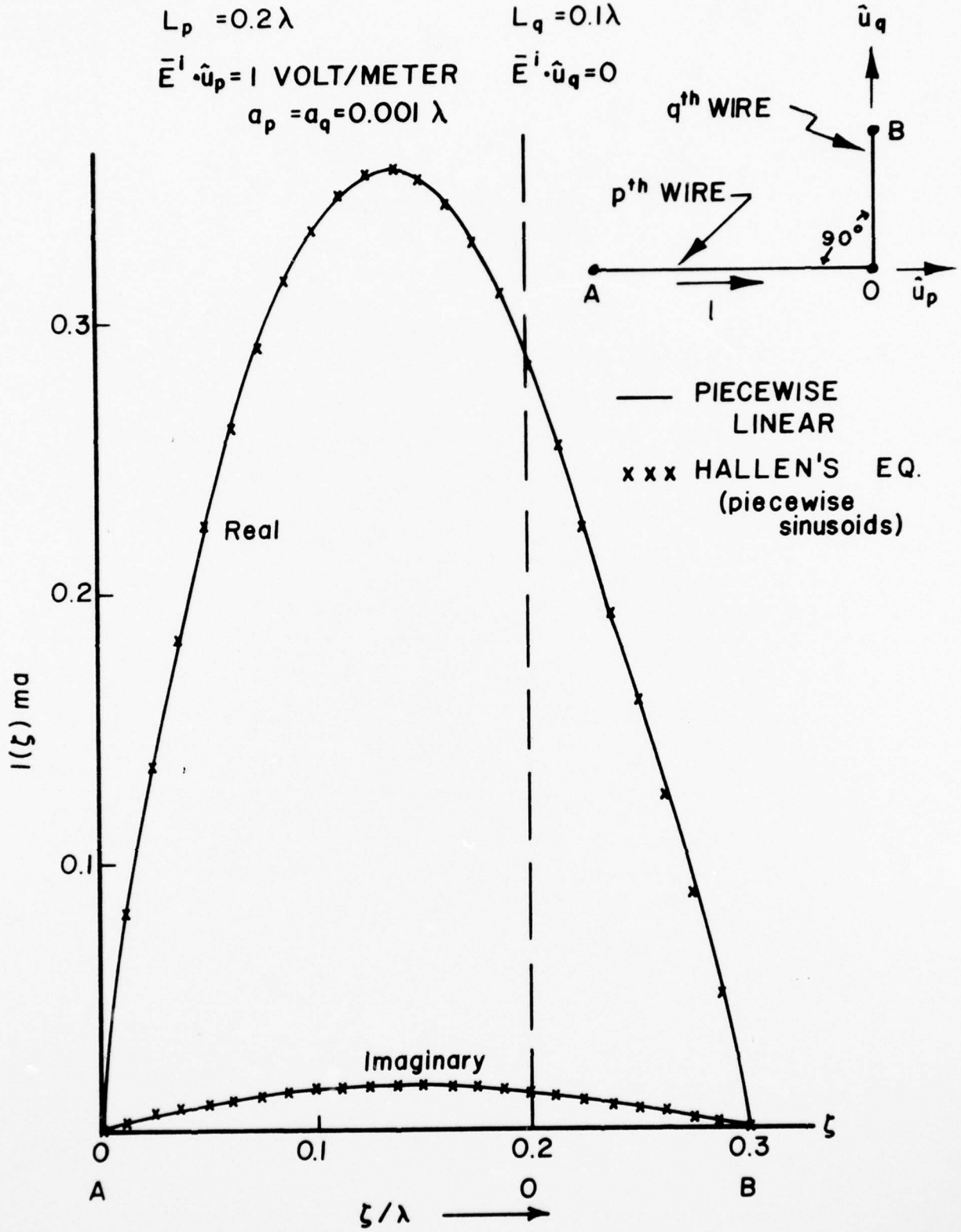

FIG. 3.6. CURRENTS INDUCED ON L-WIRE SCATTERER

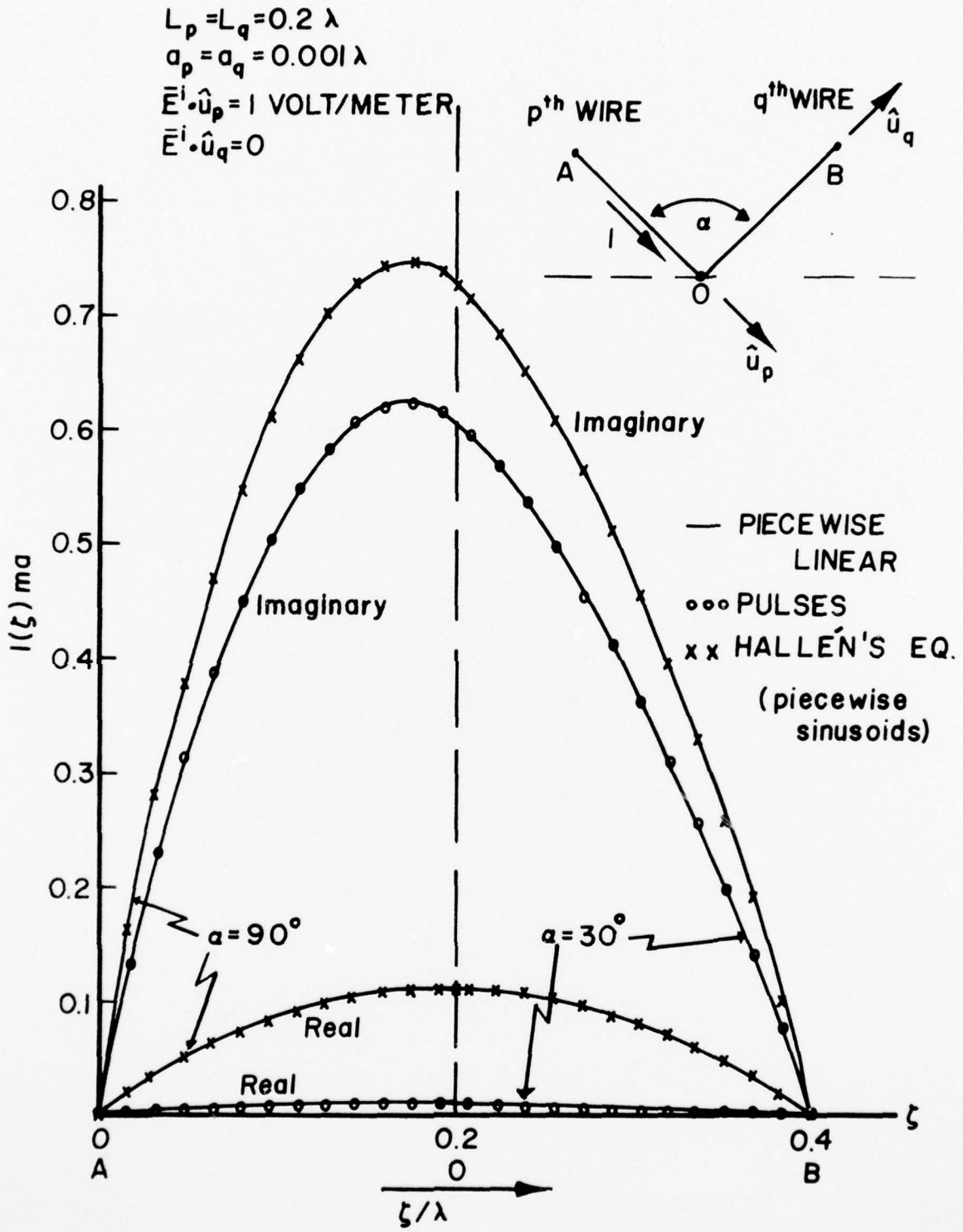

FIG. 3.7. CURRENTS INDUCED ON BENT-WIRE SCATTERER

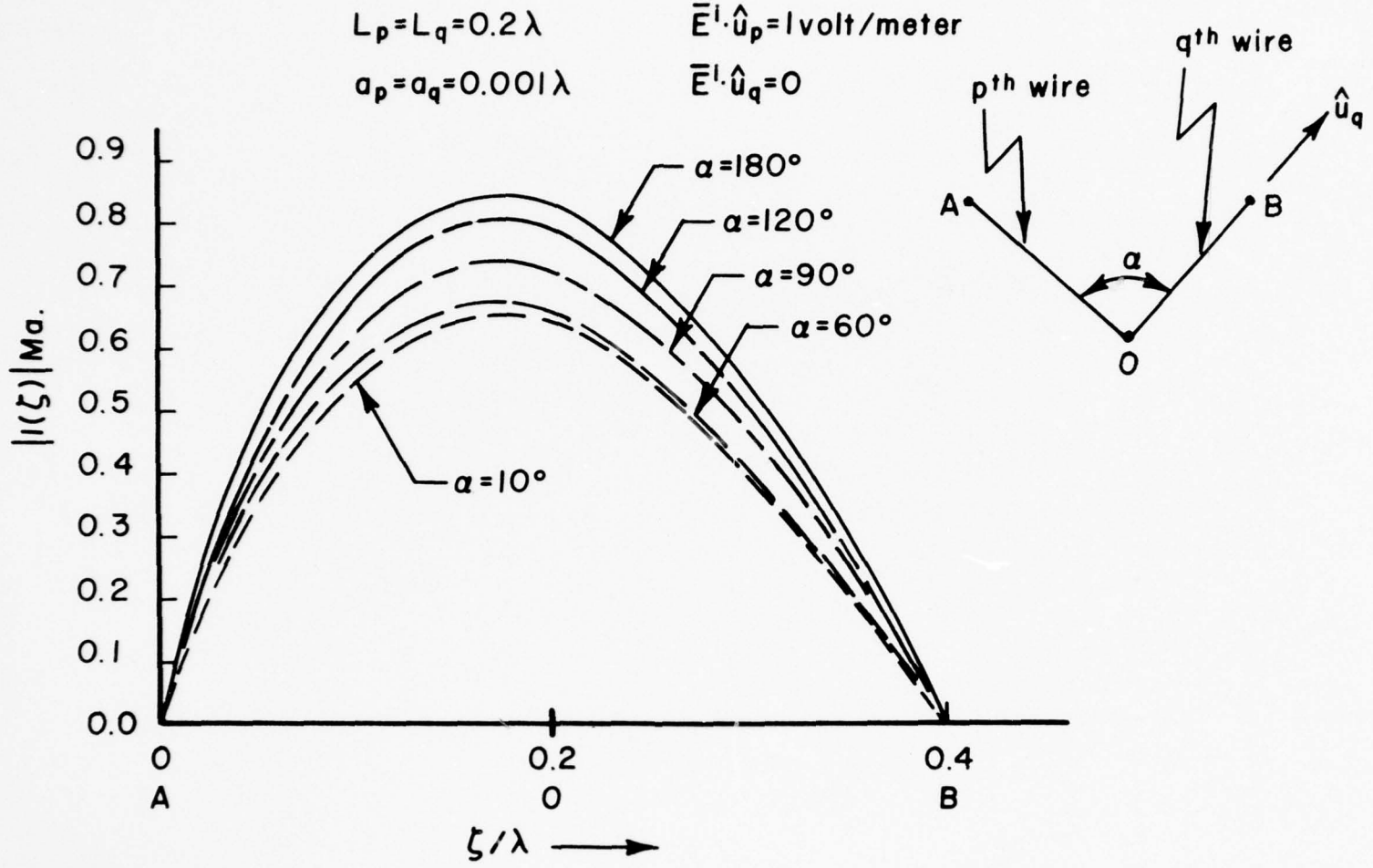

FIG. 3.8. DEPENDENCE OF CURRENT ON BENT-WIRE SCATTERER ON BEND ANGLE

REFERENCES

1. King, R.W.P., Fundamental Electromagnetic Theory, Dover Publication, New York; 1963.

CHAPTER 4

APPLICATION TO WIRE BICONICAL ANTENNA STRUCTURES

4.1 MATRIX EQUATIONS AND SYMMETRY

The coupled integral equations formulated in Chapter 3, along with either piecewise linear testing or piecewise sinusoidal testing, leads one to generalized equations (3.12) to (3.15) for analysis of wire structures. Since the pulse basis set is easy to incorporate and is as powerful as any other set, only the pulses are used in the following application to biconical antennas. Sample results, viz., the current distribution, input impedance at the feed point, and the far electric field radiation pattern, are presented for a wire biconical antenna in free space or above a ground plane in various orientations. From the developments in Chapter 3, a self matrix $[S_p^p]$ and a mutual coupling matrix $[C_p^q]$ are established for two arbitrarily oriented wires, p^{th} and q^{th}, either joined at one end or not. For the case of a biconical antenna above a ground plane, Fig. 4.1, or a biconical antenna in free space, Fig. 4.2, the following partitioned matrix equation of eight by eight is obtained,

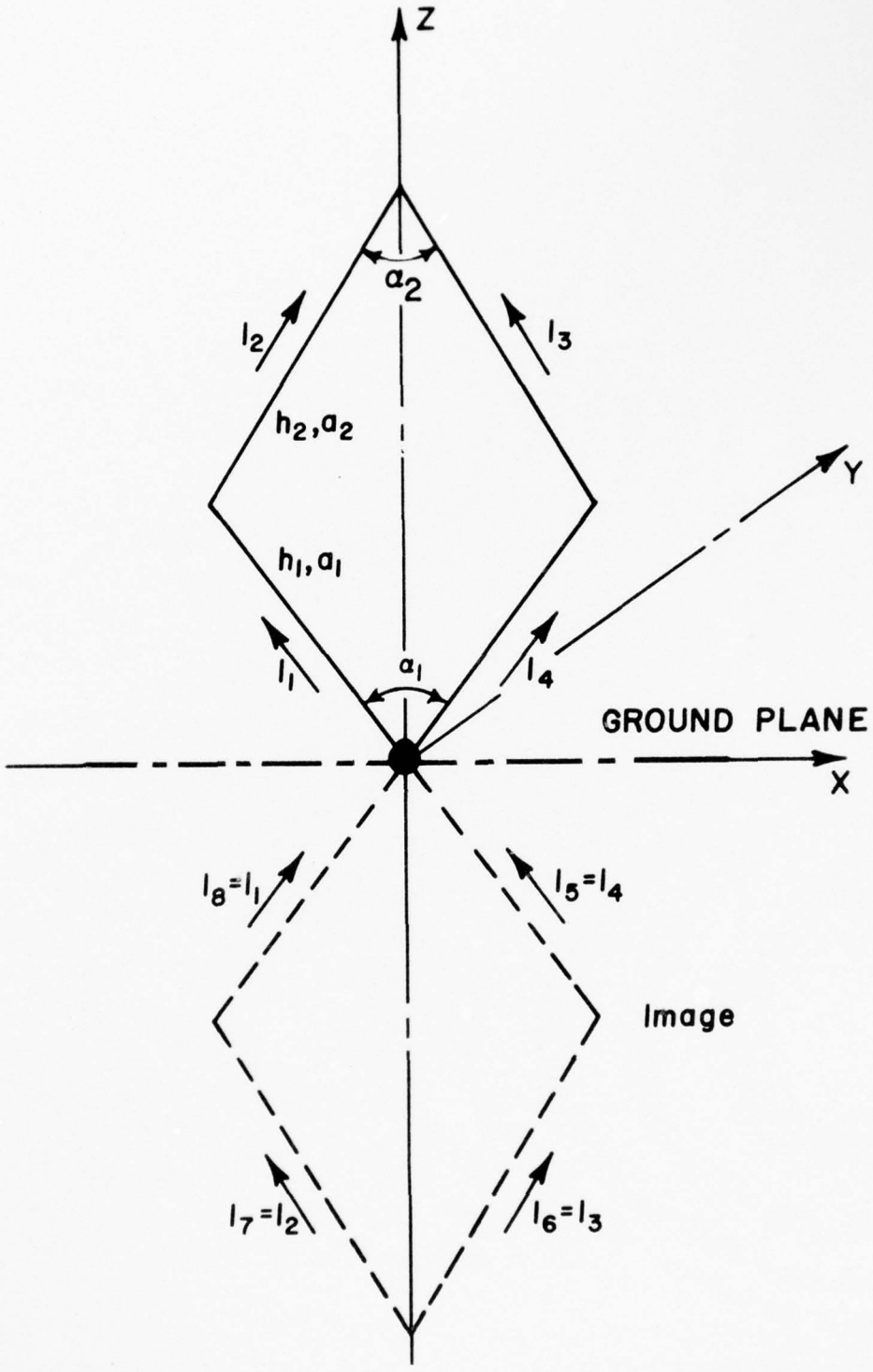

FIG. 4.1. VERTICAL WIRE BICONICAL ANTENNA ABOVE GROUND

AD-A040 477 MISSISSIPPI UNIV UNIVERSITY DEPT OF ELECTRICAL ENGIN--ETC F/G 9/5
THEORETICAL ANALYSIS OF THE WIRE BICONICAL ANTENNA.(U)
JAN 75 C M BUTLER, K R UMASHANKAR, C E SMITH DAEA18-74-C-0173

UNCLASSIFIED

NL

2 OF 2
AD A040477

END

DATE FILMED
7-77

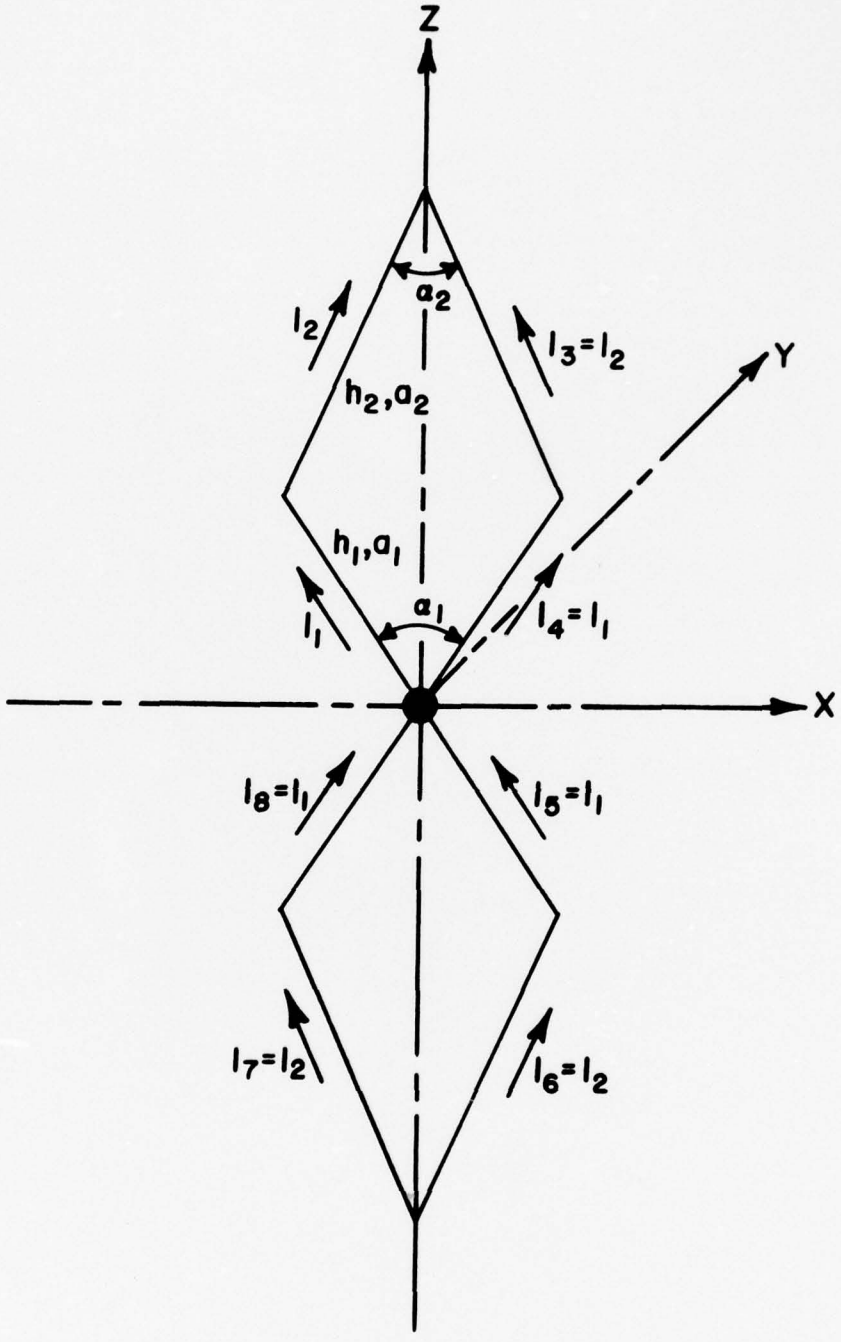

FIG. 4.2. WIRE BICONICAL ANTENNA IN FREE SPACE

$$\begin{bmatrix} [S_1^1] & [C_1^2] & [C_1^3] & [C_1^4] & \cdot & [C_1^8] \\ [C_2^1] & [S_2^2] & [C_2^3] & [C_2^4] & \cdot & [C_2^8] \\ \cdot & \cdot & \cdot & & \cdot & \cdot \\ \cdot & \cdot & \cdot & [S_p^p] \; [C_p^q] & & \cdot \\ \cdot & \cdot & \cdot & & \cdot & \cdot \\ [C_8^1] & [C_8^2] & [C_8^3] & [C_8^4] & \cdot & [S_8^8] \end{bmatrix} \begin{bmatrix} [I^1] \\ [I^2] \\ \cdot \\ [I^p] \\ \cdot \\ [I^8] \end{bmatrix} = \begin{bmatrix} [V_1] \\ [V_2] \\ \cdot \\ [V_p] \\ \cdot \\ [V_8] \end{bmatrix} \qquad (4.1)$$

where $[I^1]$, $[I^2]$, $[I^3]$,...,$[I^8]$ are partitioned column vectors representing the unknown current coefficients on the first, second, ...,eighth wires, and $[V_1]$, $[V_2]$, ... are the corresponding excitation column vectors defined by (3.35).

The self and the mutual coupling partitioned matrices, $[S_p^p]$ and $[C_p^q]$, result from piecewise linear testing on the p^{th} wire and account for contributions from the currents on p^{th} and q^{th} wires, respectively. *Due to the various symmetries** in the orientation of the wires and in the location of the feed point at the center of the structure, $[I^5] = [I^4]$, $[I^6] = [I^3]$, $[I^7] = [I^2]$ and $[I^8] = [I^1]$. The bottom half of the matrix can be generated using top-half matrix elements in the reverse order. Hence, deleting the bottom half of the partitioned matrix (4.1), one needs to generate only the top half of (4.1):

---

*These column vectors are equal subject to appropriate ordering of the elements in the columns.

$$\begin{bmatrix} [S_1^1] & [C_1^2] & [C_1^3] & [C_1^4] & [C_1^5] & \cdot & [C_1^8] \\ [C_2^1] & [S_2^2] & [C_2^3] & \cdot & \cdot & \cdot & [C_2^8] \\ [C_3^1] & [C_3^2] & [S_3^3] & \cdot & \cdot & \cdot & [C_3^8] \\ [C_4^1] & [C_4^2] & [C_4^3] & \cdot & \cdot & \cdot & [C_4^8] \end{bmatrix} \begin{bmatrix} [I^1] \\ [I^2] \\ [I^3] \\ [I^4] \end{bmatrix} = \begin{bmatrix} [V_1] \\ [V_2] \\ [V_3] \\ [V_4] \end{bmatrix} \tag{4.2}$$

Due to the symmetry in the currents as stated above, the partitioned matrix equation (4.2) can be folded and written as

$$\begin{bmatrix} [S_1^1+C_1^8] & [C_1^2+C_1^7] & [C_1^3+C_1^6] & [C_1^4+C_1^5] \\ [C_2^1+C_2^8] & [S_2^2+C_2^7] & [C_2^3+C_2^6] & [C_2^4+C_2^5] \\ [C_3^1+C_3^8] & [C_3^2+C_3^7] & [S_3^3+C_3^6] & [C_3^4+C_3^5] \\ [C_4^1+C_4^8] & [C_4^2+C_4^7] & [C_4^3+C_4^6] & [S_4^4+C_4^5] \end{bmatrix} \begin{bmatrix} [I^1] \\ [I^2] \\ [I^3] \\ [I^4] \end{bmatrix} = \begin{bmatrix} [V_1] \\ [V_2] \\ [V_3] \\ [V_4] \end{bmatrix} \tag{4.3}$$

The partitioned matrix equation (4.3) is a square matrix of four by four and can be solved for the unknown current vectors $[I^1]$, $[I^2]$, $[I^3]$, and $[I^4]$. This compact matrix form is equivalent to successive modifications of the kernel functions in the integral equations (3.12) and (3.14). Such are possible because of the symmetry in the distribution of the currents with respect to the feed point. We further note $[I^4] = [I^1]$ and $[I^3] = [I^2]$ because the wire geometry is identical about its vertical axis. Hence, one has to solve for only unknown current vectors $[I^1]$ and $[I^2]$. Also, one may delete the third

and fourths rows of (4.3) and fold the resulting matrix equation of two by four into a compact partitioned matrix equation of two by two:

$$\begin{bmatrix} \{[S_1^1+C_1^8] + [C_1^4+C_1^5]\} & \{[C_1^2+C_1^7] + [C_1^3+C_1^6]\} \\ \{[C_2^1+C_2^8] + [C_2^4+C_2^5]\} & \{[S_2^2+C_2^7] + [C_2^3+C_2^6]\} \end{bmatrix} \begin{bmatrix} [I^1] \\ [I^2] \end{bmatrix} = \begin{bmatrix} [V_1] \\ [V_2] \end{bmatrix} . \tag{4.4}$$

The above procedure can be conveniently applied to the cases of biconical wire antennas placed perpendicular to the ground plane, Fig. 4.3, and parallel to the ground plane, Fig. 4.4. The direction and symmetries in the distribution of the current in the corresponding image structures are shown in the respective figures. The partitioned matrix equation (4.1) applies to these two cases of biconical antennas perpendicular and parallel to a ground plane with a new definition for the matrix terms,

$$[C_p^q] = [C_p^q] + [C_p^q]^i , \tag{4.5}$$

where the partitioned matrix $[C_p^q]$ is the algebraic sum of two submatrices obtained for a particular element and its corresponding image element. With the new definition for the matrix terms in (4.1), step by step matrices can be folded and (4.3) can be solved for the case of a biconical antenna structure placed perpendicular to the ground plane. Similarly, (4.4) can be solved for the case of biconical antenna structure placed parallel to the ground plane.

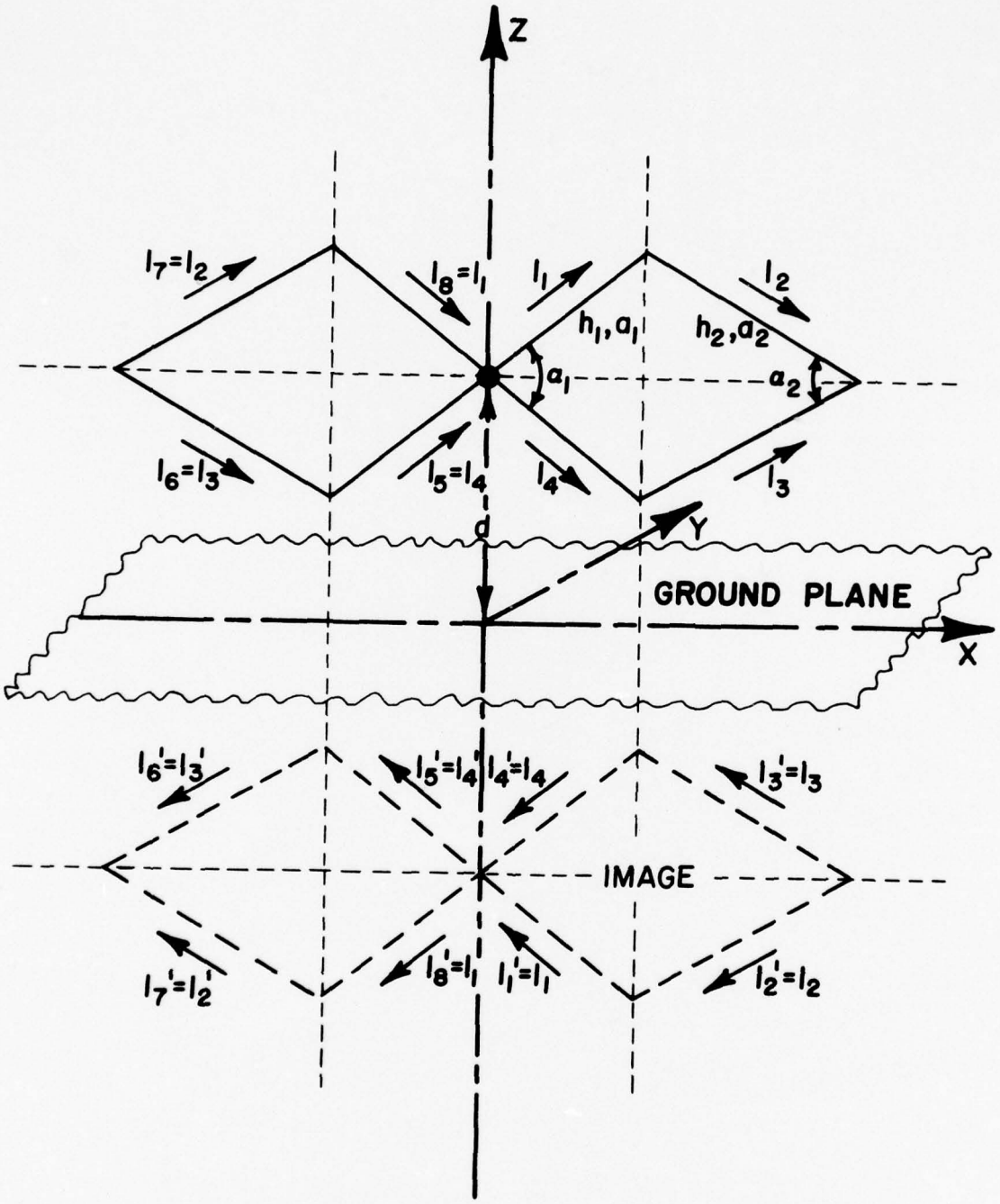

FIG. 4.3. WIRE BICONICAL ANTENNA ABOVE AND PERPENDICULAR TO GROUND PLANE

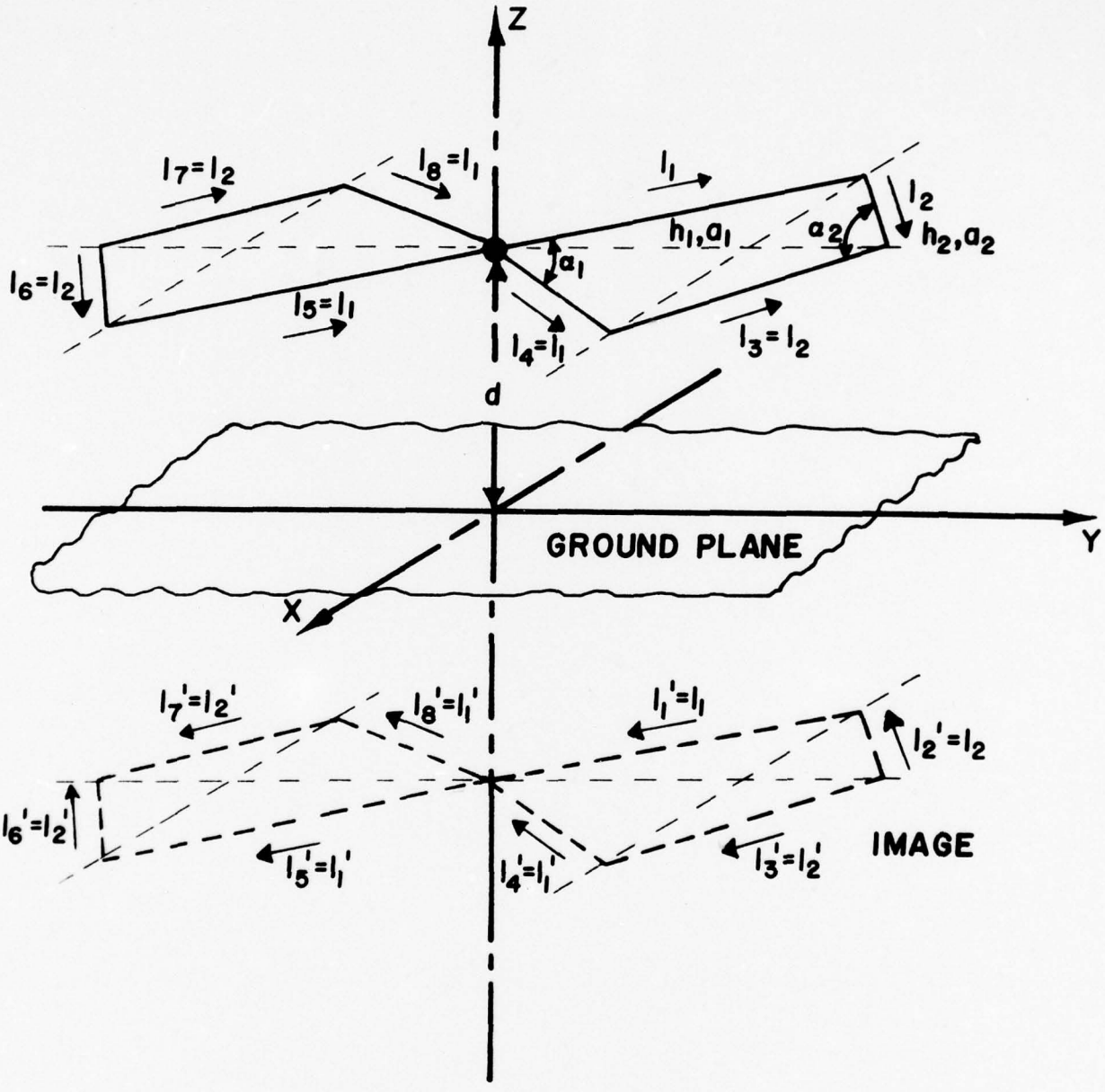

FIG. 4.4. WIRE BICONICAL ANTENNA ABOVE AND PARALLEL TO GROUND PLANE

4.2. SAMPLE RESULTS

In the following representative sample results, viz., the distribution of the current, input impedance, and far field radiation pattern, are presented for the biconical antenna structure shown in Figs. 4.1-4.4.

Fig. 4.1 shows the orientation of the biconical wire antenna placed vertically over a conducting ground plane. The structure is assumed to be in the xz-plane with the feed point at the origin of coordinates on the conducting ground plane. The geometry of the wire structure is specified by lengths, h_1 and h_2, and radii, a_1 and a_2, bottom and top conical angles, α_1 and α_2, with symmetry maintained for the other two wires. The structure becomes a Bow-tie antenna [1] with $\alpha_2=180^{\circ}$. The figure also shows the image and the various symmetries of the antenna currents. Only $[I^1]$ and $[I^2]$ are solved for this geometry and, in Figs. 4.5 and 4.6, are shown the real and imaginary parts of the current distribution on a bow-tie antenna above a ground plane at five different frequencies. The current is continuous at the bend and goes to zero at the upper end. The real and imaginary parts of the current on the vertical wire biconical antenna above ground is shown in Fig. 4.7 at three different frequencies. In Fig. 4.8 the input impedance on a bow-tie antenna above ground is plotted on a Smith chart* for frequencies from 400 MHz to 2000 MHz. The input impedance makes one complete loop in this frequency range, and one observes that calculated impedance values compare quite favorably with

*Smith chart data are normalized with respect to 50 ohms.

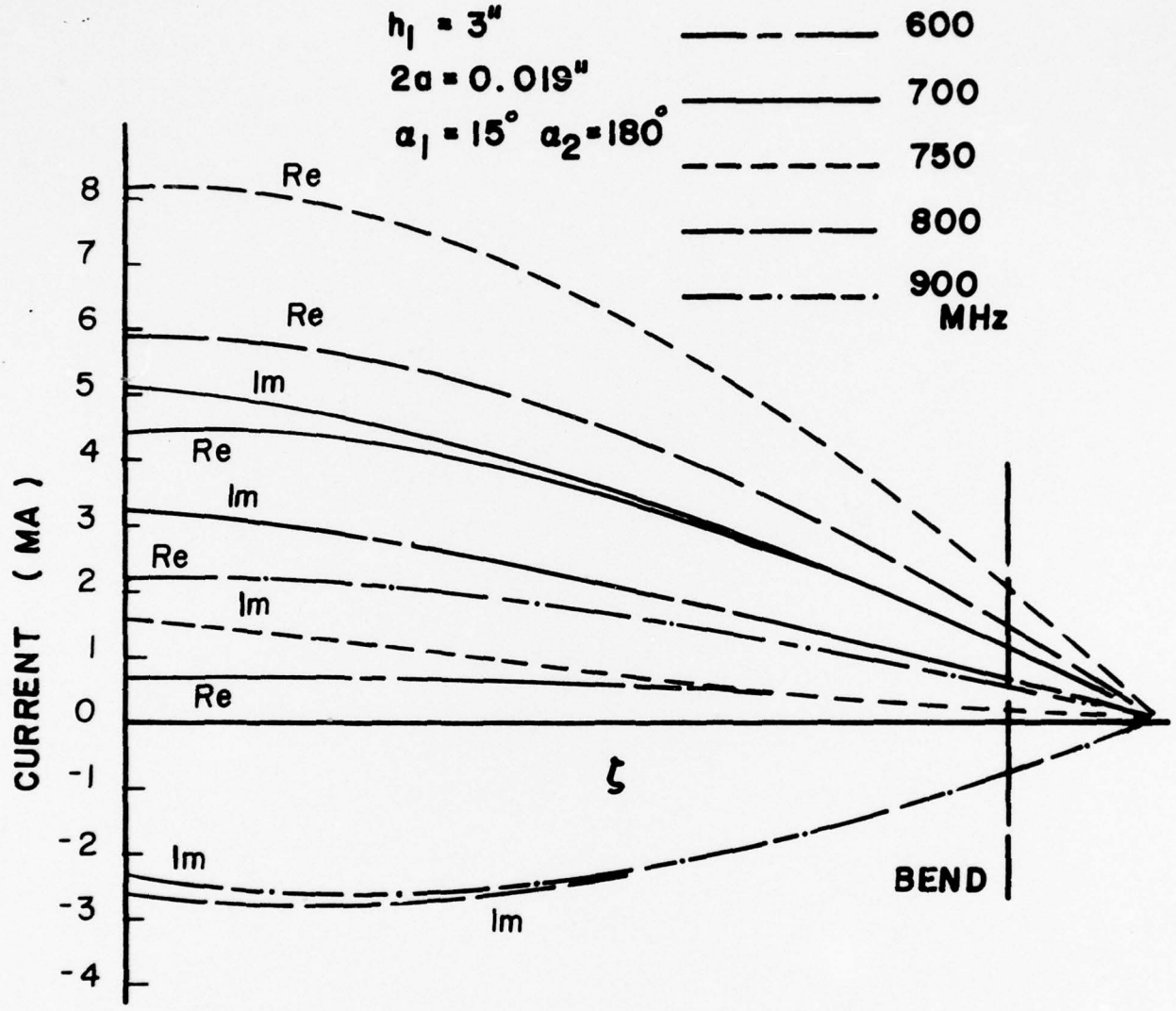

FIG. 4.5. CURRENT ON BOW-TIE ANTENNA ABOVE GROUND (α_1=15°)

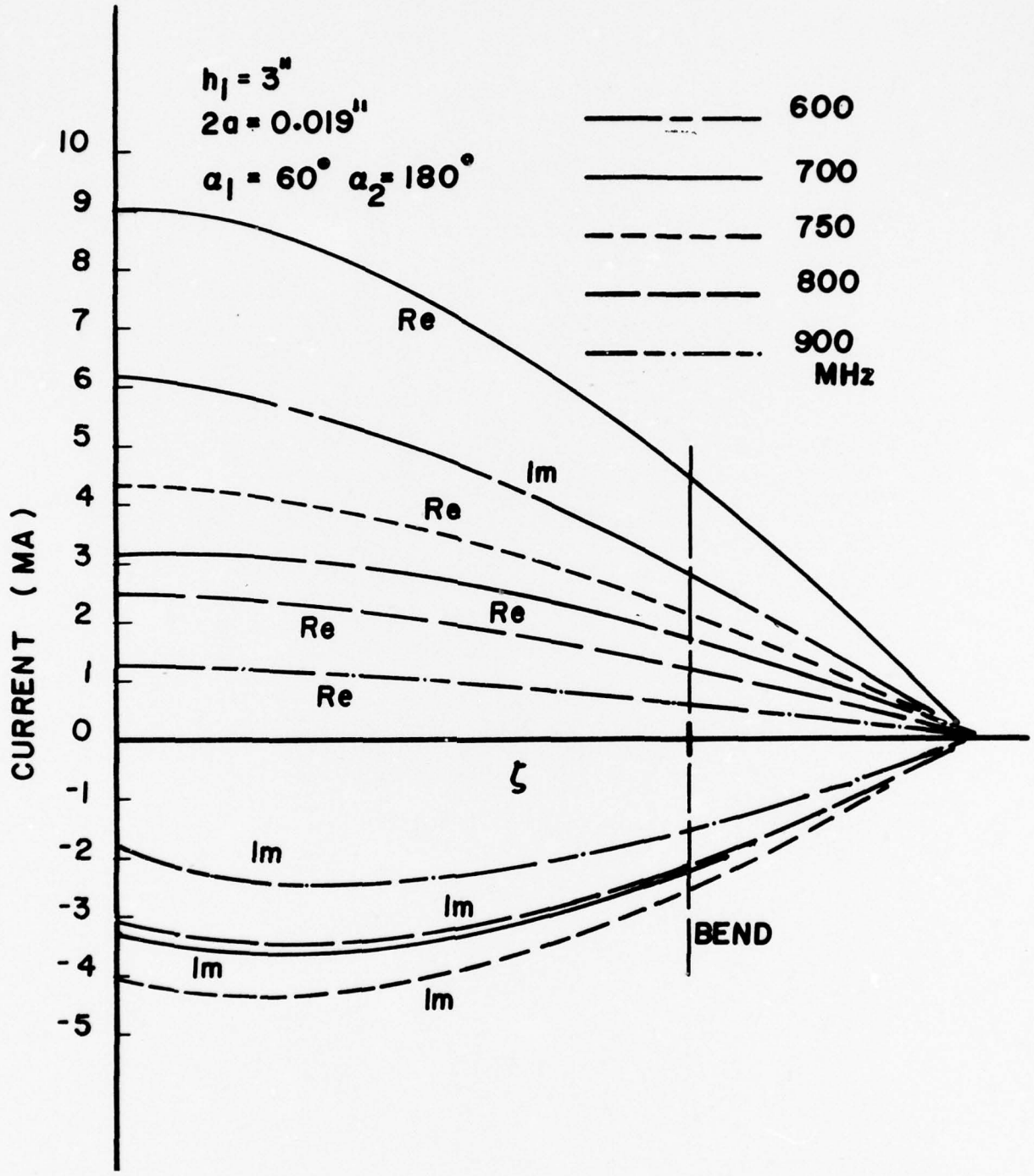

FIG. 4.6. CURRENT ON BOW-TIE ANTENNA ABOVE GROUND ($\alpha_1 = 60^0$)

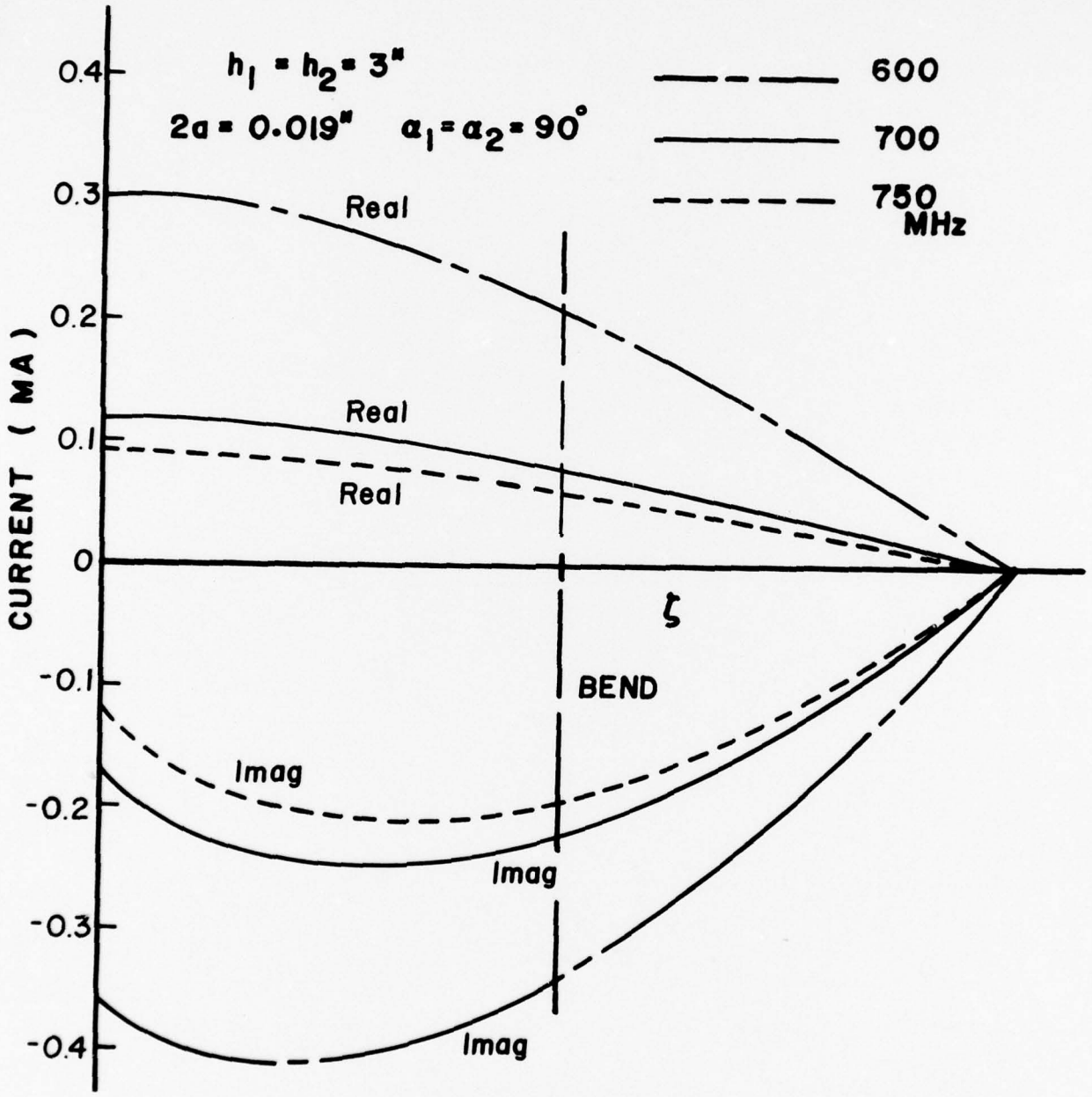

FIG. 4.7. CURRENT ON VERTICAL WIRE BICONICAL ANTENNA ABOVE GROUND

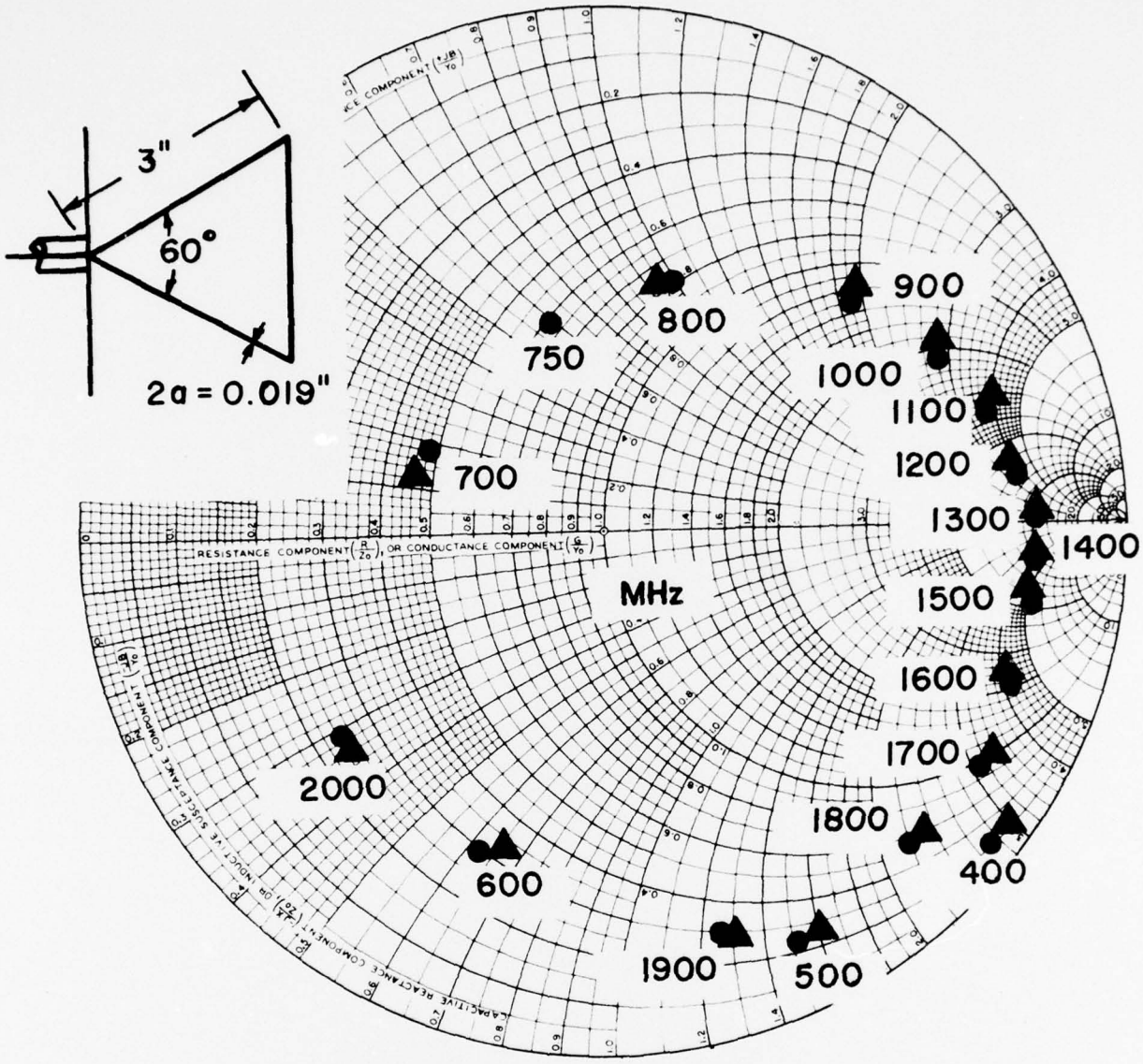

FIG. 4.8. INPUT IMPEDANCE OF BOW-TIE ANTENNA ABOVE GROUND ($\alpha_1 = 60^0$)

those which are measured. Further, the convergence of the input impedance of the bow-tie antenna as a function of number of coefficients in the current expansion is given in Fig. 4.9. Similarly, in Figs. 4.10, 4.11, and 4.12, are shown values of input impedance of other bow-tie antennas above ground compared with those of the measured results. The input impedance of a vertical biconical antenna above ground is indicated in Fig. 4.13. We note that the distribution of the current on the vertical wire biconical antenna above ground and the wire biconical antenna in free space is identical, but, for the wire biconical antenna in free space, the input impedance is twice that shown for the case of a vertical biconical antenna above a ground plane.

For convenience and ease of reading, data on Smith charts of Figs. 4.8, 4.10-4.13, 4.15 and 4.17 are tabulated in Tables III-IX.

The wire biconical antenna in free space is now placed above a ground plane, Fig. 4.3, with the plane of the wires perpendicular to the ground plane. The feed point is at a distance d above the ground plane, and the figure also shows the image structure and the current symmetries. The unknown currents $[I^1]$, $[I^2]$, $[I^3]$ and $[I^4]$ are determined for this geometry and, in Figs. 4.14 and 4.15, data for this antenna are given. Similarly, when the structure is place above and parallel to the ground plane (Fig. 4.4) at a distance d from the ground, the corresponding distribution of the current and the input impedance are as shown in Figs. 4.16-4.17.

A sample far field pattern of a wire biconical antenna in free space is given in Fig. 4.18.

TABLE III

Input Impedance of Bow-Tie Antenna
above Ground
(Data of Fig. 4.8)

Frequency (MHz)	Calculated Impedance (Ohms)	Measured Impedance (Ohms)
400	9.8 - j 136.1	12.4 - j 148.6
500	12.3 - j 75.6	12.6 - j 80.9
600	14.6 - j 31.2	16.2 - j 33.2
700	24.0 + j 9.0	23.2 + j 6.4
750	30.5 + j 29.5	
800	39.5 + j 47.8	38.5 + j 46.5
900	65.0 + j 95.0	61.8 + j 97.5
1000	108.5 + j 140.5	97.5 + j 140.0
1100	180.1 + j 192.0	160.0 + j 200.0
1200	355.2 + j 186.3	315.0 + j 180.5
1300	525.7 + j 5.2	510.0 + j 10.5
1400	390.3 - j 200.1	401.5 - j 195.0
1500	261.7 - j 275.3	280.0 - j 255.0
1600	105.6 - j 210.9	155.5 - j 205.0
1700	47.5 - j 155.2	51.5 - j 165.0
1800	27.6 - j 110.4	29.5 - j 115.0
1900	15.5 - j 61.5	14.0 - j 65.5
2000	12.2 - j 15.5	12.5 - j 17.5

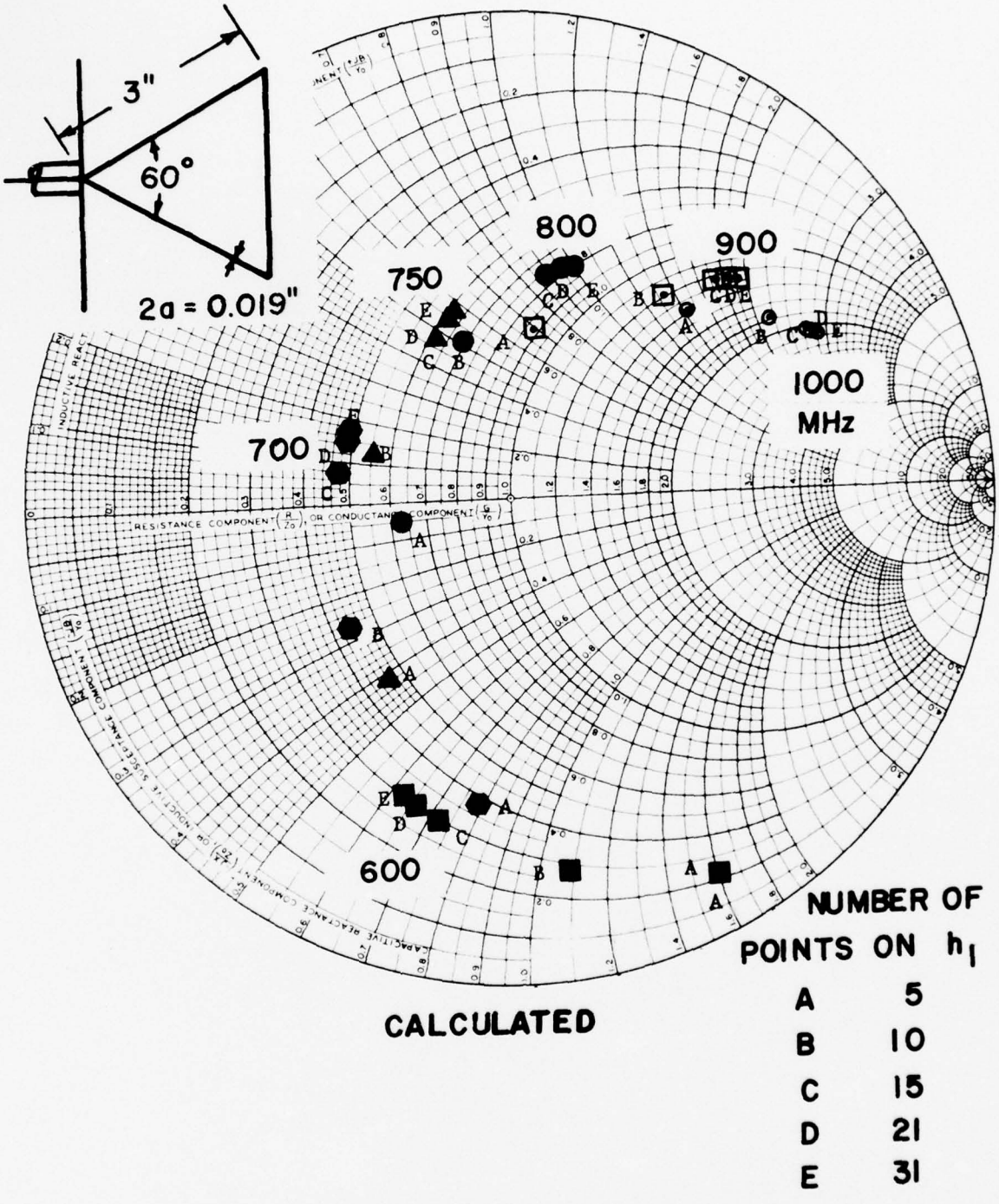

FIG. 4.9. CONVERGENCE OF THE INPUT IMPEDANCE OF BOW-TIE ANTENNA ABOVE GROUND ($\alpha_1 = 60^0$)

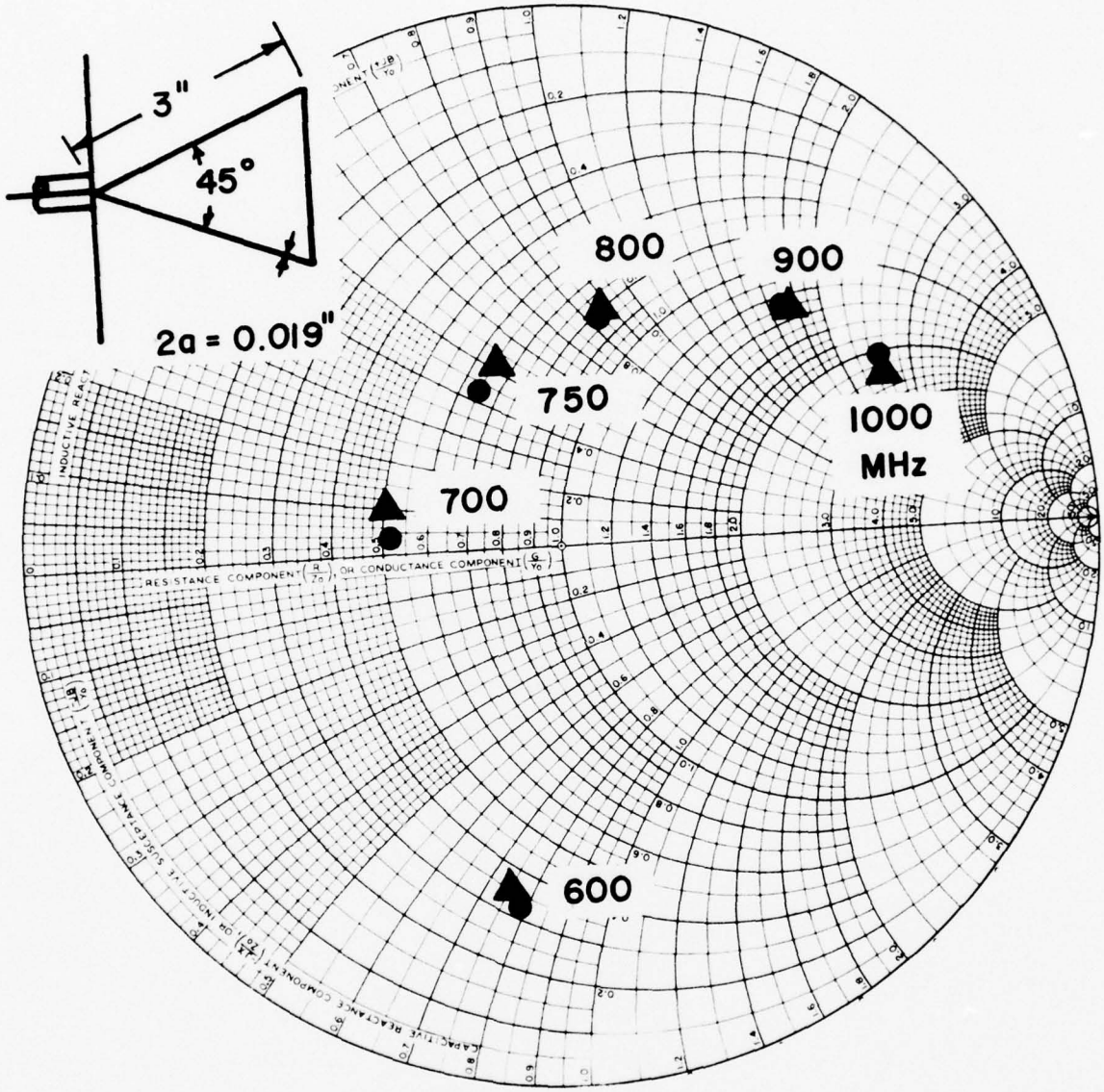

● CALCULATED

▲ MEASURED

FIG. 4.10. INPUT IMPEDANCE OF BOW-TIE ANTENNA ABOVE GROUND ($\alpha_1 = 45^0$)

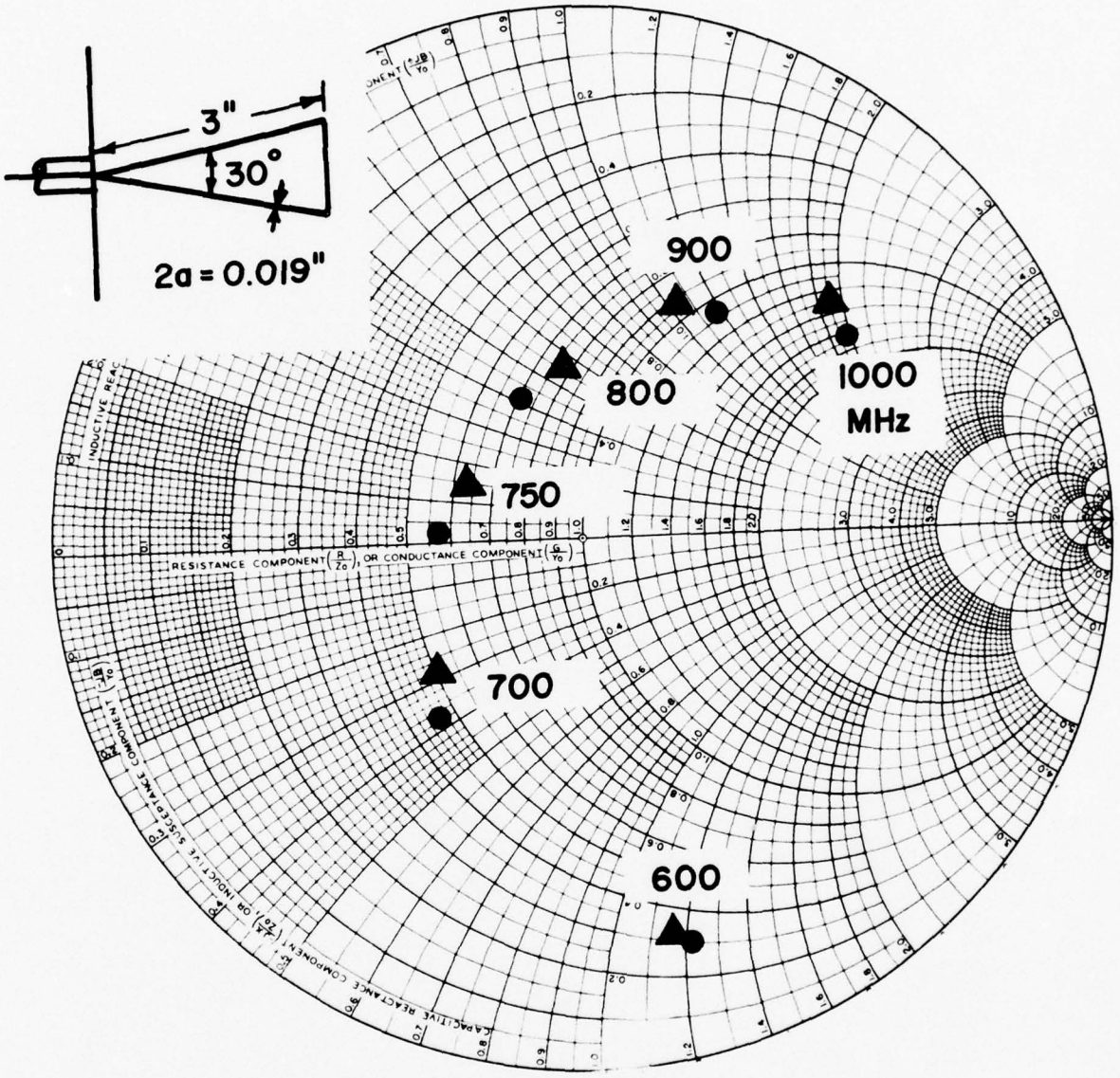

FIG. 4.11. INPUT IMPEDANCE OF BOW-TIE ANTENNA ABOVE GROUND ($\alpha_1 = 30^0$)

TABLE IV

Input Impedance of Bow-Tie Antenna
above Ground
(Data of Fig. 4.10)

Frequency (MHz)	Calculated Impedance (Ohms)	Measured Impedance (Ohms)
600	16.4 - j 39.4	17.0 - j 38.0
700	25.9 + j 4.2	25.0 + j 4.5
750	32.5 + j 21.2	33.5 + j 24.0
800	40.5 + j 42.2	39.5 + j 42.0
900	62.6 + j 80.3	67.5 + j 85.0
1000	105.1 + j 127.5	113.5 + j 120.0

TABLE V

Input Impedance of Bow-Tie Antenna
above Ground
(Data of Fig. 4.11)

Frequency (MHz)	Calculated Impedance (Ohms)	Measured Impedance (Ohms)
600	15.1 - j 61.3	15.5 - j 57.5
700	23.2 - j 18.6	25.0 - j 14.5
750	28.6 + j 1.6	32.0 + j 6.2
800	35.5 + j 21.1	39.0 + j 27.5
900	53.7 + j 59.5	47.5 + j 52.5
1000	81.4 + j 98.6	70.0 + j 95.0

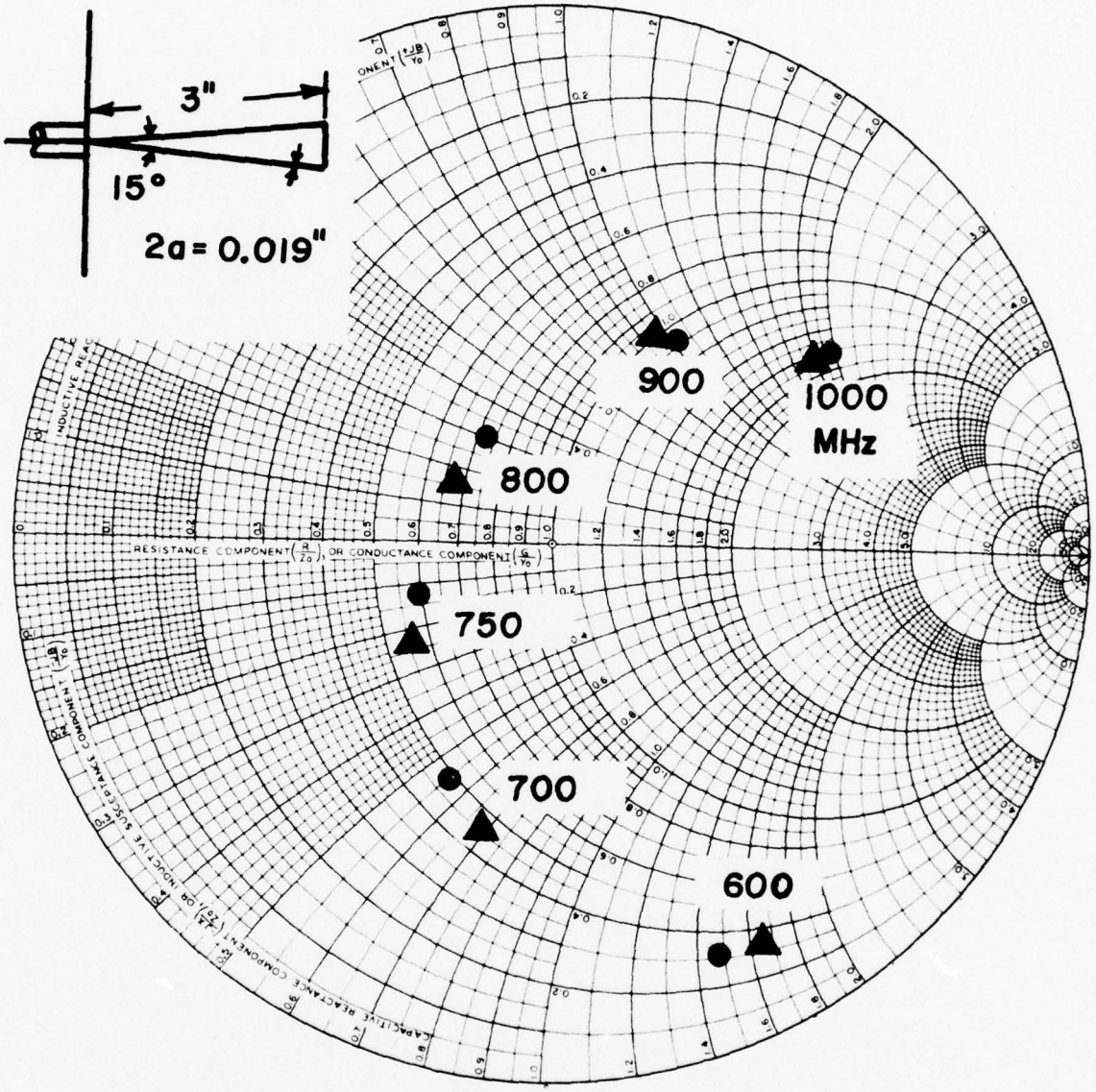

FIG. 4.12. INPUT IMPEDANCE OF BOW-TIE ANTENNA ABOVE GROUND ($\alpha_1 = 15^0$)

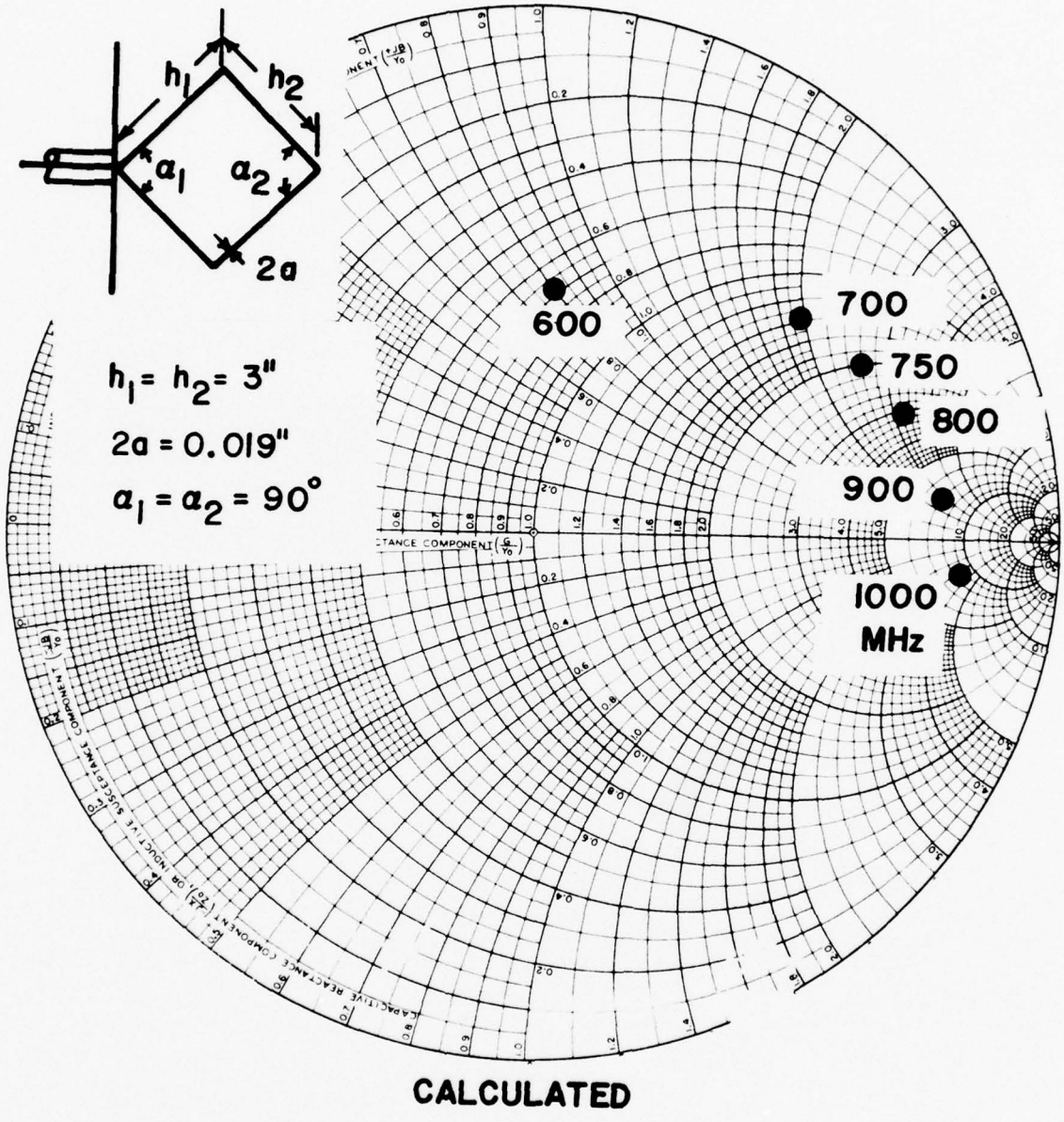

FIG. 4.13. INPUT IMPEDANCE OF VERTICAL BICONICAL ANTENNA ABOVE GROUND ($\alpha_1 = \alpha_2 = 90^0$)

TABLE VI

Input Impedance of Bow-Tie Antenna above Ground (Data of Fig. 4.12)

Frequency (MHz)	Calculated Impedance (Ohms)	Measured Impedance (Ohms)
600	15.7 - j 74.2	15.5 - j 82.5
700	24.2 - j 27.6	22.5 - j 35.0
750	29.5 - j 6.3	27.5 - j 12.0
800	36.3 + j 15.0	37.5 + j 7.5
900	54.2 + j 51.5	50.0 + j 47.5
1000	80.5 + j 99.4	85.5 + j 87.5

TABLE VII

Input Impedance of Vertical Biconical Antenna above Ground (Data of Fig. 4.13)

Frequency (MHz)	Calculated Impedance (Ohms)
600	33.9 + j 40.7
700	68.6 + j 98.2
750	100.0 + j 130.2
800	151.5 + j 161.2
900	352.7 + j 145.4
1000	411.5 - j 161.3

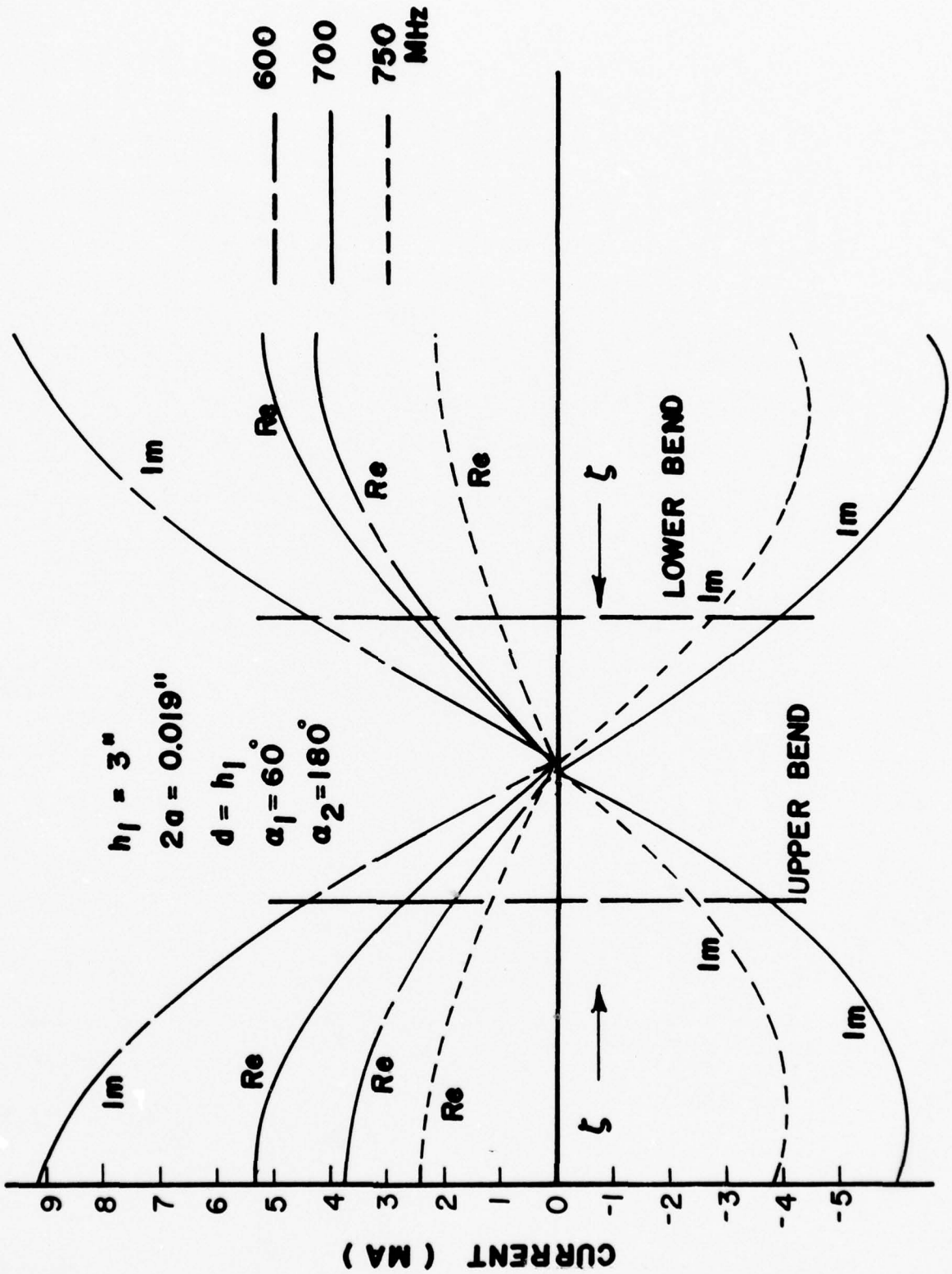

FIG. 4.14. CURRENT ON WIRE BICONICAL ANTENNA ABOVE AND PERPENDICULAR TO GROUND PLANE

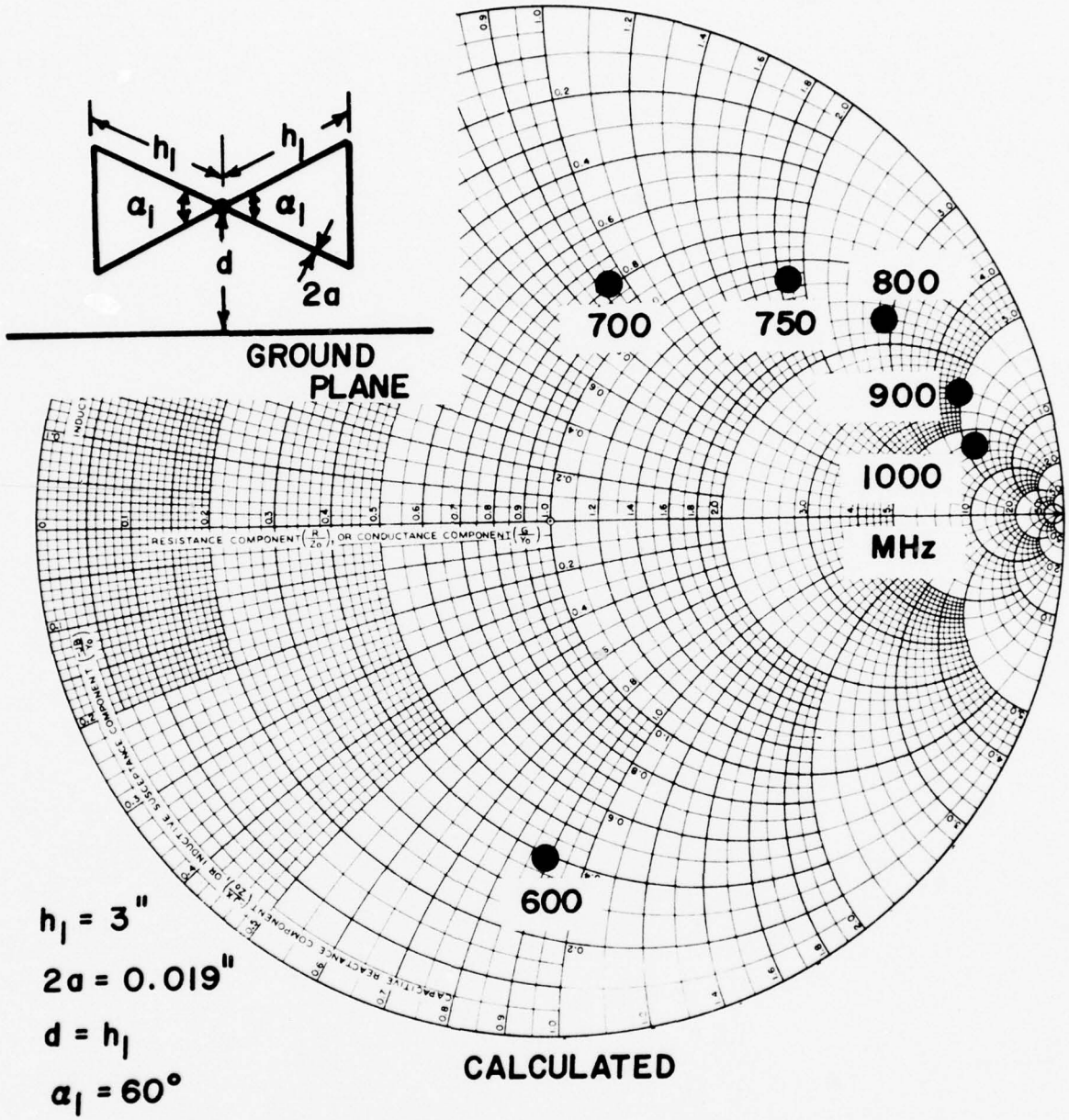

FIG. 4.15. INPUT IMPEDANCE OF WIRE BICONICAL ANTENNA ABOVE AND PERPENDICULAR TO GROUND PLANE

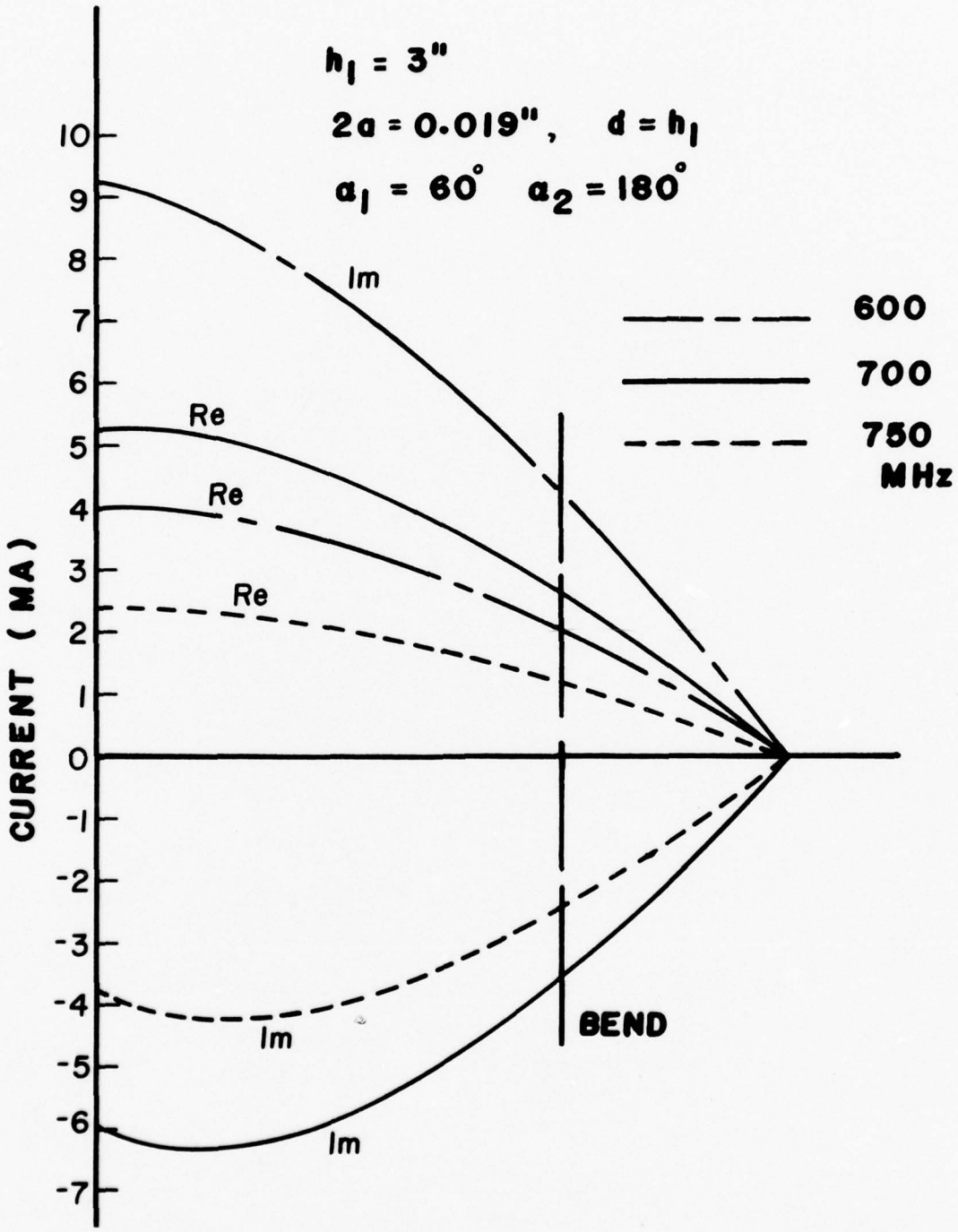

FIG. 4.16. CURRENT ON WIRE BICONICAL ANTENNA ABOVE AND PARALLEL TO GROUND PLANE

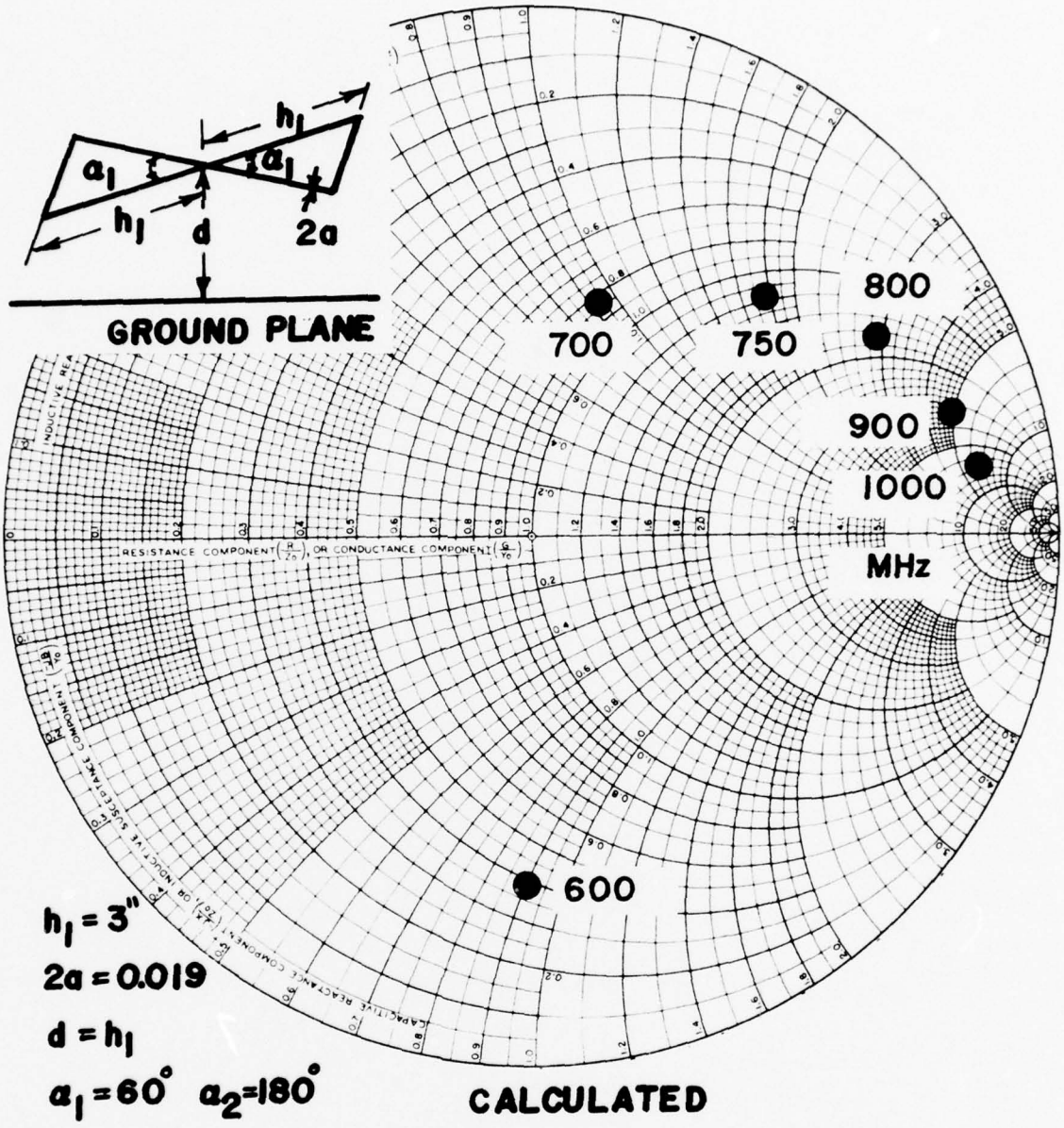

FIG. 4.17. INPUT IMPEDANCE OF WIRE BICONICAL ANTENNA ABOVE AND PARALLEL TO GROUND PLANE

TABLE VIII

Input Impedance of Wire Biconical Antenna above and Perpendicular to Ground Plane (Data of Fig. 4.15)

Frequency (MHz)	Calculated Impedance (Ohms)
600	18.9 - j 44.7
700	39.7 + j 46.8
750	56.4 + j 93.9
800	79.9 + j 142.9
900	157.9 + j 244.4
1000	306.3 + j 335.9

TABLE IX

Input Impedance of Wire Biconical Antenna above and Parallel to Ground Plane (Data of Fig. 4.17)

Frequency (MHz)	Calculated Impedance (Ohms)
600	19.5 - j 45.2
700	41.1 + j 46.7
750	58.7 + j 88.4
800	83.4 + j 142.7
900	151.1 + j 243.6
1000	319.5 + j 324.6

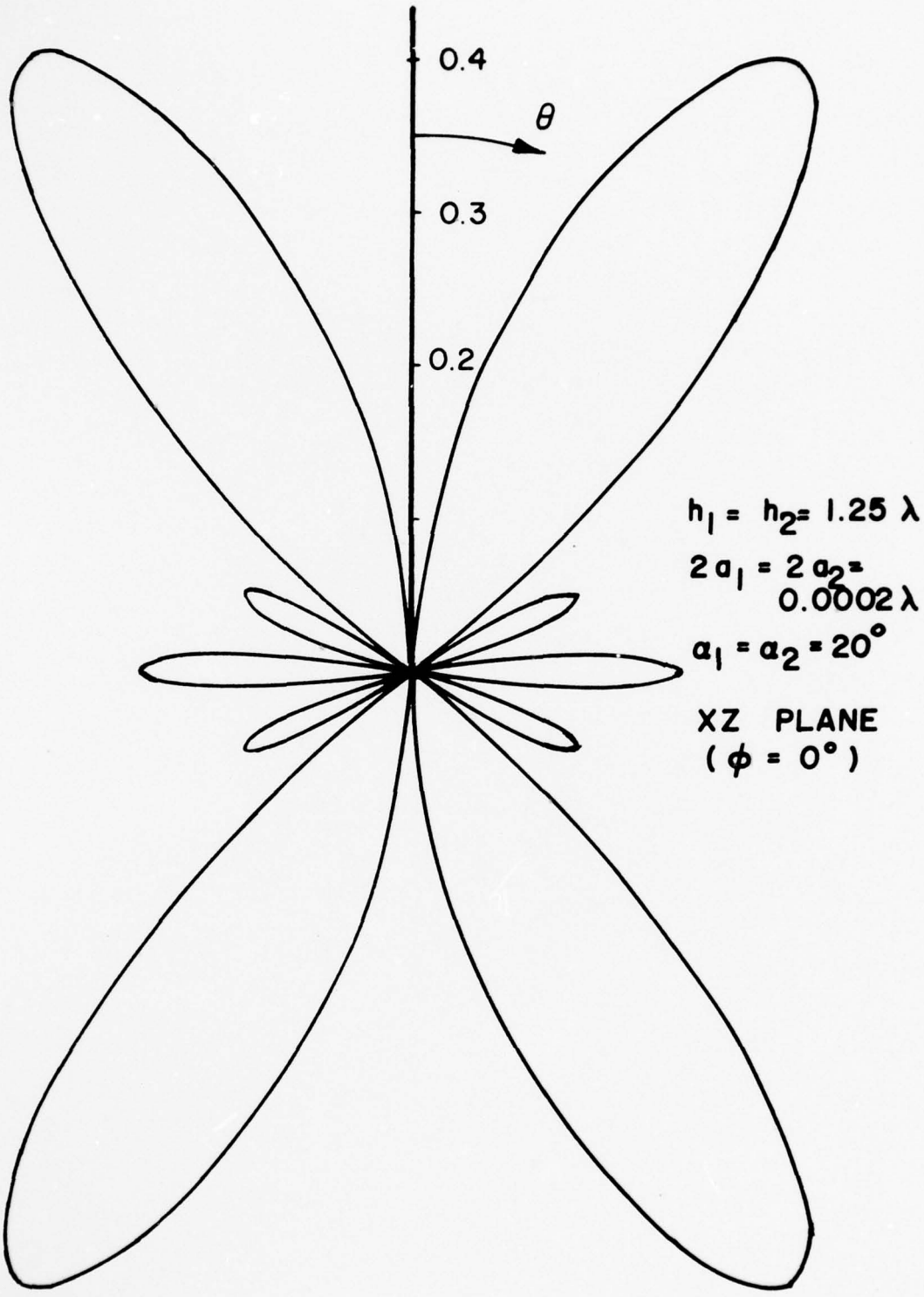

FIG. 4.18. FAR-FIELD PATTERN OF WIRE BICONICAL ANTENNA IN FREE SPACE, E_θ - COMPONENT

REFERENCES

1. Prewitt, J.O., C.E. Smith, and Butler, C.M., "The Bow-Tie Antenna," 1974 IEEE Region III Proceedings of Southeastcon, Orlando, Florida, April 29-May 1, 1974, pp. 59-62.

APPENDIX I

INTEGRALS INVOLVING PIECEWISE LINEAR AND PIECEWISE SINUSOIDAL FUNCTIONS

In solving equations by numerical techniques incorporating piecewise linear and piecewise sinusoidal testing, one encounters the need to evaluate integrals involving the piecewise linear and piecewise sinusoidal "pulses." In this appendix these integrals are tabulated.

I-1 PIECEWISE LINEAR

The piecewise linear function $\Lambda_m^{\ell}(z)$ is defined by

$$\Lambda_m^{\ell}(z) = \frac{1}{\Delta}\left(\Delta - |z-z_m|\right) , \quad z\varepsilon(z_{m-1}, z_{m+1}) \tag{I.1}$$

where

$$\Delta = (z_m - z_{m-1}) . \tag{I.2}$$

Λ_m^{ℓ} is depicted in Fig. I-1.

Piecewise Linear Testing (Against First Derivative) For a function $f(z)$ having a first derivative, one can readily show that the following are true.

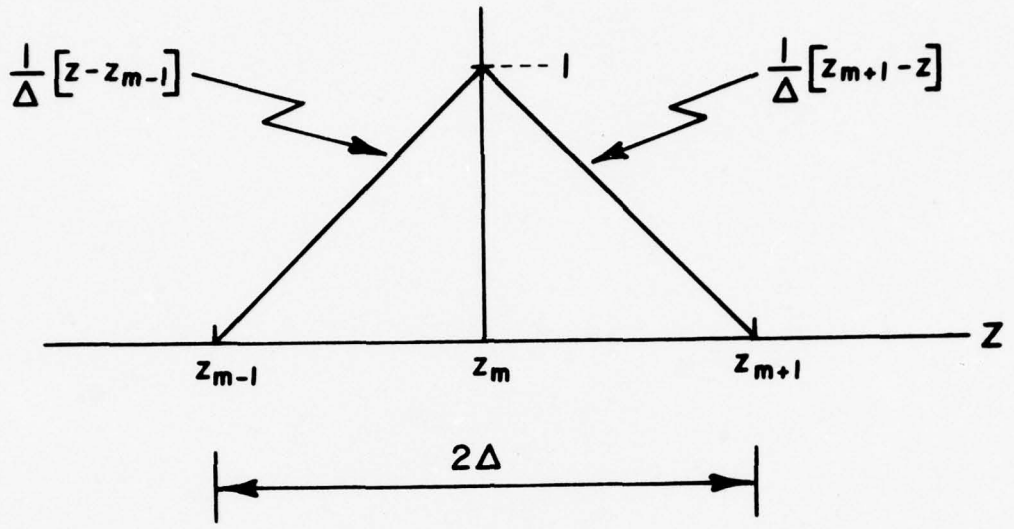

FIG. I-1. PIECEWISE LINEAR FUNCTION

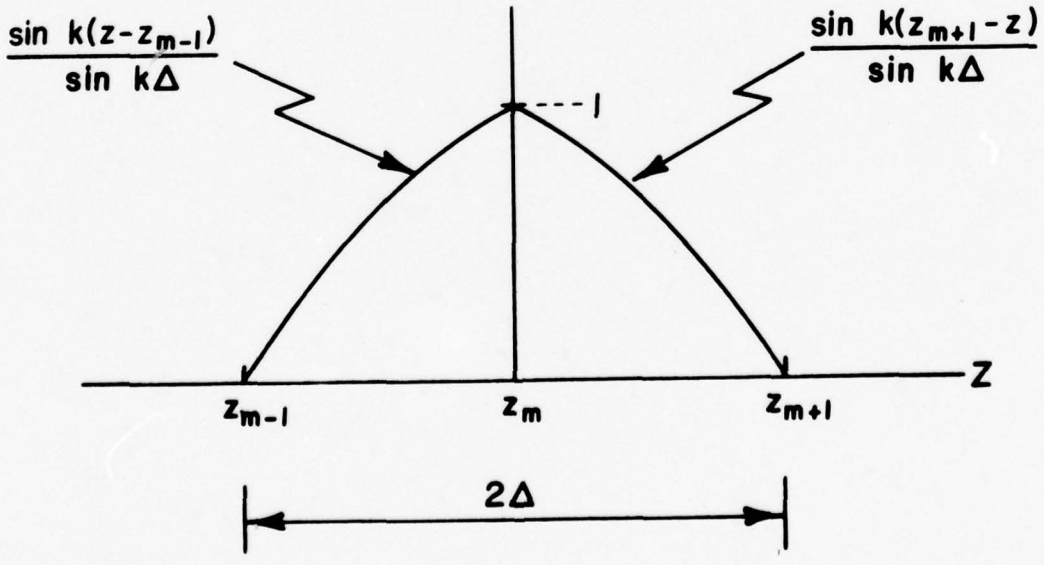

FIG. I-2. PIECEWISE SINUSOIDAL FUNCTION

$$\int_{z=z_{m-1}}^{z_m} \frac{d}{dz} f(z) \Lambda_m^{\ell}(z) dz = f(z_m) - \frac{1}{\Delta} \int_{z=z_{m-1}}^{z_m} f(z) dz \qquad (I.3)$$

$$\int_{z=z_m}^{z_{m+1}} \frac{d}{dz} f(z) \Lambda_m^{\ell}(z) dz = -f(z_m) + \frac{1}{\Delta} \int_{z=z_m}^{z_{m+1}} f(z) dz \qquad (I.4)$$

$$\int_{z=z_{m-1}}^{z_{m+1}} \frac{d}{dz} f(z) \Lambda_m^{\ell}(z) dz = \frac{1}{\Delta} \left[- \int_{z=z_{m-1}}^{z_m} f(z) dz + \int_{z=z_m}^{z_{m+1}} f(z) dz \right] \qquad (I.5)$$

Piecewise Linear Testing (Against Second Derivative) For a function f(z) possessing a second derivative, the following integrals can be established.

$$\int_{z=z_{m-1}}^{z_m} \frac{d^2}{dz^2} f(z) \Lambda_m^{\ell}(z) dz = \frac{d}{dz} f(z_m) + \frac{1}{\Delta} f(z_{m-1}) - \frac{1}{\Delta} f(z_m) \qquad (I.6)$$

$$\int_{z=z_m}^{z_{m+1}} \frac{d^2}{dz^2} f(z) \Lambda_m^{\ell}(z) dz = - \frac{d}{dz} f(z_m) - \frac{1}{\Delta} f(z_m) + \frac{1}{\Delta} f(z_{m+1}) \qquad (I.7)$$

$$\int_{z=z_{m-1}}^{z_{m+1}} \frac{d^2}{dz^2} f(z) \Lambda_m^{\ell}(z) dz = \frac{1}{\Delta}\left[f(z_{m+1}) - 2f(z_m) + f(z_{m-1})\right] \qquad (I.8)$$

I-2 PIECEWISE SINUSOIDAL

The piecewise sinusoidal function is defined by

$$\Lambda_m^s(z) = \frac{\sin k(\Delta - |z-z_m|)}{\sin k\Delta} \quad , \quad z\varepsilon(z_{m-1}, z_{m+1}) \qquad (I.9)$$

and is illustrated in Fig. I-2.

Piecewise Sinusoidal Testing (Against First Derivative) For $f(z)$ possessing a first derivative, one can derive the following.

$$\int_{z=z_{m-1}}^{z_m} \frac{d}{dz} f(z) \Lambda_m^s(z) dz = f(z_m) - k \int_{z=z_{m-1}}^{z_m} f(z) \frac{\cos k(z-z_{m-1})}{\sin k\Delta} dz \qquad (I.10)$$

$$\int_{z=z_m}^{z_{m+1}} \frac{d}{dz} f(z) \Lambda_m^s(z) dz = -f(z_m) + k \int_{z=z_m}^{z_{m+1}} f(z) \frac{\cos k(z_{m+1}-z)}{\sin k\Delta} dz \qquad (I.11)$$

$$\int_{z=z_{m-1}}^{z_{m+1}} \frac{d}{dz} f(z) \Lambda_m^s(z)\,dz = \frac{k}{\sin k\Delta} \left[- \int_{z=z_{m-1}}^{z_m} f(z) \cos k(z - z_{m-1})\,dz \right.$$

$$\left. + \int_{z=z_m}^{z_{m+1}} f(z) \cos k(z_{m+1} - z)\,dz \right] \qquad \text{(I.12)}$$

Piecewise Sinusoidal Testing (Against Second Derivative)

Finally, for f(z) possessing a second derivative, one can establish the relationships which follow.

$$\int_{z=z_{m-1}}^{z_m} \frac{d^2}{dz^2} f(z) \Lambda_m^s(z)\,dz = \frac{d}{dz} f(z_m) - k \frac{\cos k\Delta}{\sin k\Delta} f(z_m) + \frac{k}{\sin k\Delta} f(z_{m-1})$$

$$- k^2 \int_{z=z_{m-1}}^{z_m} f(z) \Lambda_m^s(z)\,dz \qquad \text{(I.13)}$$

$$\int_{z=z_m}^{z_{m+1}} \frac{d^2}{dz^2} f(z) \Lambda_m^s(z)\,dz = - \frac{d}{dz} f(z_m) - k \frac{\cos k\Delta}{\sin k\Delta} f(z_m) + \frac{k}{\sin k\Delta} f(z_{m+1})$$

$$- k^2 \int_{z=z_m}^{z_{m+1}} f(z) \Lambda_m^s(z)\,dz \qquad \text{(I.14)}$$

$$\int_{z=z_{m-1}}^{z_{m+1}} \frac{d^2}{dz^2} f(z)\Lambda_m^s(z)dz = \frac{k}{\sin k\Delta}\left[f(z_{m+1}) - 2\cos k\Delta f(z_m) + f(z_{m-1})\right]$$

$$- k^2 \int_{z=z_{m-1}}^{z_{m+1}} f(z)\Lambda_m^s(z)dz \qquad \text{(I.15)}$$

I-3 APPROXIMATIONS

The following approximations are good whenever f(z) is smooth over $z\varepsilon(z_{m-1},-z_{m+1})$ and are useful in applications of piecewise linear and piecewise sinusoidal testing.

$$\int_{z=z_{m-1}}^{z_m} f(z)\Lambda_m^{\ell,s}(z)dz \doteq \frac{\Delta}{2} f(z_m) \qquad \text{(I.16)}$$

$$\int_{z=z_m}^{z_{m+1}} f(z)\Lambda_m^{\ell,s}(z)dz \doteq \frac{\Delta}{2} f(z_m) \qquad \text{(I.17)}$$

$$\int_{z=z_{m-1}}^{z_{m+1}} f(z)\Lambda_m^{\ell,s}(z)dz \doteq \Delta f(z_m) \qquad \text{(I.18)}$$

In the above expressions $\Lambda_m^{\ell,s}$ represents either (I.1) or (I.9).

APPENDIX II

ELECTRIC SCALAR POTENTIAL DUE TO A RING CHARGE

In this appendix is presented the calculation of electric scalar potential due to a ring of uniform, discrete charge. An expression for this potential is often needed in moment method analyses of wire scatterers or antennas when the wire current is approximated by pulses. A circumferentially uniform surface current on a cylinder "deposits" a discrete ring of charge at any point where the current is discontinuous. If the total axial current on the cylinder, assumed to be coaxial with the z axis, is $I_z(z)$, then the total quantity of charge Q in the ring of charge is given by

$$Q = -\frac{1}{j\omega} \lim_{\alpha \to 0} \left[I_z(z_d+\alpha) - I_z(z_d-\alpha) \right] \qquad \text{(II.1)}$$

where z_d is the point at which I_z is discontinuous. This charge Q is uniformly distributed over the ring which can be looked upon as a circular line charge of constant linear density,

$$\rho_\ell^r = \frac{Q}{2\pi a} \quad , \qquad \text{(II.2)}$$

where a is the cylinder radius.

Knowing the density ρ_ℓ^r of the ring charge, one next determines the scalar potential due to the ring charge. If the ring charge is located at $z=\zeta$ in a cylindrical coordinate system,

with the plane of the ring parallel to the xy plane as depicted in Fig. II-1, the potential Φ at a point (r,ϕ,z) is

$$\Phi(r,\phi,z) = \frac{1}{4\pi\varepsilon}\int_{\phi'=-\pi}^{\pi}\rho_{\ell}^{r}\,\frac{e^{-jkR}}{R}\,a\,d\phi' \qquad (II.3)$$

where R is defined in Fig. II-1. Since the charge is constant in ϕ, so is Φ; thus, Φ reduces to

$$\Phi(r,z) = \frac{Q}{4\pi\varepsilon}g(z-\zeta,r,a) \qquad (II.4)$$

where

$$g(\xi,r,a) = \frac{1}{2\pi}\int_{\phi'=-\pi}^{\pi}\frac{e^{-jk[\xi^2+r^2+a^2-2ra\,\cos\phi']^{\frac{1}{2}}}}{[\xi^2+r^2+a^2-2ra\,\cos\phi']^{\frac{1}{2}}}\,d\phi' \quad . \qquad (II.5)$$

A special case of interest requires the determination of $\Phi(a,z)$ in which case g reduces to the usual kernel (exact) $K(\xi)$ used in thin-wire calculations: $g(\xi,a,a) = K(\xi)$. Therefore, in view of (II.1), the potential at (a,z) due to a current discontinuity at z_d is

$$\Phi(a,z) = -\frac{1}{j4\pi\omega\varepsilon}K(z-z_d)\lim_{\alpha\downarrow 0}\left[I_z(z_d+\alpha) - I_z(z_d-\alpha)\right]. \qquad (II.6)$$

Lastly, it is worth noting that, for $a<<\lambda$ and $|\bar{r}-\bar{r}'|>>a$, the potential at a point $\bar{r}$ due to a ring charge at $\bar{r}'$ can be written simply in the form,

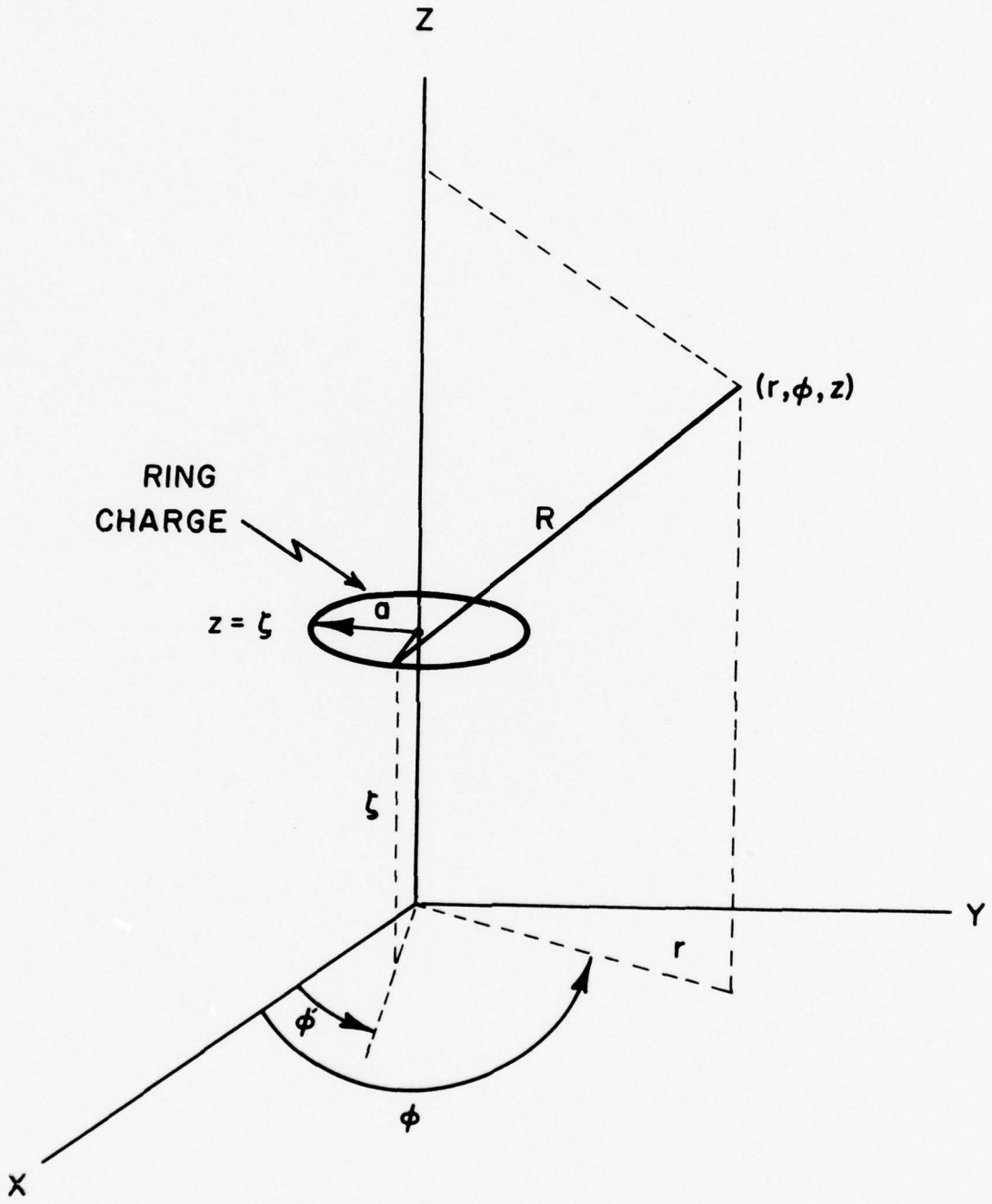

FIG. II-1. RING CHARGE IN FREE SPACE

$$\Phi(\bar{r}) = -\frac{1}{j4\pi\omega\varepsilon}\frac{e^{-jk|\bar{r}-\bar{r}'|}}{|\bar{r}-\bar{r}'|}\lim_{\alpha\to 0}\left[I_z(z_d+\alpha) - I_z(z_d-\alpha)\right], \quad (II.7)$$

again with the ring charge resulting from a discontinuity in I_z at z_d.

Singularity of Potential Due to Ring Charge The potential Φ due to the ring charge is singular in the limit as the point of observation approaches the ring. Knowledge of the behavior of the potential on a cylindrical surface due to a ring charge at the end of the cylinder (Fig. II-2) is useful in wire analyses. Thus we investigate the manner in which $\Phi(a,z)$ becomes unbounded as $z\to\zeta$. Since $\frac{Q}{4\pi\varepsilon}$ is a constant and $g(d,a,a) = K(d)$, we determine the limit of $K(d)$ as d approaches zero. $K(d)$ can be written

$$K(d) = \frac{1}{2\pi}\int_{\phi'=-\pi}^{\pi}\frac{1}{D}d\phi' - \frac{1}{2\pi}\int_{\phi'=-\pi}^{\pi}[1-e^{-jkD}]\frac{1}{D}d\phi' \quad (II.8)$$

where

$$D = [d^2 + 2a^2(1-\cos\phi')]^{\frac{1}{2}} . \quad (II.9)$$

The singularity of $K(d)$ is due to the first integral above and the second is well behaved so, being interested in the singularity, we concentrate attention on the first. For a positive number $\delta<\pi$,

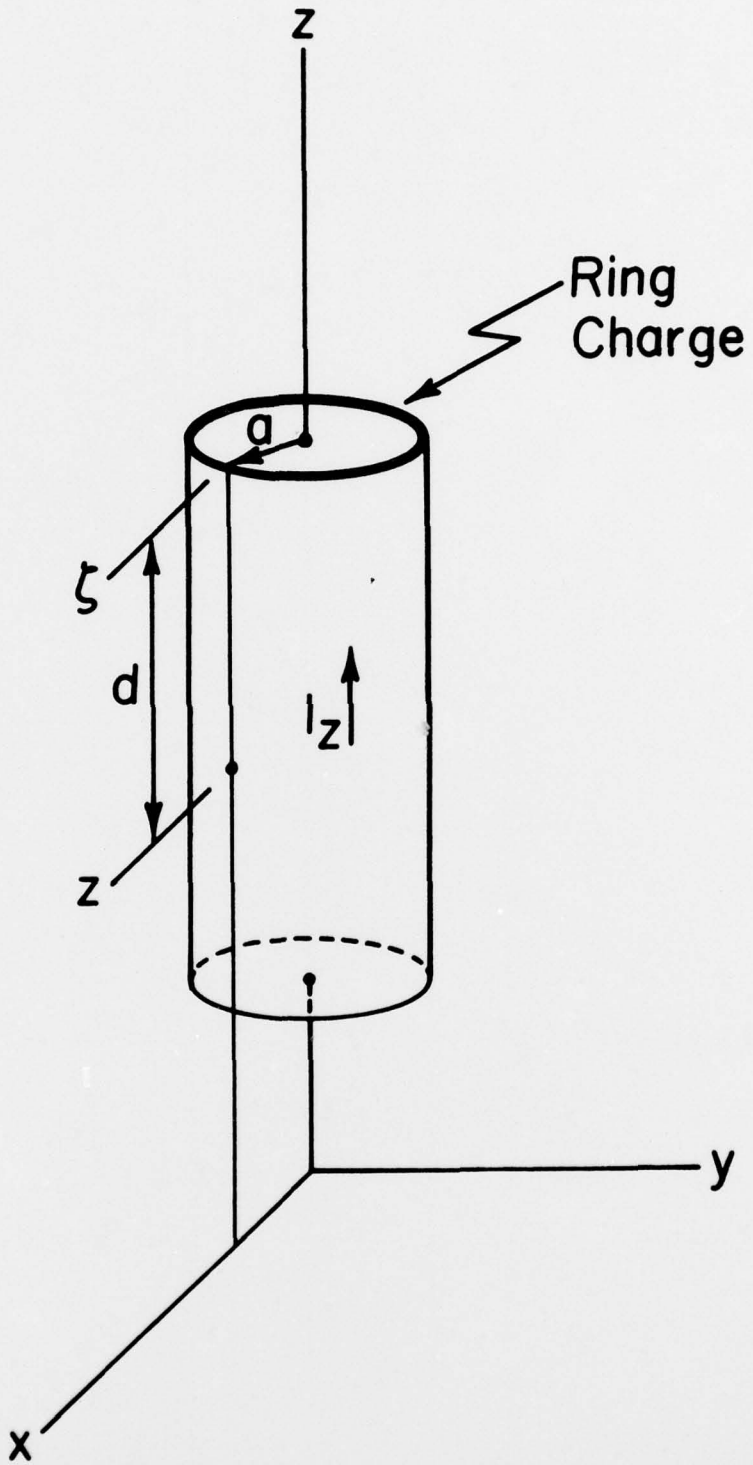

FIG. II-2. RING CHARGE ON END OF CYLINDER

$$\frac{1}{2\pi}\int_{\phi'=-\pi}^{\pi}\frac{1}{D}d\phi' = \frac{1}{2\pi}\left(\int_{\phi'=-\pi}^{-\delta} + \int_{\phi'=-\delta}^{\delta} + \int_{\phi'=\delta}^{\pi}\right)\frac{1}{D}d\phi' \quad ,$$

and, as before,we discard bounded quantities and retain only the integral over $(-\delta,\delta)$, which, for any nonzero δ, contains the singularity. Next we specify that δ be fixed but sufficiently small to justify replacing $2(1-\cos\phi')$ in (II.9) by ϕ'^2. This enables us to reduce the integral over $(-\delta,\delta)$ containing the singularity to

$$\frac{1}{2\pi a}\int_{\phi'=-\delta}^{\delta}\frac{1}{[(\frac{d}{a})^2+\phi'^2]^{\frac{1}{2}}}d\phi'$$

which can be readily integrated to obtain

$$\frac{1}{2\pi}\left\{\ell n\left(\delta+\sqrt{\delta^2+(\frac{d}{a})^2}\right) - \ell n\left(-\delta+\sqrt{\delta^2+(\frac{d}{a})^2}\right)\right\} \quad .$$

In the limit as $d\to 0$, the above behaves as

$$\frac{1}{\pi a}\lim_{d\to 0}\left(\ell n(\frac{2a}{d})\right) .$$

Hence,

$$K(d) \xrightarrow[d\to 0]{} \frac{1}{\pi a}\ell n(\frac{2a}{d}) \qquad (II.10)$$

and the limiting behavior of the potential is

$$\Phi \xrightarrow[d\to 0]{} \frac{Q}{4\pi^2 \varepsilon a} \ell n\left(\frac{2a}{d}\right) \qquad \text{(II.11)}$$

or, as a function of the current at the end of the cylinder,

$$\Phi \xrightarrow[d\to 0]{} \frac{I_z(\zeta)}{j4\pi^2 \omega \varepsilon a} \ell n\left(\frac{2a}{d}\right) \quad . \qquad \text{(II.12)}$$

APPENDIX III

WIRE-TO-WIRE DISTANCE AND LOCATION SCHEME

In the interest of flexibility in a wire analysis, one wishes to have available a general scheme for specifying the location of an arbitrary wire as well as the geometric properties of the wire which are pertinent to the calculations to be performed. Also, one must be able to specify in a general manner the distance from a point on one wire to that on another. A scheme for accomplishing the above is outlined in this appendix.

As suggested in Fig. III-1, the locations of the lower and upper end points of the axis of a given wire are denoted in Cartesian coordinates by $(x^{\ell},y^{\ell},z^{\ell})$ and (x^{u},y^{u},z^{u}), respectively. From these points, one determines the wire length **L**, the direction cosines of the wire $\cos\alpha$, $\cos\beta$, $\cos\gamma$, the unit vector along the wire axis $\hat{u}$, the location of the axis center $\bar{r}^{c}$.

Wire Length:

$$L = \left[(x^{u}-x^{\ell})^{2} + (y^{u}-y^{\ell})^{2} + (z^{u}-z^{\ell})^{2}\right]^{\frac{1}{2}} \qquad \text{(III.1)}$$

Direction Cosines:

$$\cos\alpha = \frac{x^{u}-x^{\ell}}{L} \qquad \text{(III.2a)}$$

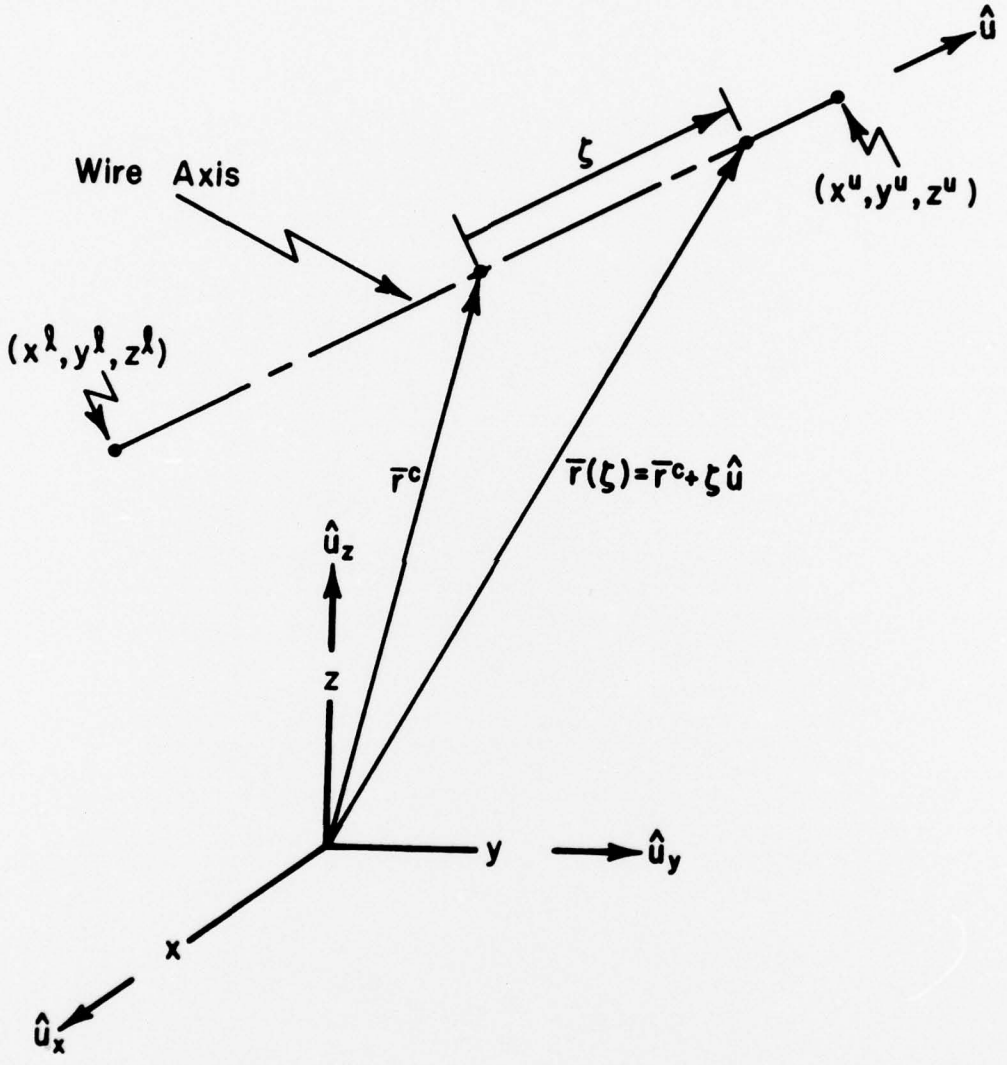

FIG. III-1. LOCATION OF WIRE AXIS

$$\cos\beta = \frac{y^u - y^\ell}{L} \qquad \text{(III.2b)}$$

$$\cos\gamma = \frac{z^u - z^\ell}{L} \qquad \text{(III.2c)}$$

Unit Vector (from lower to upper end):

$$\hat{u} = \cos\alpha\ \hat{u}_x + \cos\beta\ \hat{u}_y + \cos\gamma\ \hat{u}_z \qquad \text{(III.3)}$$

Location of Wire Center:

$$\bar{r}^c = x^c\hat{u}_x + y^c\hat{u}_y + z^c\hat{u}_z \qquad \text{(III.4)}$$

$$x^c = x^\ell + \frac{L}{2}\cos\alpha = \frac{1}{2}\,(x^u + x^\ell) \qquad \text{(III.5a)}$$

$$y^c = y^\ell + \frac{L}{2}\cos\beta = \frac{1}{2}\,(y^u + y^\ell) \qquad \text{(III.5b)}$$

$$z^c = z^\ell + \frac{L}{2}\cos\gamma = \frac{1}{2}\,(z^u + z^\ell) \qquad \text{(III.5c)}$$

The equation of a line in space can be conveniently formulated in terms of the location of a point on the line and a parameter specifying displacement along the line from this reference point to any other point. With the wire axis center as reference the equation of the wire axis is

$$\bar{r}(\zeta) = \bar{r}^c + \zeta\hat{u}\ . \qquad \text{(III.6)}$$

As depicted in Fig. III-1, $\bar{r}(\zeta)$ locates a point on the wire axis in terms of the fixed reference $\bar{r}^c$ and the displacement $\zeta\hat{u}$ from the center to a general point on this axis.

From (III.6), one may readily calculate the distance from a general point $\bar{r}$ in space,

$$\bar{r} = x\hat{u}_x + y\hat{u}_y + z\hat{u}_z \quad , \tag{III.7}$$

to the point $\bar{r}'$ on the wire axis:

$$\begin{aligned} |\bar{r}-\bar{r}'| &= \left|\bar{r} - (\bar{r}^c-\zeta'\hat{u})\right| \\ &= \Big| \left[(x-x^c) - \zeta'\cos\alpha\right]\hat{u}_x + \left[(y-y^c) - \zeta'\cos\beta\right]\hat{u}_y \\ &\qquad + \left[(z-z^c) - \zeta'\cos\gamma\right]\hat{u}_z\Big| \end{aligned} \tag{III.8}$$

Also, one may determine the distance D_{pq} from a point on the surface of the p^{th} wire to a point on the axis of the q^{th} wire (see Fig. 3.2):

$$D_{pq}(\zeta,\zeta') = \left[a_p^2 + \left|(\bar{r}_p^c+\zeta\hat{u}_p) - (\bar{r}_q^c+\zeta'\hat{u}_q)\right|\right]^{\frac{1}{2}} \tag{III.9}$$

In (III.9), a_p is the radius of the p^{th} wire, $\bar{r}_p^c$ locates its center, and $\hat{u}_p$ is the unit vector along its axis, while $\bar{r}_q^c$ locates the center of the q^{th} wire whose axis is directed along $\hat{u}_q$. The parameters ζ and ζ' denote displacement along p^{th} and q^{th} wires, respectively, from their respective centers.

APPENDIX IV

FAR FIELD COMPUTATION

The radiated fields of a complex coupled-wire antenna structure can readily be calculated with far-field conditions for a known current distribution using either reciprocity or a vector potential approach. In this analysis, the vector potential approach is used to formulate the electric field in terms of current distributions computed from the numerical procedure outlined in this report. As would be expected, this far-field formulation reduces to the computation of an equivalent array factor and pattern factor related to the subdomain basis set used to represent the antenna current distribution.

For simplicity, a single wire, as the p^{th} wire shown in Fig. IV-1, is used to illustrate the formulation which can subsequently be extended to the multiple-wire case required to fabricate the wire biconical antenna. From standard formulas, such as (3.3a), for total vector potential in the direction of the current, i.e. the wire,

$$A_p(\bar{r}) = \frac{\mu}{4\pi} \int_0^{L_p} i_p(\zeta') \frac{e^{-jk|\bar{r}-\bar{r}'_p|}}{|\bar{r}-\bar{r}'_p|} d\zeta' \qquad \text{(IV.1)}$$

where

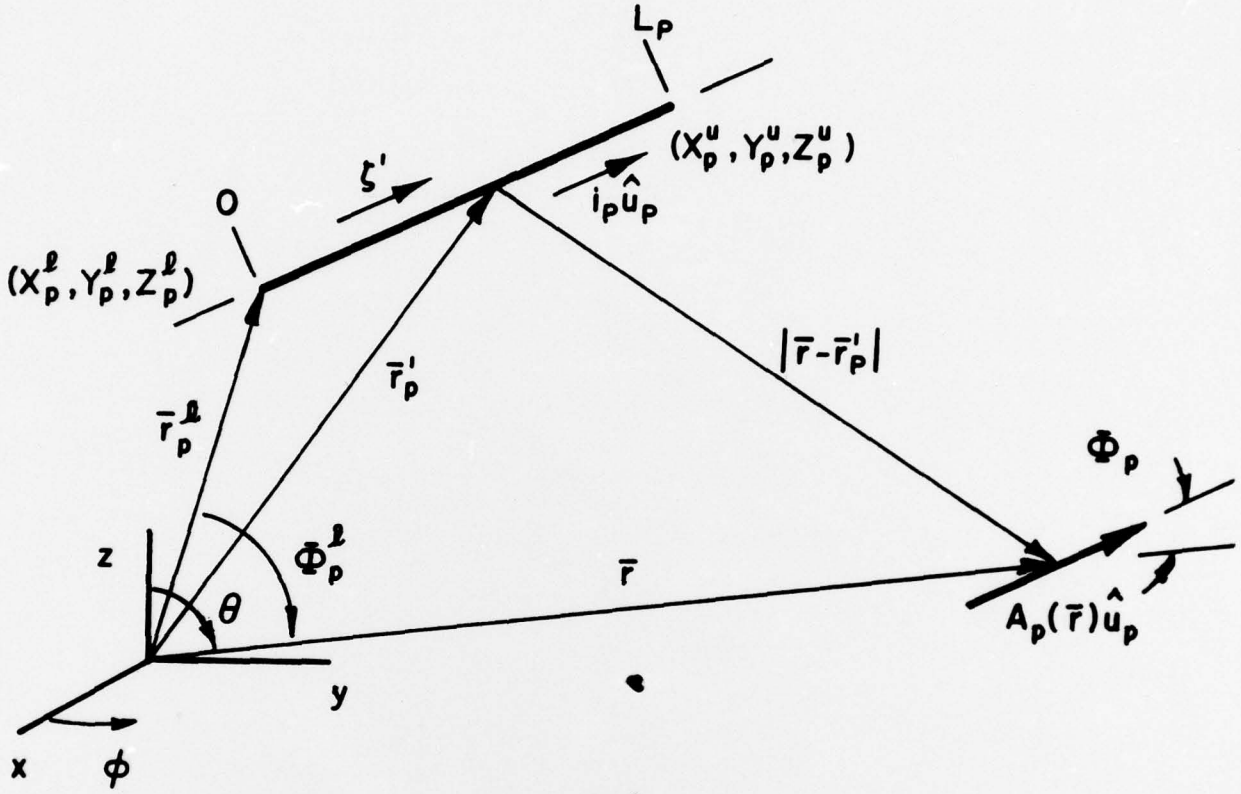

$$\cos\Phi_p = \frac{\bar{r}\cdot\hat{u}_p}{|\bar{r}|}$$

$$\cos\Phi_p^\ell = \frac{\bar{r}\cdot\bar{r}_p^\ell}{|\bar{r}||\bar{r}_p^\ell|}$$

FIG. IV-1. GEOMETRY FOR FAR-FIELD COMPUTATION FOR A SINGLE WIRE.

$$|\bar{r}-\bar{r}'_p| = (|\bar{r}|^2 + |\bar{r}'_p|^2 - 2\bar{r}\cdot\bar{r}'_p)^{\frac{1}{2}} \quad ,$$

and L_p is the total length of the p^{th} wire, as defined in Chapter 3 and Fig. IV.1. Now, for the far-field conditions, $\bar{r}$ large, $|\bar{r}'_p|$ bounded, and $\frac{|\bar{r}'_p|}{|\bar{r}|} << 1$, (IV.1) reduces to

$$A_p(\bar{r}) = \frac{\mu}{4\pi} \frac{e^{-jk|\bar{r}|}}{|\bar{r}|} \int_0^{L_p} i_p(\zeta') e^{jk|\bar{r}'_p|\cos\Phi_p} \, d\zeta' \quad \text{(IV.2)}$$

where Φ_p is the angle between $\bar{r}$ and $\hat{u}_p$. Φ_p can be expressed in terms of the direction cosines related to $\bar{r}$ and the p^{th} wire as

$$\cos\Phi_p = \cos\alpha_p\cos\alpha_r + \cos\beta_p\cos\beta_r + \cos\alpha_p\cos\alpha_r \, . \quad \text{(IV.3)}$$

If the distance $|\bar{r}'_p|$ is expressed in terms of $\bar{r}^{\ell}_p$ and the distance along the wire from the lower and to the upper end, ζ', the vector potential becomes

$$A_p(\bar{r}) = \frac{\mu}{4\pi} \frac{e^{-jk(|\bar{r}|-|\bar{r}^{\ell}_p|\cos\Phi^{\ell}_p)}}{|\bar{r}|} \int_0^{L_p} i_p(\zeta') e^{jk\zeta'\cos\Phi_p} \, d\zeta' . \quad \text{(IV.4)}$$

In this case, $\bar{r}^{\ell}_p$ is the vector from the origin of the coordinate system to the lower end of the p^{th} wire and Φ^{ℓ}_p is the angle between $\bar{r}$ and $\bar{r}^{\ell}_p$. Φ^{ℓ}_p can also be represented in terms of the related direction cosines as

$$\cos\Phi_p^{\ell} = \cos\alpha_p^{\ell}\cos\alpha_r + \cos\beta_p^{\ell}\cos\beta_r + \cos\alpha_p^{\ell}\cos\alpha_r. \qquad \text{(IV.5)}$$

Equation (IV.4) is simply an equation for the total vector potential in the far-field for an arbitrarily placed wire with a general current distribution. However, if the current distribution is expressed in terms of a linear combination of subdomain elements of the form (2.6a) and as shown in Fig. 2.3, then

$$i_p(\zeta') = \sum_1^N I_m \Lambda_m^{\ell}(\zeta') \qquad \text{(IV.6)}$$

where N is total number of subdomain elements. With the substitution of (IV.6) into (IV.4) and a subsequent translation of axis, the vector potential simplifies to

$$A_p(\bar{r}) = \frac{\mu}{4\pi} \frac{e^{-jk(|\bar{r}| - |\bar{r}_p^{\ell}|\cos\Phi_p^{\ell})}}{|\bar{r}|} \sum_1^N I_m e^{jkm\Delta\cos\Phi_p} \times \int_{-\Delta}^{\Delta} \Lambda^{\ell}(u) e^{ju\cos\Phi_p}\, du \qquad \text{(IV.7)}$$

where Δ is $L_p/(N-1)$, N is the total number of segments on the wire, u is distance measured relative to the center of an element of the subdomain basis set $\{\Lambda_m^{\ell}\}$, and Λ^{ℓ} is an subdomain element centered about zero on the u axis. Note that at each end of the wire the integral is valid only for Δ, not 2Δ, and

thus, the half-elements must be handled differently from the full elements. From (IV.7) it is evident that

$$A_p(\bar{r}) = \frac{\mu}{4\pi} \frac{e^{-jk(|\bar{r}|-|\bar{r}_p^{\ell}|\cos\phi_p^{\ell})}}{|\bar{r}|} \Big[\text{Array Factor } (A_f) \times \text{Pattern Factor } (P_f) + \text{Half-element Contribution} \Big] \tag{IV.8a}$$

where

$$A_f = \sum_{1}^{K} I_{m+1} e^{jmk\Delta\cos\Phi_p} \quad ; \; K = N-2, \tag{IV.8b}$$

$$P_f = \int_{-\Delta}^{\Delta} \Lambda^{\ell}(u) e^{jku\cos\Phi_p} \, du \, , \tag{IV.8c}$$

and the half-element contributions on the wire ends are

$$I_1 e^{jk\Delta\cos\Phi_p} \int_{0}^{\Delta} \Lambda^{\ell}(u) e^{ju\cos\Phi_p} \, du + I_N e^{jkN\Delta\cos\Phi_p} \int_{-\Delta}^{0} \Lambda^{\ell}(u) e^{ju\cos\Phi_p} \, du \, . \tag{IV.8d}$$

In the far-field of the wire, the electric field in the direction of the wire can be approximated as

$$\bar{E}_p(\bar{r}) = -j\omega A_p(\bar{r}) \hat{u}_p \, . \tag{IV.9}$$

However, the θ and ϕ components of the electric field in respect to the origin of the coordinate system are the qualities of interest, therefore, the projected components of the $\bar{E}$-field are

$$E_\theta(\bar{r}) = -j\omega A_p(\bar{r})\hat{u}_p \cdot \hat{u}_\theta \qquad \text{(IV.10a)}$$

and

$$E_\phi(\bar{r}) = -j\omega A_p(\bar{r})\hat{u}_p \cdot \hat{u}_\phi \qquad \text{(IV.10b)}$$

where the unit vectors, $\hat{u}_\theta$ and $\hat{u}_\phi$, can be represented in terms of the direction cosines related to $\bar{r}$ for computation.

A subroutine PATRN has been developed for the far-field computation of the total θ and ϕ components of the electric field from Eqs. (IV.8) and (IV.10) using the known current distribution determined for the geometry defined in the numerical procedure presented in this report for a single wire. The subroutine computes these fields for the piecewise linear subdomain basis set where the full-element pattern factor is of the well-known form

$$P_f = \Delta \left[\frac{\sin (x/2)}{(x/2)} \right]^2 \qquad \text{(IV.11a)}$$

and the half-element pattern factor is of the form

$$P_f^{\ell, u} = \Delta \left[\frac{1}{x^2} \pm \frac{j}{x} - \frac{e^{\mp jx}}{x^2} \right] \qquad \text{(IV.11b)}$$

where

$$x = k\Delta\cos\Phi_p$$

where the negative sign corresponds to the upper elements and the positive sign corresponds to the lower element.

These results are extended to the case of multiple wires encountered in the wire biconical antenna by linear superposition of the total electric field as indicated in (3.1).